KUOPION YLIOPISTON JULKAISUJA G. - A.I. VIRTANEN -INSTITUUTTI 67
KUOPIO UNIVERSITY PUBLICATIONS G.
A.I. VIRTANEN INSTITUTE FOR MOLECULAR SCIENCES 67

RIIKKA IMMONEN

Magnetic Resonance Imaging of Progressive Changes in Traumatic Brain Injury and Epileptogenesis

Doctoral dissertation

To be presented by permission of the Faculty on Natural and Environmental Sciences
of the University of Kuopio for public examination in Auditorium MET,
Mediteknia building, University of Kuopio,
on Thursday 18th December 2008, at 12 noon

Department of Neurobiology
A.I. Virtanen Institute for Molecular Sciences
University of Kuopio

KUOPION YLIOPISTO

KUOPIO 2008

Distributor: Kuopio University Library
P.O. Box 1627
FI-70211 KUOPIO
FINLAND
Tel. +358 40 355 3430
Fax +358 17 163 410
http://www.uku.fi/kirjasto/julkaisutoiminta/julkmyyn.html

Series Editors: Research Director Olli Gröhn, Ph.D.
Department of Neurobiology
A.I. Virtanen Institute for Molecular Sciences

Professor Michael Courtney, Ph.D.
Department of Neurobiology
A.I. Virtanen Institute for Molecular Sciences

Author's address: Department of Neurobiology
A.I. Virtanen Institute for Molecular Sciences
University of Kuopio
P.O. Box 1627
FI-70211 KUOPIO
FINLAND
Tel. +358 40 355 2023
Fax +358 17 163 030
E-mail: Riikka.Immonen@uku.fi

Supervisors: Research Director Olli Gröhn, Ph.D.
Department of Neurobiology
A.I. Virtanen Institute for Molecular Sciences

Professor Asla Pitkänen, M.D., Ph.D.
Department of Neurobiology
A.I. Virtanen Institute for Molecular Sciences

Reviewers: Professor Annemie Van der Linden, M.D., Ph.D.
Bio-Imaging Lab
University of Antwerp, Belgium

Professor Leif Østergaard, M.D., Ph.D.
Center for Functionally Integrative Neuroscience
Århus University Hospital, Denmark

Opponent: Mark Lythgoe, Ph.D.
Center for Advanced Biomedical Imaging
University College London, United Kingdom

ISBN 978-951-27-1126-0
ISBN 978-951-27-1108-6 (PDF)
ISSN 1458-7335

Kopijyvä
Kuopio 2008
Finland

Immonen, Riikka. Magnetic Resonance Imaging of Progressive Changes in Traumatic Brain Injury and Epileptogenesis. Kuopio University Publications G. - A.I. Virtanen Institute for Molecular Sciences 67. 2008. 80 p.
ISBN 978-951-27-1126-0
ISBN 978-951-27-1108-6 (PDF)
ISSN 1458-7335

Abstract

Epilepsy can develop as a consequence of known etiology like traumatic brain injury, stroke, or prolonged febrile seizures. Brain insult is typically followed by a latent period (i.e., epileptogenesis) during which various neurobiological changes occur, including neurodegeneration, gliosis, neurogenesis, angiogenesis, alterations in the extracellular matrix, molecular changes in cellular membranes and axonal sprouting. The axonal plasticity and circuitry reorganization is believed to underlie the change in network excitability, and eventually lead to the occurrence of spontaneous seizures. Traumatic brain injury (TBI) launches insidiously progressive brain pathology which can, in addition to epilepsy, lead to functional and cognitive impairment.

In this thesis work multiple *in vivo* magnetic resonance imaging (MRI) techniques including quantitative mapping of relaxation and diffusion, a novel technique called manganese enhanced MRI (MEMRI), susceptibility contrast enhanced MRI of cerebral blood volume changes, and magnetic resonance spectroscopy were targeted to probe the pathological cellular phenomena during the pre-symptomatic latent phase. The aim was to find surrogate markers for epileptogenesis and predictive factors for long-term functional and histopathological outcome after TBI utilizing experimental animal models.

It was shown that MEMRI was able to detect axonal sprouting in the hippocampus of the epileptogenic rat. Manganese accumulated in the the dentate gyrus and CA1 sub regions of the hippocampus, where axonal sprouting was present. The fact that the signal rose from mossy fibers was verified by cross comparison of MEMRI findings with several histological stainings and eliminating astrogliosis, microgliosis, seizure activity and the leakage of blood-brain barrier as the primary sources of MEMRI signal. Thereby, enhancement by manganese was proven to be a potential surrogate marker for epilepsy in the experimental setting.

The progression of tissue damage was followed by quantitative MRI for over 11 months after fluid percussion induced TBI and a distinct temporal pattern was found in the irreversibly damaged lesion area as compared to the more mildly affected perifocal and hippocampal regions. The chronic metabolic changes in the hippocampi were studied using ^{1}H magnetic resonance spectroscopy (MRS), and the long-term outcome was assessed by Morris water maze testing the learning ability, by brain atrophy measurements, and by histological stainings. Importantly, correlations between the early quantitative MRI findings (T_2, $T_{1\rho}$, average diffusion, atrophy, hemorrhage) and the long-term outcome were found promoting the predictive value of quantitative MRI after TBI.

Furthermore, since haemodynamic disturbances may be one factor affecting the secondary damage progression after TBI, the CBV changes in different brain regions were followed for two weeks post-injury. Simultaneously the impairment of motor functions was tested by a composite neuroscore test. The main finding was that the perilesional CBV drops rapidly acutely after injury and then slowly recovers over the 2 weeks period, and this accurately coincides with similar drop and recovery in the motor function performance.

Taken together, MRI probes tailored for epilepsy, TBI or other neurodegenerative diseases have potential to provide early biomarker and may aid the prediction the long-term outcome.

National Library of Medicine Classification: WL 141, WL 354, WL 385, WN 185, QY 58
Medical Subject Headings: Brain Injuries; Epilepsy; Magnetic Resonance Imaging; Magnetic Resonance Spectroscopy; Manganese; Markers, Biological; Hippocampus; Mossy Fibers, Hippocampal; Behavior; Maze Learning; Motor Activity; Hemodynamics; Histological Techniques; Prognosis; Disease Models, Animal

From the largest scale of the infinite space
to the smallest scale of atomic interactions.
From the detailed mechanisms of brain function
to the intriguing capabilities of human mind.
As far as you can imagine - and beyond
One could not ask for more fascinating subject to study
than the combination of abstract and concrete
in the field of neurobiological NMR...

Acknowledgements

The represented studies were carried out during the years 2003-2008 as a collaboration of Biomedical imaging unit and Epilepsy research group at the A. I. Virtanen Institute for Molecular Sciences, University of Kuopio.

I want to express my gratitude to my supervisors, who both have invested a respectable amount of time and effort in this thesis project and in my education and inspiration. I owe enormous thanks to my principal supervisor Research Director, Docent Olli Gröhn, who successfully runs the Biomedical imaging unit, works with uncompromised quality, and yet manages to be available when needed and never loses his good spirit. I am also indebted to my second supervisor Professor Asla Pitkänen, for her guidance into the fascinating world of epilepsy and the perspective she provides to the science in the field of neurobiology.

I wish to thank Professor Annemie Van der Linden and MD, PhD, Leif Ostergaard, MD, PhD, the official reviewers of this thesis, for their efforts and constructive criticism.

I want to thank my co-authors, Irina Kharatisvili, Heidi Gröhn, Alejandra Sierra, Juha-Pekka Niskanen, Christine Einula, Taneli Heikkinen, Leena Tähtivaara and Juha Yrjänheikki. Particularly Irina Kharatishvili for her massive input to these studies and ever so warm attitude.

I want to show my respect for the whole NMR group. One could not hope for more energetic, warm and brilliant set of co-workers - nor more stimulating coffee-room conversations. I also want to express my appreciation to the whole Epilepsy research group and to Jari Nissinen, Merja Lukkari and Jarmo Hartikainen for their assistance. I want to thank Maarit - 'the power woman' - Pulkkinen for all the technical and practical help and input to these studies.

I'm grateful to M.Sc Nick Hayward for revising the language of the manuscript and generously taking time when necessary.

This study was financially supported by the Finnish Academy, the Sigrid Juselius Foundation, the Finnish Cultural Foundation of Northern Savo, the Emil Aaltonen Foundation, the Finnish Epilepsy Society and the University of Kuopio Foundation.

I want to express my deepest gratitude and admiration to my parents, Reetta and Niilo, for providing me with solid and every-obstacle-overcoming self esteem and curiosity for science, and their constant support, and to my brother Kari for his existence, attitude and most of all for his drive to keep in contact with the big, the best and the only sister. Greetings also to all my honorary-sisters around Finland!

And finally, to my husband Timo. Your flying ideas together with the ability and unstoppable, fearless attitude of actually realizing them all, is the best refreshment to the body and mind. With you by my side everything is possible, and any worries shrink into their correct proportions.

Kuopio, November 2008

Riikka Immonen

Abbreviations

ADC	apparent diffusion coefficient
AEDs	antiepileptic drugs
B_0	external magnetic field
B_1	magnetic field component of radio frequency pulse
B_{1SL}	spin-lock magnetic field
BBB	blood-brain barrier
CBF	cerebral blood flow
CBV	cerebral blood volume
CCI	controlled cortical impact injury
CNS	central nervous system
CSF	cerebrospinal fluid
CHESS	chemical shift selective radio frequency pulse
Cho	choline containing compounds
Cr	creatine and phosphocreatine
D_{av}	1/3 of the trace of the diffusion tensor
DTI	diffusion tensor imaging
DWI	diffusion weighted imaging
EEG	electroencephalography
FASTMAP	fast automatic shimming method along projections
FID	free induction decay
FOV	field of view
FPI	fluid percussion injury
GABA	γ-aminobutyric acid
γ	gyromagnetic ratio
GFAP	glial fibrillary acidic protein
$\hbar$	Planck's quantum constant
i.p.	intraperitoneally
i.v.	intravenously
IR	inversion recovery
J	coupling constant
k	Boltzmann's constant
KA	kainic acid
LASER	localization by adiabatic selective refocusing
M	magnetization
μ	magnetic moment
MEMRI	manganese enhanced magnetic resonance imaging
MION	monocrystalline iron oxide nanoparticle
MR	magnetic resonance
MRI	magnetic resonance imaging
MRS	magnetic resonance spectroscopy
NAA	N-acetyl aspartate
NMR	nuclear magnetic resonance
OVS	outer volume suppression
PTZ	pentylenetetrazole
r	correlation
R_2	apparent transverse relaxation rate (measured by spin echo sequence)
R_{2*}	transverse relaxation rate (measured by gradient echo sequence)

RF	radio frequency
ROI	region of interest
S	signal intensity
S_0	initial signal intensity
SE	status epilepticus
SEM	standard error of mean
SL	spin-lock
SNR	signal-to-noise ratio
STEAM	stimulated echo acquisition mode
θ	flip angle
T	temperature (in Kelvin)
T_1	longitudinal relaxation time / spin-lattice relaxation time
$T_{1\rho}$	longitudinal relaxation time / spin-lattice relaxation time in a rotating frame
T_2	apparent transverse relaxation time / spin-spin relaxation time
T_2*	transverse relaxation time
τ_c	correlation time
TBI	traumatic brain injury
TE	echo time
TI	inversion time
TLE	temporal lope epilepsy
TR	repetition time
ω_0	frequency of the main magnetic field / Larmor frequency
ω_{1SL}	frequency of the spin-lock field

List of original publications

This thesis is based on the following original publications referred to by their corresponding Roman numerals in the thesis.

I

Immonen R, Kharatishvili I, Sierra A, Einula C, Pitkänen A, Gröhn O: *Manganese Enhanced MRI detects mossy fiber sprouting rather than neurodegeneration, gliosis or seizure-activity in the epileptic rat hippocampus.* NeuroImage, 40:1718-30 (2008)

II

Immonen R, Kharatishvili I, Niskanen J-P, Gröhn H, Pitkänen A, Gröhn O: *Distinct MRI pattern in lesional and perilesional area after traumatic brain injury in rat - 11 months follow-up.* Experimental Neurology, in press, doi:10.1016/j.expneurol.2008.09.009 (2008)

III

Immonen R, Kharatishvili I, Gröhn H, Pitkänen A, Gröhn O: *Quantitative MRI predicts long-term structural and functional outcome after experimental traumatic brain injury*. NeuroImage, in press

IV

Immonen R, Heikkinen T, Tähtivaara L, Nurmi A, Stenius T-K, Puoliväli J, Tuinstra T, Phinney A, Van Vliet B, Yrjänheikki J, Gröhn O: *Cerebral blood volume alterations in the perilesional areas in the rat brain after traumatic brain injury - comparison with behavioural outcome*. manuscript

Table of contents

1 Introduction

Magnetic resonance imaging and spectroscopic methods offer a variety of approaches to study the different features of the brain pathologies non-invasively. Particularly, in complex nervous system diseases with slow progressive nature and largely unknown mechanisms the application of multimodal MRI techniques that target different underlying phenomena can provide crucial information about the spatio-temporal developments of the tissue damage and thereby provide more insight into the disease mechanisms.

Epilepsy is one of the most common groups of neurological diseases affecting over 1% of the worlds population, which means over 68 million people worldwide, and it can develop as a consequence of different etiologies: febrile seizures, stroke, brain infection, status epilepticus or traumatic brain injury (Engel 1989). After the initial insult there is a latent period, epileptogenesis, that can last from weeks to years, during which several neurobiological processes take place eventually leading to the occurrence of spontaneous seizures, that is, to the beginning of the actual epilepsy phase. The neurobiological sequels include neurodegeneration and neurogenesis, gliosis and axonal sprouting, angiogenesis and reorganization of the extracellular matrix (Jutila et al., 2002).

Traumatic brain injury (TBI) is the most common cause of new-onset epilepsy among young people (Annegers, Rocca, Hauser 1996). In addition to being one of the etiologies of epilepsy, traumatic brain injury itself is a devastating condition and a prevalent cause of disability and mortality in industrialized countries (Leon-Carrion et al., 2005a). TBI possess a progressive complex nature and variety of functional and cognitive outcome disabilities which can manifest several years after the initial insult (Cohen et al., 2007; Gennarelli and Graham 1998; McIntosh et al., 1996). In TBI the primary impact causes immediate damage through mechanical forces and launches a cascade of secondary damage. The direct consequences are lesion formation at the contusion site, diffuse axonal injury and intracerebral hemorrhages, while the secondary processes include progressive neuronal death, glial hypertrophy, haemodynamic disturbances and problems with energy metabolism leading to further tissue atrophy (Graham et al., 2000b). The mechanism of destructive cascades and the role of recovery processes are still mainly unknown.

Experimental animal models of epilepsy and TBI express many of the features of the human conditions and allow a targeted investigation of the pre-symptomatic period. The chemically induced status epilepticus in rat launches epileptogenesis and the pathophysiological cascades cause the seizures to appear a few months later. Histological studies have verified reorganization of neural circuits, that is, axonal sprouting called mossy fiber sprouting in the hippocampus of these animals similarly to the human patients (Sutula et al., 1989; Tauck and Nadler 1985b) and cellular level alterations mimicking the complex human condition (McIntosh et al., 1996; Pirttila et al., 2001; Pitkanen et al., 2000). Fluid percussion induced brain injury is the best characterized animal model for TBI and it has been proven to develop functional deficits, such as memory decline, resembling the symptoms in patients (Thompson et al., 2006).

Several drugs could potentially benefit epileptogenic or TBI patients if only the treatment could be started in the early latent phase and targeted to the patients undergoing the early steps of the pathological cascades. There is a great need for diagnostic methodology that

could detect the early surrogate markers of the disease, help to predict the long-term outcome, guide interventions and monitor the treatment response.
The full potential of available MRI methodology needs to be investigated with the help of animal models in order to tailor for each disease modality an optimal combination of MRI assessments, which could then be transferred into clinical use.

2 Literature overview

2.1 Theory and principles of NMR

The nuclear magnetic resonance phenomenon is an interaction between the charged nuclear particles, possessing a property called spin, and the external magnetic field. Atomic nuclei with an uneven number of protons or neutrons possess a non-zero angular momentum, called spin angular momentum $\vec{S}$. Intuitively, the electromagnetic nature of the nuclei, *nuclear magnetism,* can be visualized as a small loop with electrical current creating a magnetic field through the loop, perpendicularly (Faraday's law of induction[1]) and causing the loop (atomic particle) to behave as a small bar magnet when interacting with the external magnetic field. Further in the classical mechanics point of view, this small bar magnet can be thought to rotate about its own axis, that is, to spin, and thereby have property analogous to mechanical angular momentum[2]. Strictly speaking this analogy can not be taken too far, and according to the quantum mechanical point of view the spin, described by wavefunctions and propability distributions, carries intrinsic angular momentum, which has nothing to do with motion in space (Griffiths 1995). In the following presentation, the theory of NMR starts with a quantum mechanical approach and moves then to classical physics, because the concepts of classical physics enable a more fluent description of the phenomena in the context of practical applications and NMR techniques. The theory beyond the scope of this thesis can be found in several books (de Graaf 2007; Gadian 1995; Griffiths 1995; Haacke 1999).

Key features in the quantum mechanical principles of NMR are briefly described in the following section. The physical property of spin angular momentum is quantised, meaning that it can have only certain discrete values. This derives from the fact that the spin of the nucleus (I), also called as the quantum number of the nucleus, can have only integral or half-integral values: integral if the nucleus has an even mass number, zero if there is an even numbers of both protons and neutrons, and half-integral if the nucleus has an odd mass number. The spin angular momentum $\vec{S}$ is a vector property and is in turn defined as $\vec{S} = m\hbar$, where m (magnetic quantum number) can only get values I, I-1,I-2,...,-I, hence spin angular momentum is quantised with the respect of both magnitude and orientation. The most studied nucleus in the field of in vivo NMR, the hydrogen ^{1}H, has nuclear spin quantum number (I) of 1/2, m of either +1/2 or -1/2 and the spin angular momentum $\vec{S} = \pm 1/2\ \hbar$. This means that the hydrogen has two possible eigen states (and the spin state is a superposition of them), and upon measurement the spin state is determined to be one of the two states. The external magnetic field creates an energy difference between these states (so called Zeeman effect) while in the absence of external magnetic field the states would be at the same energy level (degenerate). The external magnetic field interacts with the nuclei because the spin angular momentum $\vec{S}$ causes the nuclei to possess also adjacent magnetic moment μ

$$\mu = \gamma \vec{S} \qquad [1]$$

which depends on its characteristic gyromagnetic ratio γ.

[1] According to the Faraday's law of induction a moving electrical charge creates a magnetic field and, vice versa, a changing magnetic field induces electromotive force (emf) and thereby current in a closed loop.
[2] A rigid object in classical mechanics admits orbital angular momentum, associated with the motion *of* the center of mass, and spin angular momentum, associated with the motion *about* the center of mass.

Due to the magnetic moment the nucleus behaves as a magnetic dipole and experiences a torque, $T = \mu \times B$, which depends on the field strength and tends to align the dipole parallel to the external field. Now, hydrogen nucleus has two allowed energy states in a magnetic field, parallel to the magnetic field is the lower energy state (with population of n^+) and anti-parallel the higher (with population of n^-). The energy difference ΔE between the eigenstates depends on the magnetic field B_0

$$\Delta E = \gamma \hbar B_0 \qquad [2]$$

The NMR signal is based on the transitions between the adjacent energy states. Irradiating the object with an energy-quantum that satisfies the so-called resonance condition, that is carries energy equal (or multiple) to the energy difference between the levels, can induce a transition from the lower energy state to the higher one. In NMR techniques this *excitation* is accomplished by applying an additional oscillating magnetic field B_1. When the object is thereafter returning towards the lowest energy state (favourable state) and transitions back to the lower energy state take place, the object transfers a quantum of energy corresponding to the ΔE to its surroundings as heat. The requirement for energy absorbance (and transfer) is as follows

$$\Delta E = h\nu_0 \qquad [3]$$

where h is the Planck constant and ν is the frequency of the electromagnetic radiation quanta[3]. When combining equations 2 and 3 (and noting that ħ = h/2π) the resonance condition becomes

$$\nu_0 = \gamma B_0 / 2\pi \quad \text{, and further} \quad \omega_0 = \gamma B_0 \quad , \qquad [4]$$

where ω_0 is called Larmor frequency (angular frequency, $\omega_0 = \nu_0 2\pi$). The applied oscillating magnetic field B_1 is generated with electromagnetic radiation (often referred as RF-pulse) having frequency is in the order of hundreds of megahertz (~10^8 Hz), which is within the radiofrequency (RF) range. In the case of hydrogen the gyromagnetic ratio is 2.67 *10^8 rad/s/T and the magnetic field strengths range from typical clinical 1.5 T scanner to *in vivo* experimental 9.4 T and even 16.4 T scanners.

The imbalance between the spin populations in the two energy states is the fundamental feature that gives rise to the NMR signal. In the absence of any external magnetic field the magnetic moments of a nuclei population would be randomly oriented, cancelling each other out, but in the magnetic field B_0 they find a new equilibrium defined by the Boltzmann's distribution

$$\frac{n^-}{n^+} = e^{-\Delta E / kT} = e^{-\gamma \hbar B_0 / kT} \qquad [5]$$

which states that the number of antiparallel and parallel nuclei depends on the external magnetic field strength B_0 and the absolute temperature T (k is the Boltzmann's constant).

[3]The NMR techniques use the magnetic component of the electromagnetic radiation

In this equilibrium there is a small excess of nuclei in the lower energy state n^+ parallel to the B_0 field and this generates a net magnetization M_0. The magnitude of the population difference is only about 10 spins out of every million, however since a few grams of tissue contains $\sim 10^{23}$ protons the excess population gives rise to a detectable signal. The ^1H concentration in human body is about 88 M while the concentrations of other nuclei of interest in NMR (possessing non-zero spin angular momentum), such as ^{31}P, ^{23}Na, ^{17}O or ^{19}F, range from μM to mM and therefore give rise to a notably smaller signal.
From this point onward the NMR theory and principles are easiest to explain by using the concepts of classical physics. The above mentioned net magnetization M_0 can be thought as a sum vector which is slightly tilted and precesses about the B_0 at so called Larmor frequency ω_0 (rad/s), $\omega_0 = \gamma B_0$ as derived in equations 3 and 4. The following description of magnetization is done in a Cartesian coordinate system of rotating frame of reference which rotates at the Larmor frequency about the B_0 and where the orientation of M_0 (net magnetization at equilibrium) is defined to be along the z-axis. The M_z component of the magnetization is termed longitudinal magnetization. At the perpendicular x and y orientations there is no magnetic field, hence the net transverse (xy) component of the magnetization vector (M_{xy}) is zero.

Only the xy-component of the magnetization can be detected. The magnetization oscillating/precessing on the xy-plane induces an alternating current into the receiver coil (that is, a conductor wire loop perpendicular to the xy-plane and tuned to the Larmor frequency). The tilting of the magnetization vector onto the xy-plane, excitation, is achieved when an oscillating magnetic field B_1 is applied on the resonance frequency ω. The characteristics of the applied RF-pulse determine how strong torque it imposes on the net magnetization and how much the net magnetization becomes tilted. A pulse which causes a 90º flip onto the xy-plane is called 90º pulse, and a pulse causing a 180º flip is a 180º pulse, respectively.

NMR signal induced in the receiver coil is called a free induction decay (FID), an alternating current carrying frequency and phase [phase change $\Delta\theta = \omega t$] information and showing exponential decay of amplitude. The amplitude decay begins immediately when the applied RF-pulse (electromagnetic radiation) is turned off, because the system starts to return back to the equilibrium recovering the M_z and losing the M_{xy}.

This so-called relaxation of the components of magnetization vector M_z and M_{xy} is the key concept in magnetic resonance imaging since the relaxation rates depend on the biochemical/physical surroundings of the nuclei. The relaxation can be described by the Bloch equations (Bloch, 1994)

$$\frac{dM_z}{dt} = \frac{M_0 - M_z}{T_1} \qquad [6]$$

$$\frac{dM_{xy}}{dt} = -\frac{M_{xy}}{T_2} \qquad [7]$$

2.1.1 Recovery of M_z: T_1 relaxation

T_1 relaxation is the relaxation of the longitudinal z-component of the magnetization [Eq. 6] and happens because the system returns towards equilibrium by transferring energy between

the nuclear spin and the surrounding lattice. T_1 relaxation is therefore termed spin-lattice relaxation. The nucleus transfers energy to its molecular environment as heat energy (spontaneous emissions are so unlikely that they have only negligible role in the loss of energy). The thermal translational, rotational and vibrational motion of the nucleus itself and the motions of the surrounding molecules cause the nuclei to experience fluctuating magnetic field variations. Those fluctuations taking place at the Larmor frequency or at double the Larmor frequency evoke stimulated emissions and lead to the recovery towards the equilibrium, that is, recovery of the M_z component. The spectral density function $J(\omega)$ describes the frequency distribution of the random tumbling of the molecules.

$$J(\omega) \propto \frac{\tau_c}{1+\omega^2\tau_c^2} \qquad [8]$$

where τ_c is the time required for the molecule to rotate one radian (τ_c is short for fast molecular motion and long for slow molecular motion). In the case of dipole-dipole interactions the dependency of T_1 relaxation on the frequencies of the surrounding molecular motion can be formalized as follows

$$\frac{1}{T_1} \propto \frac{\tau_c}{1+\omega_0{}^2\tau_c^2} + \frac{4\tau_c}{1+4\omega_0^2\tau_c^2} \qquad [9]$$

and it can be noted that relaxation rate is at highest (meaning T_1 is at shortest) when $\tau_c = 1/\omega_0$, that is when the molecular tumbling happens at Larmor frequency (corresponding τ_c of 10^{-7}-10^{-9} s depending on the external magnetic field strength).

2.1.2 Transverse relaxation: T_2* and T_2

T_2 relaxation is the relaxation of the transverse xy-component of the magnetization [Eq. 7] and it takes place due to interactions of spins with other spins, and is therefore termed spin-spin relaxation. Furthermore, all phenomena contributing to the T_1 relaxation affect also the T_2 relaxation. T_2 relaxation time is always shorter (or equal) to the T_1 relaxation time. Immediately after the 90º pulse the individual spins are in phase coherence at the xy-plane. Their precession frequency depends on the magnetic field they experience [Eq.4], and because of the local field inhomogeneities and the interactions between individual spins, the spins experience different local fields, start to precess at different frequencies and dephase (i.e. lose their phase coherence) and hence the net M_{xy} magnetization starts to decay.

A transverse relaxation time constant T_2* describes the combined effect of all the dephasing processes on transverse relaxation. $1/T_2$* is the decay rate of the FID signal. The main two effects on transverse relaxation are the dephasing due to the static magnetic inhomogeneities ($T_{2,\Delta B0}$), caused by inhomogeneous static magnetic field B_0 or large magnetic susceptibility differences within a heterogeneous sample, together with so called apparent transverse relaxation T_2

$$\frac{1}{T_2*} = \frac{1}{T_{2,\Delta B0}} + \frac{1}{T_2} \qquad [10]$$

The apparent transverse relaxation T_2 can be further divided into the dephasing caused by intrinsic relaxation properties $T_{2,intr}$, dephasing caused by diffusion $T_{2,diff}$ and dephasing by proton exchange $T_{2,exch}$.

$$\frac{1}{T_2} = \frac{1}{T_{2,\mathrm{int}\,r}} + \frac{1}{T_{2,diff}} + \frac{1}{T_{2,exch}} \qquad [11]$$

The dephasing effects caused by inherently inhomogeneous static magnetic field B_0 ($T_{2,\Delta B0}$) are referred as static dephasing and can be reversed by a 180º refocusing pulse in a spin echo measurement (described below in chapter 2.1.4). The dephasing caused by diffusion through local field gradients or due to exchange processes is referred to as dynamic dephasing (if the time scale of the changes is faster than the echo-time or the interval between refocusing pulses) and it can not be reversed. The dephasing effects caused by microscopic field fluctuations by neighbouring spins and dipole-dipole interactions ($T_{2,intr}$) are irreversible. The term apparent T_2 is used, because T_2 measured with spin-echo contains several different dynamic dephasing mechanisms in echo-time dependent manner.

In the case of dipole-dipole interactions the dependency of T_2 relaxation on the frequency distribution of surrounding molecular motion can be formalized as follows

$$\frac{1}{T_{2,\mathrm{int}\,r}} \propto 3\tau_c + \frac{5\tau_c}{1+\omega_0^2\ \tau_c^2} + \frac{2\tau_c}{1+4\omega_0^2\tau_c^2} \qquad [12]$$

and it can be noted that slow molecular motion (large τ_c value) has a dominant effect on the T_2 relaxation (the first term of the equation causes the T_2 relaxation rate to be highest when τ_c is large) and thereby T_2 probes the slow molecular motion. The very fast molecular motion is non-significant regarding the T_2 relaxation, because in the case of extreme fast molecular rotational motion (small τ_c, such that $\omega^2\ \tau_c^2 << 1$) T_2 becomes longer, and approaches T_1. This is called motional narrowing, and the condition $T_2 \sim T_1$ is true, for example, in the cerebrospinal fluid (CSF), which in its physical properties is close to free water with only low consentration of molecules.

2.1.3 $T_{1\rho}$ relaxation

$T_{1\rho}$ measures the relaxation at very low magnetic fields while benefiting from the high signal-to-noise ratio at a high B_0 field (Sepponen et al., 1985). The idea of $T_{1\rho}$ experiment is that the spins are flipped first by 90º and are then locked in the xy-plane by a continuous RF-pulse, that is, an additional on-resonance spin-lock field B_{1SL}. Spins precess now about the B_{1SL} field. This continuous spin-lock pulse causes the net magnetization vector to remain in the xy-plane and creates preferred energy states for spins in that direction while there is no net magnetization orthogonal to B_{1SL}. The system starts to return towards the equilibrium and the magnetization starts to relax along the B_{1SL} (Santyr et al., 1994). In the relaxation process spins at the higher energy level lose energy via heat transfer (analogous to the T_1 spin-lattice energy transfer, and the $T_{1\rho}$ relaxation is therefore often referred as T_1 relaxation in the rotating frame.). However, the quanta of energy transfered are now much smaller than in T_1 relaxation due to much smaller difference ΔE_{SL} between the energy states, and therefore, the $T_{1\rho}$ measurement probes different molecular interactions than T_1. Taken together, $T_{1\rho}$ probes the relaxation under the influence of very low magnetic fields, typically <1 mT). The dependency of $T_{1\rho}$ relaxation on the frequencies of surrounding molecular motion (dipole-dipole interactions) can be written

$$\frac{1}{T_{1\rho}} \propto \frac{3\tau_c}{2(1+4\omega_{eff}^2\tau_c^2)} + \frac{5\tau_c}{2(1+\omega_0{}^2\tau_c^2)} + \frac{\tau_c}{1+4\omega_0^2\tau_c^2} \quad [13]$$

where the ω_{eff} is frequency of the effective spin-lock field and $T_{1\rho}$ relaxation rate is highest when the molecular motion is close to $\omega_{eff} = \gamma B_{1SL}$ which corresponds to slow motion with frequency in kHz range and τ_c around 10^{-2}-10^{-4}s .

2.1.4 Measurement of the different relaxation times

Signal can be detected only from the xy-plane where the oscillation of the xy-component of the net magnetization induces wave-form signal in the receiver coil. The magnitude of measured signal determines how much of the longitudinal magnetization had recovered at the moment of signal acquisition. The choice of the timing of signal refocusing actions (pulses or bipolar gradient) and signal collection in the sequence determines which relaxation process is probed, that is, if transversal or longitudinal relaxation process is dominating the acquired signal.

Measuring the T_1 relaxation can be done with a so-called inversion recovery experiment. In the inversion recovery procedure the magnetization is first inverted by 180º, that is, to the -z direction, and allowed to recover along the z-axis for a time period called inversion time (TI) before applying the 90 º pulse and acquiring the signal. The magnitude of the detected signal is

$$M_z = M_0(1-2e^{-TI/T1}) \quad [14]$$

and depends on the initial net magnetization M_0, T_1 relaxation and inversion time. T_1 relaxation time has been defined to be the time when magnetization has recovered to 63% of its initial maximal value. When repeating the measurement with different known inversion times and fitting the Eq.14 to the acquired signal intensity values the absolute T_1 relaxation time constant can be calculated. Eq.14 assumes exponential recovery with a starting point of M_0 at -z direction. Another option to measure T_1 is the so-called saturation recovery technique where the 90º pulses (or pulses of smaller flip angle) are repeated in intervals short enough so that the longitudinal component of magnetization M_z does not have time to completely recover (system does not return to equilibrium) within the repetition time (TR). The formulae of magnetization in the saturation recovery approach is similar to Eq.14 with factor 2 removed (because now the flip is only half of full inversion) and repetition time term replacing the inversion time term

$$M_z = M_0(1-e^{-TR/T1}) \quad [15]$$

Measuring the T_2 relaxation can be done by first tilting the magnetization to the xy-plane by 90º pulse and, after some dephasing, rephasing the spins on the xy-plane and thereby generating a so-called echo. A technique called spin-echo or Hahn spin-echo sequence (Hahn 1950; Carr and Purcell 1954) achieves this by applying a 180º pulse that reverses the phase of spins (flips them 180º at xy -plane), which causes the dephased spins to rephase again, and restore (most of) the net M_{xy} magnetization. The time from 90º pulse to the restored coherence (i.e. the echo signal) is called echo time (TE). When the echo signal intensity is

assessed with different known TEs, T_2 relaxation time can be calculated by fitting the exponential decay function

$$M_{xy} = M_0 e^{-TE/T2} \quad [16]$$

T_2 relaxation time has been defined to be the time when xy magnetization has decayed to 37% of its original value. Multiple echoes can be obtained by adding refocusing pulses to the spin echo sequence and again (similar to the Hahn echo) the amplitude of the consequent echoes decay according to the apparent T_2 relaxation. By shortening the interval of refocusing pulses the contribution of dynamic dephasing phenomena to the observed transverse decay can be minimized (Carr and Purcell 1954).

The echo signal can be also created without the 180º refocusing pulse by using bipolar field gradients instead. The presence of a gradient accelerates the dephasing of the spins, but by applying a field gradient in the opposite direction the spins can be rephased, the coherence restored and the echo signal generated. Gradient echo techniques can be used to measure the T_2* since they do not reverse any of the relaxation phenomena listed with Eq. 10 and Eq. 11.

$T_{1\rho}$ measurement (principles described in chapter 2.1.3) can be made as follows. First, a 90º pulse is applied in the x' direction (that is x in the rotating frame of reference) and it tilts the net magnetization to the y' axis. Then a long lasting RF-pulse called the spin-lock pulse B_{1SL} is applied along the same y' axis. The magnetization relaxes along the y' (field defined by B_{1SL}) and signal decays exponentially according to

$$M = M_0 e^{-TSL/T1\rho} \quad [17]$$

where TSL is the duration of the spin-lock pulse. $T_{1\rho}$ can be assessed by recording the signal decay (free induction decay, FID) immediately after the spin-lock pulse. The absolute $T_{1\rho}$ relaxation time constant can be calculated when repeating the measurement with different known TSL times.

2.1.5 Diffusion

The physical phenomenon of diffusion is caused by the thermal Brownian motion of molecules. The diffusion properties of the sample provide information about its morphology, whether there are diffusion limiting structures or the diffusion is unrestricted. In the case of isotropic unrestricted diffusion the random thermal motion of molecules can be written as

$$\langle r^2 \rangle = 6Dt \quad [18]$$

where $\langle r^2 \rangle$ is the mean square displacement. The signal decay caused by diffusion can be measured either by a bipolar gradient setup or by adding an identical pair of gradients in the spin-echo sequence both before and after the 180º refocusing pulse (Stejskal and Tanner 1965; Tanner 1983). If the spins are stationary the first gradient dephases the spins and the second gradient rephases the spins. Depending on the measurement technique this second gradient can be either the second half of the bipolar gradient with opposite direction or the second identical gradient after the 180 phase reverse. However, if the spins are not stationary but diffuse around and therefore do not experience the second gradient completely, the result

is signal decay. The stronger the diffusion (*i.e.,* the higher the diffusion coefficient D), the greater the signal decay. The decay is also affected by the configuration of the diffusion gradients

$$M = M_0 e^{-bD} \quad \text{, where} \quad b = \gamma^2 \delta^2 G^2 (\Delta - \delta/3) \qquad [19]$$

Here the b-value is shown for two rectangular gradients and γ is the duration of the diffusion gradients, δ is the amplitude and Δ is the delay between them. Diffusion coefficient D can be quantified by repeating the diffusion measurement with different b-values and fitting the decay function to the measured signal intensities.
By using a combination of diffusion gradient pairs in different directions and thereby measuring a diffusion tensor, a more complete description of diffusion can be achieved (Basser, Mattiello, Le Bihan 1994; Le Bihan et al., 2001)

$$D = \begin{bmatrix} D_{xx} & D_{xy} & D_{xz} \\ D_{yx} & D_{yy} & D_{yz} \\ D_{zx} & D_{zy} & D_{zz} \end{bmatrix} \qquad [20]$$

which describes the water diffusion in 3D and thereby in biological samples provides information about the the favourable directions for water diffusion dictated by fiber structures and membranes as well as the density of the diffusion restricting structures. Diffusion tensor imaging (DTI) is currently applied particularly in research of brain connectivity and neuronal pathway integrity. The sum of the diffusion along the main axes x, y and z is called the trace of the diffusion tensor (de Graaf, Braun, Nicolay 2001; Mori and van Zijl 1995). This divided by three is the average of the diffusion in x. y and z directions can be called the average diffusion $D_{av.}$

$$D_{av} = \frac{1}{3} TraceD = \frac{D_{xx} + D_{yy} + D_{zz}}{3} \qquad [21]$$

The average diffusion provides information about the amount of water (edema for example), mobility of water, turtuosity of the microscopic structures restricting the free diffusion, cellular density and so forth. The average diffusion is not orientation dependent, thus it describes the total diffusion more reliably than any of the individual diffusion directions does, avoiding any errors due to the positioning of the sample.

2.2 Magnetic Resonance Imaging

2.2.1 Image formation and signal localization

Magnetic resonance imaging (MRI) generates 2D or 3D signal intensity images about the object by translating the amplitude, frequency and phase information of the detected FID signal is into information about the signal intensity in the voxel of the signal origin. The fact that the precession frequency of a nucleus linearly depends on the local field strength ($\omega = \gamma B_{eff}$) is the main principle of the signal localization in MRI. The localization is based

on application of linear magnetic field gradients across the imaged sample in the directions of principal axis x, y and z. The gradients linearly alter the magnetic field strength along the direction of application and as a consequence the spins experience location dependent field, and thereby have location dependent ω or change of phase. This property of location dependent effective precession frequency can be used to selectively excite only a certain slice or volume of the sample object. Selective excitation pulses have certain nominal carrier frequency and frequency bandwidth and they can transfer energy only to those nuclei, whose resonance frequency matches the carrier frequency of the excitation pulse (or are within the frequency bandwidth). Thereby, with linear magnetic field gradient across the sample, the excitation pulse flips only the spins within the slice selected by carrier frequency of the pulse, and the slice thickness is dictated by the slope of the field gradient and the pulse bandwidth. The stronger the field gradient the steeper is the change of field strength in adjacent points along the gradient direction and the thinner is the slice excited by the pulse with a certain bandwidth.

The acquired FID is decoded by the mathematical technique called Fourier transform, which converts the signal from the time domain into the frequency domain, that is, reveals the frequency components of the signal. In order to form a 2D or 3D image of the sample a range of field gradient conditions are introduced and arising signals recorded. The waveform information is collected in a 2D or 3D matrix called k-space, where the N different rows of N by M matrix (the vertical encoding) are encoded with different phases (characteristic phase offset) and the M points of each row along the horizontal encoding direction (so called read-direction) are determined by different frequencies. That is, during the read-gradient application the signal is recorded and encoded to a k-space row as a function of time. The third dimension can be encoded by adding a second phase gradient along this third (or slice) direction. The k-space data can be collected in numerous different ways depending on the required speed, resolution and nature of the measurement. Then the Fourier transform is applied to form the image. The data in the center of the k-space define the contrast in image and the edges of k-space determine the fine details, such as sharpness, of the image.

2.2.2 Contrast

One great advance of MRI is that just by small modifications to the measurement technique and parameters several contrasts can be generated that each depend on, and thereby are descriptive of, a variety of tissue properties and molecular interaction phenomena. The contrast can rise from proton density (in the case of hydrogen imaging), relaxation properties of tissue, diffusion environment in the tissue or a variety of other phenomena out of the scope of this thesis. The techniques to sensitize the measurement to T_1, T_2, $T_{1\rho}$ or T_2* relaxation or diffusion are described in chapter 2.1.

2.2.3 Contrast agents

Substances can be divided into categories according to how they interact with magnetic field. Paramagnetic substances enhance the magnetic field locally when placed into a magnetic field. As a response to the external magnetic field paramagnetic material experiences small positive magnetization, that is, it has small positive magnetic susceptibility. This property can be utilized to create contrast in MRI. The magnetic-susceptibility contrast agents cause alterations in to the local magnetic field and the resultant non-homogeneous field has an effect on the local magnetization. Upon administration, the contrast agents locally enhance (with

appropriate selection of imaging parameters) the obtained signal by accelerating the T_1 relaxation.

Iron oxide and gadolinium
Iron oxide particles coated with dextrans or siloxanes are used as a MRI contrast agents both in clinical and experimental settings. When administered intravenously, iron decreases the T_1 time of blood and also enhances the T_2* relaxation. Ultrasmall superparamagnetic iron oxide (USPIO) particles have diameter less that 50 nm. Gadolinium is also a paramagnetic substance and gadolinium compounds in a chelated form (chelated to reduce the toxicity of the metal ion), such as DTPA, are also in routine clinical use. Intravascular contrast agents are mainly used for the evaluating of tissue perfusion, integrity of blood-brain barrier and for the detection of angiogenesis related to tumor growth.

Manganese enhanced MRI
Manganese as free Mn^{2+} ion is paramagnetic. A novel and presently very intensively studied MRI technique, manganese enhanced magnetic resonance imaging (MEMRI), can reveal structural, connectional and also functional alterations at high spatial resolution (Natt et al., 2002; Silva Afonso C. , L.J.H., Aoki Ichio and Koretsky Alan P. 2004; Watanabe et al., 2002; Watanabe, Frahm, Michaelis 2004). Manganese is administered as $MnCl_2$. The manganese shortens T_1 (and to some extent T_2) relaxation times causing a local signal enhancement in T_1 weighted images. Manganese is known to have some neurotoxic effects in higher concentrations but it is in use in animal studies because of the fact that in addition to the paramagnetic property Mn^{2+} is a calcium Ca^{2+} analogue and this enables studies of several biological systems that involve calcium. The free Mn^{2+} ion can bind to similar sites and behave similarly to Ca^{2+} in neurons. Upon neuronal depolarization, i.e an *action potential* event, voltage gated Ca^{2+} channels open and Mn^{2+} can enter cells. Thus MEMRI can provide information about neural activity. After uptake manganese can be transported both anterogradely and retrogradely by axons and it can also pass synapses.

2.3 ^{1}H - Magnetic Resonance Spectroscopy

^{1}H - MR spectroscopy allows the identification and quantification of a large number of biologically important compounds *in vivo*. After its excitation the system emits a set of radiofrequency quanta each characteristic of different nuclei. The acquired FID signal is the superposition of these individual signals, which can be extracted by Fourier transform and plotted as a frequency spectrum. The spectrum presents the amplitude and phase content of the (detectable) frequencies. The real part of a spectrum is the absorption spectrum and the imaginary part is the so-called dispersion spectrum.

2.3.1 Chemical shift and other features of the spectrum

When exciting a certain nuclei, such as hydrogen ^{1}H (which is highly sensitive to NMR due to its high gyromagnetic ratio and high natural abundance), in a simple case the resonating nuclei would induce an FID of plain exponential decay shape and that would produce a spectrum with perfect Lorentzian-line-shape peak at the characteristic frequency. However, in the case of more intriguing true biological samples the collected spectrum contains complex biochemical information and consists of multiple resonance peaks at different frequencies.

The shift in frequency peaks, called chemical shift δ, happens because the nuclei resonate at different frequencies in dissimilar chemical environments. The nuclei can be partially shielded from the magnetic field by the electrons surrounding it. This so called shielding effect can be described as

$$B_\sigma = (1-\sigma)B_0 \qquad [22]$$

where B_σ is the magnetic field that the shielded nucleus experiences and σ is the chemical shield constant depending on the electron density. The chemical shift δ is

$$\delta = \frac{\omega - \omega_{ref}}{\omega_0} * 10^6 \qquad [23]$$

and it quantitatively measures the difference between the resonance frequency of the reference compound and the frequencies that are shifted due to the shielding. This difference is denoted as part per million (ppm). The reference compound at 0.00 ppm by default is the nine equivalent protons of 2,2-dimethyl-2-silapentane-5-sulfonate (DSS).

The spectrum can display further information by its fine splitting of resonances (fine structures or multiplicity). The splitting can arise due to the existence of so-called scalar coupling (referred to also as spin-spin coupling or J-coupling), which arise from interactions through electrons in chemical bonds between two protons in different chemical groups. However, in *in vivo* spectra the spectral resolution is rarely high enough (*i.e.* line width is not narrow enough) to distinguish the fine splitting, but the coupling does have echo time dependent effect on the spectrum trough so-called J-modulation which have to be taken into account in designing (N)MR spectroscopy (MRS) experiments and in data analysis.

2.3.2 Water suppression and spatial localization

In the case of ^{1}H - MRS, water resonance originating from the two protons in a water molecule at about 4.7 ppm is several orders of magnitude larger than the resonances from low concentration metabolites. This can be overcome by water suppression techniques where the frequency selective excitation and dephasing gradient (crusher gradient) are used to selectively destroy the water signal by a magnetic gradient dephasing pulse (CHESS) (Frahm et al., 1989). The idea of the CHESS pulse is that it excites only frequency bandwidth of the pulse in the spectrum, and in a typical *in vivo* water suppression scheme would then consist of 3 to 7 CHESS pulses. An efficient water suppression method derived from CHESS is the use of seven variable power pulses with optimized relaxation delays (so called VAPOR water suppression technique) (Tkac et al., 1999).

Another prerequisite for metabolic detection and good spectrum quality is the accurate spatial localization which excludes the unwanted signals emerging outside the ROI. The choice of a restricted voxel translates into more homogeneous magnetic field within the acquisition voxel as well as more homogeneous tissue within the sample voxel. Benefits are seen as narrower resonances and elimination of large unwanted resonances. In the single voxel spectroscopy the voxel of interest is selected by using a combination of gradients and selective RF-pulses. Stimulated echo acquisition mode (STEAM) is one of the localization methods and it selects the volume element where to acquire the signal from by a pulse sequence utilizing a combination of three orthogonal slice selective 90º pulses [90-TE/2-90-mixing time-90-TE/2-acquisition].

Outer volume (outside of the volume of interest) can be excluded by a method called outer volume suppression where the outer volume is first exited and then dephased by crusher gradients.

2.3.2 ^{1}H-MRS Metabolites detectable at 4.7 T

The field strength and the nuclei of interest determine which metabolites can be detected. The short T_2 prevents the direct observation of several metabolites by traditional spectroscopy methods. The spectral resolution is limited by the chemical shift range which is only 5 ppm for non-exchangeable protons. In this range many of the metabolic resonances overlap hindering their separate quantification. In the optimal cases of *in vivo* ^{1}H spectroscopy (high magnetic field with short TE acquisition) up to 20 brain metabolites can be simultaneously obtained (Mlynarik et al., 2008; Tkac et al., 1999). The most important metabolites of the central nervous system (CNS) studied by *in vivo* ^{1}H-MRS are listed here.

N-acetyl aspartate (NAA) gives rise to one the most prominent resonance in ^{1}H-MRS at 2.01 ppm and the NAA concentration in the normal adult human brain is 7.5-17.0 mmol/L. NAA is often used as a marker of neuronal density. However, the NAA concentration differs among neuron types (Simmons, Frondoza, Coyle 1991), increases during development (van der Knaap et al., 1990), and has been reported to change dynamically, suggesting that NAA levels may also reflect neuronal function / dysfunction rather than simply neuronal number. The fact that NAA levels have been reported to recover after reversible ischemia (Brulatout et al., 1996) and brain injury (De Stefano, Matthews, Arnold 1995) and show reduction even in the absence of neuronal loss in multiple sclerosis (Tsai and Coyle 1995) support this suggestion.
N-acetyl aspartate glutamate (NAAG) is a source of glutamate and is thought to have a role in excitatory neurotransmission. NAAG resonates at 2.04 (the largest resonance) and is therefore difficult to distinguish from NAA at 2.01 ppm. The combined peak of NAA+NAAG provides, however, a good estimate of NAA containing compounds. NAAG concentration in the normal adult human brain is 0.5-2.5 mmol/L.

Creatine (Cr) and phosphocreatine (PCr) are the next prominent resonances at 3.03 and 3.93 ppm, respectively. Together they are referred to as total creatine (tCr). They are present both in neuronal and glial cells, and have an important role in the energy metabolism (Wallimann et al., 1992). The total creatine is often used as an internal concentration reference in spectroscopy since its concentration is relatively constant across ages and in several diseases. However, creatine has been found to decrease in the chronic phases of some pathologies, such as stroke (Federico et al., 1994; Fenstermacher and Narayana 1990) and tumors (Okunieff et al., 1986; Stubbs et al., 1990), and in Huntington's disease evident reduction in the creatine level can be seen already in the presymptomatic phase (Sanchez-Pernaute et al., 1999; Tkac et al., 2001). Creatine concentration in the normal adult human brain is 4.5-10.5 mmol/L and phosphocreatine 3.0-5.5 mmol/L.

Choline containing compounds (free choline, glycerophosphorylcholine and phosphorylcholine) sum up to total Choline (tCho), which is one of the most evident resonances in ^{1}H-MRS besides NAA and Cr compounds. The choline resonates at 3.2 ppm. Choline reflects membrane turnover since it is involved in phospholipid synthesis pathways and degradation. Choline concentration is found to be increased in multiple sclerosis (Narayana 2005), cancer (Gillies and Morse 2005) and Alzheimer's disease (Firbank, Harrison, O'Brien 2002), and decreased in stroke (Malisza, Kozlowski, Peeling 1998). Choline (tCho) concentration in the normal adult human brain is 0.5-2.5 mmol/L

Glutamate (Glu) has multiple roles in brain biochemistry. It is a nonessential amino acid and important excitatory neurotransmitter (Erecinska and Silver 1990) as well as precursor for another neurotransmitter GABA. Glutamate also is involved in the synthesis of other metabolites and large peptides and proteins (Erecinska and Silver 1990). Glutamate is present in all cells but at highest amount in glutamanergic neurons and a smaller concentration in astroglia and GABAergic neurons. Glutamate has multiple resonances at 3.75 and between 2.04-2.35 ppm. Glutamate is transformed (by glutamine synthase) into glutamine (Gln) in the glutamate-glutamine neurotransmitter cycle. Glutamine structure is thereby very close to glutamate structure with similar chemical shift and scalar coupling features causing the resonances to be similar as well (distinguishable only in higher fields). Glutamate concentration in the normal adult human brain is 6.0-12.5 mmol/L and glutamine 3.0-6.0 mmol/L (glutamine resonances are 3.76, 2.12, 2.46, 6.82 and 7.53). Glutamine is primarily present in astroglia, it has essential role in intermediary metabolism and its main function is ammonia detoxification.

γ-aminobutyric acid (GABA) is an inhibitory neurotransmitter (in mature brain). Altered concentrations of GABA have been associated with several neurological disorders such as epilepsy (Petroff et al., 2001), depression (Sanacora et al., 1999; Sanacora et al., 2004) and panic-disorder (Goddard et al., 2001). Antiepileptic drugs (for example vigabatrin) have been developed to increase GABA level. GABA has three resonances (1.89, 2.28 and 3.01 ppm) which overlap with other metabolites and (at 4.7 T field) the spectral editing methods are needed to detect GABA. GABA concentration in the normal adult human brain is 1.0-2.0 mmol/L.

Myo-inosotol (Ins) is a cyclic sugar alcohol including six NMR detectable protons. The resonances are located at 3.52, 3.61, 3.27, 4.05 ppm. Myo-inosotol concentration in the normal adult human brain is 4.0-9.0 mmol/L but its exact role is unknown. It has been thought to be a glial marker (Brand, Richter-Landsberg, Leibfritz 1993), but it has been found in neurons as well (Godfrey et al., 1982; Sherman et al., 1977). Changes in the Myo-inosotol concentrations have been reported in mild cognitive impairment, Alzheimer's disease and after brain injury (Ross et al., 1998).

Lactate (Lac) concentration in the normal adult human brain is only 0.2-1.0 mmol/L, however in pathologies such as stroke, hypoxia and tumors, where the blood supply, and thereby the oxygen supply, is impaired so lactate is greatly increased. This is because lactate is an end product of anaerobic glycolysis. Transient increases in lactate levels can also be linked to functional activation (Prichard et al., 1991). Lactate resonances are at 1.31 and 4.10 ppm.

Macromolecule resonances affect the observed signal by underlying the metabolite resonances and greating superimposition effect on the spectrum (Behar and Ogino 1993; Kauppinen, Kokko, Williams 1992; Kauppinen et al., 1993). Macromolecules give rise to at least 10 characteristic resonances (between 0.93 and 4.3 ppm) associated to methyl and methylene resonances of protein amino acids. Macromolecules have much faster T_1 and T_2 relaxation rates that the metabolites, and that feature can be utilized to either emphasize or eliminate the macromolecular signal. Alterations in the spectrum of macromolecules have been reported in stroke (Graham et al., 2001) and tumors (Howe et al., 2003).

Taurine (Tau) is a nonessential amino acid, but it is mostly obtained from food. The function of taurine is partially unknown, but it has osmoregulatory role and it modulates the

neurotransmitter action. Taurine concentrations differ between brain regions but it is present in all cells in CNS. Taurine levels decrease by age and the concentration in normal adult human brain is 2.0-6.0 mmol/L. Taurine resonances are at 3.21, 3.25 and 3.42 ppm.

Metabolite concentrations in the rat brain are very close to the above mentioned concentrations for humans. The concentration values are taken from a recent book of Robin de Graaf (de Graaf 2007).

2.4 Imaging of epileptogenesis and epilepsy

2.4.1 Epilepsy

Epilepsies are a neurological disorders affecting about 1-2% of people worldwide. Epilepsy is defined as a central nervous system disorder where excessive or abnormal neuronal activity causes the subject to experience recurrent seizures (Engel 1989). Epilepsies are classified according to the etiology as *idiopathic* or *symptomatic*, where idiopathic refers to epilepsy without any predisposing pathology or incident, and symptomatic refers to epilepsy developed as a consequence of such predisposing disorder or incident.

Temporal lobe epilepsy (TLE) is the most common of the symptomatic epilepsies (Engel 1996). In TLE the seizures arise from structures of thehippocampus, subicular complex, amygdala, entorhinal cortex, perirhinal cortex, parahippocampal cortex and lateral cortex (Squire and Zola-Morgan 1991). TLE can develop as a sequel from pathologies like stroke, febrile seizures, brain infections, brain tumor, head trauma or *status epilepticus* (SE). SE is a life-threatening situation of prolonged seizure or repeated seizures (for over 30 minutes without full recovery of consciousness in between, Waterhouse, 2001). In TLE there is a latent period after the initial insult and before the occurrence of the spontaneous seizures. This latent period is called *epileptogenesis* and it can last from weeks to several years. During epileptogenesis several neurobiological processes take place, such as neurodegeneration, gliosis, neurogenesis, angiogenesis, alterations in the extracellular matrix, and molecular changes in cellular membranes (Jutila et al., 2002). Particularly the hippocampus has been well documented (both in human patients and more extensively in experimental models) to suffer from early pyramidal neuron cell loss in the CA1 and CA3 sub regions of hippocampus proper and pyramidal and granule cell dispersion as well as marked loss of hilar neurons (including hilar mossy cells and neurons containing somatostatin and neuropeptide Y)(Babb et al., 1992; Houser 1990; Mathern et al., 1993; Mello et al., 1992; Mello et al., 1993). Loss of hippocampal hilar cells may be one cause for the seizure activity in the dentate gyrus since hilar mossy cells normally excite neurons that mediate granule cell inhibition (Sloviter 1994).

Another potential cause of seizures is neuronal plasticity, manifested as axonal sprouting and thereby circuitry reorganization, which is known to occur during epileptogenesis. *Mossy fiber sprouting* is abnormal axonal sprouting from the granule cell layer of the dentate gyrus into the inner molecular layer and it has been reported both in human epilepsy patients, in tissue samples of operated drug-refractory patients (Houser et al., 1990; Isokawa et al., 1993; Mathern et al., 1994; Sutula et al., 1989), and in experimental models (Nissinen et al., 2000a; Pitkanen et al., 1999; Pitkanen et al., 2000; Tauck and Nadler 1985a; Wenzel et al., 2000). In animal models, mossy fiber sprouting has been shown to occur before the spontaneous seizures start (Nissinen, Lukasiuk, Pitkanen 2001).

2.4.2 MRI findings in epilepsy patients and in experimental models of epilepsy

MRI imaging is used in epilepsy patients mainly when trying to find an underlying cause for the seizures and thereafter to guide the possible surgical treatment. The structural MR imaging techniques in the clinic aim to detect lesions, tumors or signs of brain infections, and the volumetric atrophy of epilepsy related brain structures. Functional MRI is used prior to epilepsy surgery to identify the regions the surgeon needs to avoid, or to identify the abnormal activation patterns.

In experimental models for epilepsy the scale of the MRI methods are used on a wider scale. The studies have concentrated on lesion size and distribution, and also quantification of the volumetric atrophy of related brain structures using volumetric methods together with T_2 and diffusion contrasts (Grohn and Pitkanen 2007). The findings can be divided into the edematic alterations during the first few days after the induced seizures and the delayed tissue changes and atrophy during the epileptogenesis. The reports include acute diffusion decrease due to cytotoxic edema caused by seizures (Zhong et al., 1995), increased T_2 weighted signal intensity (King et al., 1991) and increased T_2 (Dube et al., 2004) due to the vasogenic edema during the following days. Thereafter the delayed diffusion increase (Tokumitsu et al., 1997), secondary delayed T_2 increase (Roch et al., 2002b) the enlargement of ventricle and cortical atrophy (Nairismagi et al., 2004) and the detection of mossy fiber sprouting by MEMRI (Nairismagi et al., 2006b) are the major epileptogenesis related findings. Furthermore, the T_2 hyperintensity 24 hours after status epilepticus in the piriform and entorhinal cortices has been found to have predictive value for the development of temporal lobe epilepsy in the lithium-pilocarpine rat model (Roch et al., 2002a).

2.4.3 MRS findings in epilepsy patients and in experimental models of epilepsy

Metabolic changes during epileptogenesis and particularly in the chronic epilepsy phase are one important focus of research since the ultimate underlying cause of epileptic seizures is an imbalance between inhibitory and excitatory functions. The mediators of these functions could potentially be detected by MRS. MRS can also detect the neurodegenerative and inflammatory processes that histologic studies have reported to take place (Hammen et al., 2003). In epilepsy patients decreased levels of NAA have been reported reflecting both decreased neuronal number and transiently disturbed neurometabolism by the insult (Connelly et al., 1994; Simister et al., 2008). Creatine and choline levels have found to be increased in the hemisphere ipsilateral to the seizure focus in TLE patients suggesting reactive astrocytosis ((Connelly et al., 1994). Also other disturbances in glutamate-glutamine metabolism, especially in the levels of glutamate (which is one major exitatory neurotransmitter), are common feature in epilepsy (Simister et al., 2003a). The inhibitory neurotransmitter GABA is found to be decreased in epilepsy (Simister et al., 2003b), however in immature brain GABA functions as an excitatory neurotransmitter and increased levels at this developmental stage may in turn promote seizures (Ben-Ari and Holmes 2005). In experimental models, decreased NAA and creatine levels in the ipsilateral hippocampus have been reported 3 - 84 days after kainic acid induced epileptogenesis (Tokumitsu et al., 1997). Lactate levels have been found to increase as a consequence of seizures, presumably since lactate is the product of anaerobic glycolysis (Petroff et al., 1986).

2.4.5 MEMRI findings in experimental studies of epilepsy and brain activation

MEMRI has been recently widely used in research into neuronal connections. In the context of epilepsy it has been shown that intracerebral injection of $MnCl_2$ into the entorhinal cortex results in Mn^{2+} transport via the perforant pathway to granule cell dendritic regions, and from there to the mossy fibers that thereby become labelled (Nairismagi et al., 2006a). Animal studies report that Mn^{2+} can enter the hippocampus also after systemic administration with intact blood-brain barrier (BBB) (Kuo et al., 2005; Lee et al., 2005). This approach is used mainly to visualize the whole neuroarchitecture, since the transfer of manganese into the brain through choroid plexus and ventricular system is slow (optimal contrast after about 22 hours) and non-specific to any neural circuit (as compared to the activity induced uptake).

One way of manganese to reach the brain is by circumventing the BBB. This can be done by nostril injections, which have been used in mice to study olfactory activation (Pautler and Koretsky 2002). Nostril injections and administration into the eye are two examples of *activity induced tract tracing* techniques with Mn. Another option is to induce trancient opening of the BBB by an osmotic challenge (Aoki et al. 2002). Manganese administration directly into the brain parenchym have been used to stydy the projections from that target area (Van der Linden et al., 2004a; Soria et al., 2008). Upon combining with specific stimulus this becomes again activity induced tract tracing and it is used to show cerebral activation patterns. Recent studies show that even without breaking the BBB, Mn^{2+} uptake after systemic administration can be promoted by inducing brain activation, such as hypothalamic activation due to fasting (Kuo et al., 2006) or by persistent exposure to acoustic stimuli (Watanabe, Frahm, Michaelis 2008). In the latter case a combination of activating the region of interest to promote the manganese uptake from extracellular fluid, and thereafter activity induced tract tracing were used to highlight the stimulated pathways.

The transport of manganese across the BBB and its subsequent transport in the extracellular space, inside the cells and across synapses are not fully understood and manganese can have neurotoxic effects (Aschner and Aschner, 1991). Therefore manganese contrast enhanced MRI techniques are non-transferable to clinical trials. However, for the purposes of experimental studies $MnCl_2$ has variety of uses, and the toxic effects have been found negligible or absent when administrating doses low enough. Even with repeated administration directly into the somatosensory cortex, lesioning, astrogliosis, functional impairment and distress can be avoided (Soria et al. 2008).

2.5 Imaging of Traumatic Brain Injury

2.5.1 Traumatic Brain Injury

Traumatic brain injury is one of the underlying etiologies of epilepsy development. According to epidemiologic studies approximately 53% of patients with penetrating head injury develop epilepsy later in life (Salazar et al., 1985). Even without the epileptic seizures TBI itself is a devastating disease with variety of cognitive and motor function deficits manifesting both immediately after the impact and even several years later. According to data from Center for Disease Control (Traumatic Brain Injury in the United States: A Report to Congress) on average every 21 seconds one person in the USA sustains a traumatic brain injury. Two recent large reviews of TBI epidemiology in Europe show that the long-term outcome and the level of disability among patients are mixed and inconsistent (Leon-Carrion et al., 2005b; Tagliaferri et al., 2006).

The mechanisms of TBI are largely unknown. The primary damage is caused by the shear forces of the impact itself, which initiates ionic, molecular, and cellular alterations within seconds (Dietrich, Alonso, Halley 1994a; McIntosh 1994; Rink et al., 1995) followed by immediate cytotoxic edema and later vasogenic edema (Faden et al., 1989; Katayama et al., 1990). Thereafter the secondary injury begins to develop and continues to worsen for days to months, or even years. The secondary injury cascades are composed of a complex combination of molecular, cellular (Karhunen et al., 2005), and metabolic (Kharatishvili et al., 2006b) alterations. Finally, these cascades lead to functional disabilities including somatomotor impairment, cognitive decline, emotional disturbance, or epilepsy (Kharatishvili et al., 2006b; Thompson et al., 2006).

Histological studies have verified the robust cellular loss and cavity formation in the primary cortical contusion site during the first weeks post-injury (Bramlett et al., 1997; Pierce et al., 1998; Smith et al., 1997). The degeneration has found to be selective to cell types and brain regions (Conti et al., 1998; Cortez, McIntosh, Noble 1989a; Hallam et al., 2004; Raghupathi et al., 2002; Rink et al., 1995; Sato et al., 2001) and it has been demonstrated to go on up to 1 year (Bramlett et al., 1997; Pierce et al., 1998; Smith et al., 1997). Histological studies of TBI report also chronic inflammation, glial hypertrophy, and axonal injury (Lenzlinger et al., 2001; Morganti-Kossmann et al., 2002; Philips et al., 2001; Soares et al., 1995; Toulmond and Rothwell 1995).

2.5.2 MRI findings in humans and experimental models

In patients, intracerebral hemorrhage (Caroli et al., 2001; Kurth, Bigler, Blatter 1994; Morais et al., 2008; Scheid et al., 2007), lesion and edema formation in the acute phase are common clinical MRI findings. Axonal damage following TBI has been frequently detected using diffusion tensor imaging (DTI) and the changes in the diffusion anisotropy have been reported in both acute and chronic TBI patients (Sidaros et al., 2008).

In experimental studies MRI findings resemble the clinical findings, but most of the experimental MRI studies of TBI have focused only on the time period extending from hours to days or a few weeks post-injury. MRI alterations associated with edema and hemorrhage have been reported (Graham et al., 2000b; Iwamoto et al., 1997) and axonal damage has been linked to changes in diffusion MRI (Mac Donald et al., 2007). TBI studies in rats have described T_2 hyperintensity (edema related, neuronal loss related or a consequence of tissue atrophy and partial volume effect) and decreased apparent water diffusion (ADC) acutely (<24 hours) after TBI followed by increased diffusion days or weeks after TBI (Albensi et al., 2000; Obenaus et al., 2007; Onyszchuk et al., 2007; Van Putten et al., 2005; Vink et al., 2001). The hippocampal T_2 relaxation time has been reported to decline in mild fluid percussion injury and increase in controlled cortical impact during 7 days post TBI (Obenaus et al., 2007). A 3 month follow-up showed enlarged ventricles, cisterns and that the necrotic tissue in the primary contusion site was absorbed and replaced by cerebrospinal fluid (Iwamoto et al., 1997).

2.5.3 Hemodynamic disturbances in both human and experimental TBI

In severely brain injured patients also the cerebral autoregulation has been found to be impaired (Bouma and Muizelaar 1990; Golding, Robertson, Bryan 1999; Overgaard and Tweed 1974). Three distinct cerebral hemodynamic phases in severe head trauma patients have been recognized based on cerebral blood flow (CBF) changes (Martin et al., 1997):

hypoperfusion (decreased CBF during the day of the injury), hyperemia (i.e. the increased amount of blood in the tissue / tissue vasculature during the next 3 days), and vasospasm (including fall in the CBF, lasting the next two weeks). CBV reduction has been reported in sub acute phase following severe traumatic brain injury (Marmarou et al., 2000). Decreased CBF acutely after impact has been documented (Kelly et al., 1996; Kelly et al., 1997; Martin et al., 1997). Even patients with symptomatic mild traumatic brain injury but without any other abnormal MRI findings have shown persistent regional hypoperfusion (Bonne et al., 2003). In the primary contusion site there is often hemorrhagic focus of necrosis, blood-brain barrier (BBB) disruption, vasogenic edema and decrease in regional blood flow (Graham et al., 2000a). There are also recovery processes, such as angiogenesis known to take place in the later post-injury phase (Dunn et al., 2004).

Hemodynamic disturbances have been found also in experimental models of TBI. Cerebral blood volume (CBV) and flow has been found to decrease 3 - 4 hours post-injury in the rat model of closed head injury (Prat 1997; (Thomale et al., 2002)). Local CBF has been found to decrease 15 minutes post-injury and remain decreased up to 4 hours in LFP rat models (Ginsberg et al., 1997; Muir, Boerschel, Ellis 1992; Ozawa et al., 1991). In experimental models transient hypoperfusion has also been detected in the contralateral hemisphere (Pasco et al., 2007). Perfusion deficits after impact can lead to local ***ischemic state of the tissue*** where the oxygen and glucose delivery is so severely impaired that it causes disturbances in energy metabolism and mitochondrial function. This has been studied in the fluid percussion TBI model by Dietrich and collaborators who report severe ischemia (i.e., mean local CBF < 0.25 ml/g/min) after severe TBI within lateral parietal cortex, moderate reductions in CBF throughout the traumatized hemisphere, including the frontal and occipital cortices, hippocampus, thalamus, and striatum and milder decreases in CBF also throughout the contralateral cerebral cortex. In histological studies they also report subarachnoid hemorrhage, blood-brain barrier (BBB) breakdown overlying the pial surface and superficial cortical layers of the injured hemisphere, focal leakage at the gray-white interface of the lateral cortex, petechial hemorrhages associated with small venules and focal platelet accumulation. (Dietrich et al., 1994; Dietrich, Alonso, Halley 1994b; Dietrich et al., 1998).

Impact may locally generate contusional damage to the vasculature, blood clots causing occlusions or other conditions where the blood supply to tissue is seized or hindered. The thresholds for tissue perfusion reductions and adjacent cellular consequences are common for both TBI and ischemia. In cerebral ischemia the tissue in the core region suffers the irreversible damage when the perfusion drops below threshold level of around <10-15 ml/100 g/min, corresponding to the anoxic cell depolarization (Hossmann and Schuier 1980), and is not restored immediately. The hemodynamically compromised surrounding region with reduced tissue perfusion is called the ischemic penumbra. Tissue with impaired perfusion suffers from protein synthesis inhibition [cerebral blood flow (CBF) 35-55 ml/100g/min] and impairment of glucose metabolism [CBF 22-35 ml/100g/min] which causes anaerobic glycolysis, adjacent build up of lactate and acidosis (Allen et al., 1993; Obrenovitch et al., 1988). The functional impairment, cessation of evoked potentials and electroencephalographic (EEG) activity, follows marked reduction in adenosine triphosphate (ATP) [CBF <20 ml/100g/min]. Ischemic penumbra is defined as the CBF region between the functional impairment and the anoxic depolarisation [CBF: 10-15 ml/100g/min < penumbra < 20 ml/100g/min] and it is thought to be salvageable if the blood supply is restored in time. The aforementioned perfusion thresholds are approximate and the factors such as the variability between species and measurement techniques should be considered in each case (Baron 2001; Takasawa et al., 2008). Regarding the state of the tissue the perfusion

findings are complemented by data from diffusion studies. Diffusion is found to reduce about 40-50% hours after severe focal ischaemia in experimental models, thereafter pseudo-normalization of values is observed followed by a gradual secondary increase (Hoehn-Berlage et al., 1995). Chronically increased values coincide with cell death, gliosis and cyst formation (Garcia et al., 1995; Takahashi et al., 1993). Acute diffusion decrease is indicating the region of ischaemic core and the region of reduced perfusion extends further including the penumbra (Baird et al., 1997; Finelli et al., 1992; Pierce et al., 1997; Roberts et al., 1993; Sorensen et al., 1996). The shifting of water between intra- and extracellular space is observed both in the initial phase of perfusion disturbances due to anaerobic glycolysis (the anaerobic glycolysis elevates intracellular osmolarity and thereby leads to influx of water from extracellular space), and later after the anoxic cell depolarization and failure of the function of ion pumps leading to cytotoxic edema in the severely impaired core region. This shift of water between compartments causes the observed diffusion to decrease because of the influx of water from extracellular space to more diffusion restricting intracellular space. The destructive signalling cascades (triggered by intracellular calcium and neurotransmitters) launched at the time of cytotoxic edema lead to the development of secondary damage. In the experimental models of ischemic stroke the final lesion volume detected by diffusion imaging has been reached within 24 hours (Minematsu et al., 1992b), and in the case of restored blood flow (early reperfusion) the lesion size is decreased as compared to the situation with permanent occlusion (Minematsu et al., 1992a; Mintorovitch et al., 1991). While in traumatic brain injury the lesion development and expansion is slower continuing up to several months, and is therefore most likely mediated by different cellular cascades. Also, the oedema formation after traumatic brain injury is most likely much more complex than after ischemia, and the origins of oedema after impact can include free oxygen radicals etc. Thus one consequence of traumatic impact has been shown to be local ischemia which causes disturbances in brain metabolism and functionality, but the role of perfusion and blood supply deficits in head injury mechanisms are largely unknown.

2.5.4 MRS findings in humans and experimental models

Nuclear magnetic resonance spectroscopy (MRS) has been used to assess metabolite changes during the acute and sub acute phases after TBI, but there are no thorough long-term studies available on chronic metabolic profile after TBI. The acute and sub acute studies have reported a decrease in N-acetylaspartate/creatine ratio (NAA/Cr) and an increase in choline/creatine (Cho/Cr) ratio in the lesion area and/or in the ipsilateral parietal cortex in rodents that have experienced fluid percussion injury or controlled cortical impact injury (Berry et al., 1986; Choi et al., 2005; Schuhmann et al., 2002). Also, in the pericontusional zone Cr+PCr, NAA, and Glu have found to be decreased from 1 hour to 28 days post-injury (Dube et al., 2001) and persistently continue to decrease in the combined hippocampus basal ganglia region up to 4 weeks after trauma (Schuhmann et al., 2002). These studies suggest that tissue damage in the hippocampus and pericontusional cortex may share similarities in their MRS signature. Importantly, the metabolic changes found in experimental models resemble the metabolic changes found in TBI patients (Ashwal et al., 2004; Shutter et al., 2006).

2.5.5 Prediction of the outcome based on MRI findings

In clinical studies the intracranial and intracerebral hemorrhage has been found to be associated with poor long-term outcome, as assessed with the Glasgow Outcome Scale (Chieregato et al., 2005). Correlation between increased diffusivity of white matter structures

and later impairment of learning and memory functions have also been reported (Salmond et al., 2006; Sidaros et al., 2008). In the case of mild TBI (MTBI; Glasgow coma score > 13) there are only weak associations with the outcome found to date and the only quantitative correlations are related to the diffuse axonal injury. The lowered magnetization transfer ratio in the corpus callosum and abnormal fractional anisotropy values obtained by diffusion tensor imaging also in other white matter tracts reveal diffuse axonal injury which correlates with cognitive recovery in MTBI (Belanger et al., 2007). In a recent review Metting and collagues listed the early MRI findings that had displayed predictive value for the chronic outcome in mild-to-moderate head injury (defined by having Glasgow coma score > 8) (Metting et al., 2007). The list included the number of lesions (detected by T_2* weighted gradient echo technique), lesion size, perfusion abnormalities, reduced cerebral blood volume and lowered N-acetyl aspartate/creatine ratio observed days to weeks (< 3 weeks) post-injury. These findings could be linked to the outcome 3 to 12 moths later. In moderate-to-severe TBI the metabolic abnormalities detected by magnetic resonance spectroscopy (MRS), such as decreased level of N-acetyl aspartate, increased level of choline containing compounds, and increased level of lactate, have been found to correlate with functional outcome measured 1-2 months after TBI (Garnett et al., 2000; Marino et al., 2007; Signoretti et al., 2008). Acute diffusion drop 3 hours post lateral fluid percussion injury has been recently reported to have predictive value for seizure susceptibility one year later (Kharatishvili et al., 2007). However, overall the MRI findings and their correlations with outcome have been inconsistent. Recent reviews emphasized the need for predictive markers (Belanger et al., 2007; Catroppa et al., 2008; Gallagher, Hutchinson, Pickard 2007; Lewine et al., 2007; Metting et al., 2007).

3 Aims of the study

In the research projects presented in this thesis work a variety of NMR techniques were used to study the complex pathophysiology of epileptogenesis and traumatic brain injury. The dual goal was to study the nature and characteristics of these progressive pathologies, and to find out the potential of different NMR techniques and their combination to function as diagnostic and prognostic tools in these diseases.

To be able to meet these goals each step of these pathologies was followed. Several different advanced MRI techniques were used to target the different destructive and/or recovery processes in the brain.

A crucial question was *how did the observed MRI changes correlate with the functionality*? Did the abnormal MRI findings reveal the functional impairment? The functionality was evaluated with different carefully conducted behavioural tests. Another question was *what were the true histopathological changes underlying the MRI findings*? To characterize the complex cellular phenomena: degeneration of neurons, proliferation of glia, axonal plasticity etc. several histological stainings were conducted.

Different experimental models were chosen to provide novel information about the spatio-temporal progression of these devastating diseases and the unique features of each model were utilized to mimic different aspects of brain changes. The transferability of the techniques to the clinics was considered as an important starting point for the studies, and besides the MEMRI, all the presented 'tools' can be relatively easily integrated to the clinical use.

The major questions addressed in this thesis work were divided among the four studies as follows:

First, can MEMRI detect the axonal sprouting in the epileptogenic hippocampus and can it therefore function as a surrogate marker in the epileptogenic and epileptic animals?

Secondly, how does the tissue damage in different brain regions differ after traumatic brain injury, and how long and at what rate do the brain alterations progress?

Thirdly, can the early MRI findings predict the long term outcome, final extent of the atrophy, functional outcome and the severity of the final histopathology?

Fourth, how does the CBV change in different brain regions in acute and sub acute phases after traumatic brain injury, and do the changes correlate with the motor performance?

4 Materials and Methods

4.1 Animal models

When studying neuronal diseases animal models are needed because they provide homogenous populations, allow frequent follow-up of the complex and slow disease development and the outcome, and most importantly, allow complete analysis of cellular level changes by histological methods. This is crucial when aiming to understand the mechanisms and thereafter develop treatments. There are several models available for epilepsy that all characterize different etiologies and different aspects of the disease. In this thesis work three different animal models were used. For the MEMRI project **I** the rat model of kainic acid induced status epilepticus was chosen because in that model the epilepsy develops within two months and all the cellular processes along with the mossy fiber sprouting are well characterized and very pronounced already at the 2 months time point. For the long-term MRI follow up of TBI (study **II**) and study **III** searching predictive factors for the long-term outcome, a rat model of lateral fluid percussion (LFP) induced TBI was chosen because it is the most widely used and best characterized animal model for closed head injury in humans. For the last study **IV** assessing the CBV changes during 2 weeks after TBI another model for TBI, namely the controlled cortical impact injury model (CCI), was chosen.

All animal procedures were approved by the Animal Care and Use Committee of the University of Kuopio, and all procedures were conducted in accordance with the guidelines set by the European Community Council Directives 86/609/EEC. The rats were housed in individual cages and kept under controlled laboratory conditions (*ad libitum* access to food and water,12 hours-12 hours light-dark cycle with lights on at 07:00 a.m., temperature 22 ± 1°C, air humidity 50-60%,).

4.1.1 Kainic acid induced epilepsy

To induce epileptogenesis a generalized seizure called *status epilepticus* (SE) was inflicted to adult male Wistar rats (n=27, weight 305-355 g, University of Kuopio, National Laboratory Animal Center, Finland). The rats were treated with kainic acid (KA, Sigma-Aldrich, St. Louis, USA, 10 mg/kg, i.p.), which induced SE. After the kainate administration the development of behavioural seizure activity was observed. Rats were considered to experience SE if they expressed continuous generalized seizure activity for 30 minutes (this could be a series of consecutive seizures without full recovery in between). The beginning of SE was defined as the time point when the animals expressed their first Class 3 seizure on Racine's scale (Racine 1972). About two hours after the beginning of SE, that is three hours after the KA injection, the seizure activity was suppressed by halothane (and the animals were imaged under halothane anesthesia).

4.1.2 Lateral fluid percussion induced TBI

The lateral fluid-percussion (LFP) brain injury was induced as previously described (Kharatishvili et al., 2006a; McIntosh et al., 1989) to adult male Harlan Sprague Dawley rats (total n=48 for TBI animals, of which 34 survived the operation, weight 305-390 g; Harlan Netherlands B.V., Horst, the Netherlands). Identical anesthetic and surgical operation without the fluid percussion impact was performed on the control animals (i.e. the sham-operated animals, n=15). A mixture containing sodium pentobarbital (58 mg/kg), chloral hydrate (60 mg/kg), magnesium sulfate (127.2 mg/kg), propylene glycol (42.8%), and absolute ethanol

(11.6%), (i.p., 6 ml/kg) was used as anesthetic. A 5 mm diameter craniectomy was drilled with a trephine between bregma and lambda on the left convexity (anterior edge 2.0 mm posterior to the bregma; lateral edge adjacent to the left lateral ridge). The temperature was monitored by rectal probe and maintained at 37.5±1.0°C using a homeothermic blanket system. The impact injury was induced by a brief (21-23 ms) transient pressure fluid pulse against the exposed dura using a fluid percussion device (AmScien Instruments, Richmond, Virginia, USA). The pressure of the impact was adjusted to 2.6-3.3 atm and measured by a transducer extracranially. The visual inspection was made to verify that the dura remained intact.

4.1.3 Controlled cortical Impact injury induced TBI

A controlled cortical impact injury (CCI) was induced to 61 adult male Sprague-Dawley rats weighting 250-350 g while 12 rats served as sham-operated controls (total n=73, Charles River Laboratories, Sulzfeld, Germany). In CCI the pressure impact is delivered similarly via craniectomy, but now with mechanical tip. The CCI was first described in the ferret (Lighthall JW.1988), and later adapted for use in the rat (Dixon et al., 1991). In the study **IV** the unilateral TBI was induced as follows. Rats were anesthetized with halothane (1% halothane in 30/70 O_2/N_2) rats were placed in a stereotaxic frame. Craniectomy of 6 mm in diameter was performed unilaterally in the midway between the bregma and the lambda (1 mm lateral to the midline). The dura was kept intact and care was taken not to cause any injury to vascular structures. The rectal temperature was maintained at 37.0±1.5°C by a homeothermic blanket system. Controlled cortical pneumatic impact (CCI) device (AmScien Instruments, Richmond, VA) was used to induce severe grade traumatic brain injury. This device has a 5-mm-diameter tip travelling at a velocity of 3 m/s which created a 2.0-mm-deep deformation when it entered the brain for 50 ms. After delivering the impact the exposed cortex was covered with the previously removed piece of skull and sealed with Spongostan™, and the wound was closed and disinfected.

4.2 NMR Methods

4.2.1 Hardware

The NMR measurements in this thesis work were all performed using a horizontal 4.7 T magnet (Magnex Scientific Ltd, Abington, UK) with actively shielded imaging gradients (Magnex) interfaced to a Varian (Palo Alto, CA) UNITYINOVA console. The transmitter/receiver system was either a quadrature half volume RF coil (diameter 28 mm, HF Imaging LLC, Minneapolis, MN) (studies **I,II** and **III**) or an actively decoupled volume transmission coil and quadrature surface receiver coil (Rapid Biomedical, Germany), in study **IV**. All analysis was performed using an in-house written program in Matlab 7.1 (MathWorks, Natick, MA).

4.2.2 Study designs, MRI protocols and data analysis

4.2.2.1 Study design and MRI protocol in MEMRI study (I)

The MEMRI study was designed to answer two major questions. Does the epileptiform activity affect the manganese accumulation after systemic manganese administration? And how do the structural cellular level changes, particularly the axonal sprouting, affect the observed MEMRI signal? The study is outlined in Fig. 1, in **I**. Briefly, the total number of 38 rats in the MEMRI study were divided into five experimental groups. Group 1 (n=11) was the main group of interest including rats receiving both KA (that is, epileptogenic and later epileptic rats) and the manganese contrast agent. The imaging of Group 1 acutely after KA administration was performed to address a the question whether the generalized seizure (now SE) related neuronal activity affects Mn^{2+} accumulation. First $MnCl_2$ (45 mg/kg in 0.1 M bicine buffer, pH 7.4) was administered intraperitoneally (i.p.). After 12 hours Mn^{2+} had already reached the hippocampus and Mn^{2+} accumulation was still ongoing (Lee et al., 2005). At this point rats were treated with kainate (KA, Sigma-Aldrich, St. Louis, USA, 10 mg/kg, i.p.) which induced SE. Development of behavioural seizure activity was allowed to continue for three hours (actual status therefore lasted about 2 hours) and then animals were anesthetised for MRI by halothane (1 % halothane in 7:3 mixture of N_2O:O_2). MRI data were assessed 3 and 25 hours after KA injection (*i.e.*, 15 and 37 h after $MnCl_2$ injection). The same Group 1 was imaged also 2 months later to address the second major question and investigate the association of Mn^{2+} accumulation with chronic structural neuropathologic changes, particularly neurodegeneration, astrocytosis, microgliosis, and sprouting of granule cell axons (mossy fibers). This chronic time point MRI was performed before and 24 hours after systemic $MnCl_2$ injection. Thereafter, animals were implanted with electrodes to detect spontaneous seizures using video-EEG monitoring, and finally, they were intracardially perfused for histology. Groups 2 and 3 were control groups for Group 1. Group 2 (n=6) underwent the same protocol as Group 1 (including video-EEG) but did not receive KA (i.e. experienced no SE), thus providing information about the MEMRI contrast in the normal brain. Group 3 (n=6) received KA and experienced SE but was not injected with $MnCl_2$, and therefore, provided control data to differentiate the changes caused by KA induced brain pathology only, without the effects of Mn^{2+} on signal intensity and T_1. Since the contribution of gliosis to the manganese contrast was unknown, Group 4 (n=5) was added to test that aspect. The SE was induced with KA and suppressed by halothane 3 hours post-KA to keep the duration of SE comparable to that in Groups 1 and 3. The MRI was performed 3-4 days after SE, when the cell loss and gliosis are already present but there is not yet any mossy fiber sprouting contributing to the MEMRI signal. MRI data were assessed without manganese at 3 days post-SE, then $MnCl_2$ injection was given, and 24 hours later MRI scanning was repeated. Thereafter, rats were transcardially perfused for the histological examination of the gliosis and other cellular phenomena. Group 5 (n=5) was added to investigate, whether BBB damage could contribute to enhanced MEMRI signal in the hippocampus. Again, SE was induced with KA and gadolinium (0.5 M Gd-DTPA, 0.4 ml/kg i.v., Gadovist, Schering) enhanced MRI was performed at 1 day, 4 days, and 2 months post-SE. Imaging took place before and 13 min after Gd injection and subtraction images (post-Gd minus pre-Gd at the given time point) were calculated. The timing of Gd imaging corresponds to that of MEMRI imaging in the Group 1. Group 6 (n=5) received only Gd and served as a control group for the Group 5.

The MRI protocol was as follows. The coronal slice of interest (-3.6 mm caudally from bregma according to Paxinos rat brain atlas, (Paxinos and Watson 1986)) for the single slice T_1 maps was chosen among the T_2 weighted multi-slice image set that was acquired using a spin echo sequence (TE = 65 ms, TR = 2.5 s, 128*256 points over field of view 3.5*3.5 cm^2,

slice thickness 0.9 mm, 17 slices covering rat cerebrum). Data for T_1 maps were then acquired from a 0.9 mm slice using an inversion recovery fast spin echo -sequence with adiabatic BIR-4 refocusing pulses (TR = 4 s, echo spacing 13 ms, 4-8 echoes / excitation, 128*256 points, field of view 2.56*2.0 cm^2, array of inversion times (TI) 10, 400, 1000, 1600 ms). T_1 weighted 3D images from the whole brain were collected using a gradient echo sequence (TE = 2.7 ms, TR = 120 ms) incorporating an adiabatic 70º BIR-4 excitation pulse to reduce the influence of B_1 inhomogeneity. A 3D volume of 2.5*2.5*3.5 cm^3 was covered with 192*64*256 points, with 2 averages per phase encoding step. The identical protocols were used both with and without manganese contrast agent.

The MEMRI data were analyzed using manually drawn ROIs (cortex, hippocampus, DG, CA1, see Fig. 2A in **I**) and profiles across the hippocampus (Fig. 2B in **I**). The bias due to the possible differences in background manganese level was eliminated by normalizing the values to a reference area (cortex or corpus callosum).

4.2.2.2 Study design and quantitative MRI protocol in TBI studies II and III:
The study of quantitative MRI changes in TBI had two major goals. To characterize the dynamics of long-term developments of tissue damage with MRI, and to compare the early MRI findings with the chronic outcomes. The study is outlined in Fig. 1 in **II** and Fig. 2 in **III.** Taken together, a first group of animals (14 TBIs and 5 controls) was imaged at 3 hours, 3 days, 9 days, 23 days, 2 months, 3 months and 6 months after TBI. Later, a second group was added (20 TBIs and 10 controls) and it went through MRI at 7 and 11 months after TBI and MRS at 5 and 10 months after TBI. For the first group with acute and sub acute MRI data we performed later behavioral Morris water maze test (7 months post-injury) and histology after 12 months to evaluate the long-term outcomes.

The MRI protocol was as follows. Anatomical details and structures were detected using a T_2 weighted spin echo multi-slice sequence with two adiabatic refocusing RF pulses to minimize the influence of the moderately inhomogeneous B_1 field (TE = 70 ms, TR = 3 s, field of view 30*30 mm^2 covered with 128*256 data points, slice thickness 0.75 mm, 19 consecutive slices covering rat cerebrum). The presence of hemorrhage in the brain tissue was determined by T_2* weighted multi-slice images measured using a gradient echo sequence (TE = 15 ms, TR = 1500 ms, flip = 70º, 128*256 points). Quantitative maps of T_2, $T_{1\rho}$ and the 1/3 of the trace of diffusion tensor (D_{av}; D_{av} = 1/3 trace D) were quantified from the same single 1.50 mm coronal slice (corresponding to the antero-posterior level of -3.80 mm from the bregma according to Paxinos rat brain atlas) using a magnetization prepared fast-spin-echo sequence with adiabatic BIR-4 refocusing pulses (TR = 3.0 s, 16 echoes/excitation, center-out k-space filling, echo spacing 10 ms, field of view of 30*30 mm^2 covered with 128*256 data points). T_2 relaxation time was measured using a spin-echo preparation block consisting of 90º-180º-180º-90º series of adiabatic pulses, that is, adiabatic half passage (AHP), two hyperbolic secant (HS) adiabatic full passages, reverse AHP and crusher gradient in front of the fast spin echo sequence (TE = 20, 38, 52, 76 ms). On-resonance longitudinal rotating frame ($T_{1\rho}$) relaxation time was measured using a preparation block with variable-length adiabatic spin lock preparation pulse (spin lock times (SL) = 18, 38, 58, 78 ms, $B1_{SL}$= 0.8 G) and crusher gradients placed in front of the fast spin echo sequence. The spin lock pulse consisted of three parts: AHP, continuous wave on-resonance spin lock period and reverse AHP pulse, (Grohn et al., 2005). 1/3 of the trace of the diffusion tensor (D_{av}) was quantified using the same pulse sequence as in the above described T_2 measurement with a diffusion sensitising gradient pair added around each refocusing RF pulse in the magnetization preparation block. Three images with different degree of diffusion weighting (b = 90, 496, 1014 s/mm^2, diffusion time = 29

ms) were all obtained in each three different orthogonal orientations: x, y and z. To assess the possible B_1 heterogeneity within the regions of interest the B_1 field was mapped. Data for B_1 field map were acquired using variable length square preparation pulse with a crusher gradient in front of a FLASH pulse sequence (TR = 4.5 ms, TE = 2.2 ms), thereafter by fitting a cosine function to the measured signal intensity oscillation B_1 maps could be calculated.

Quantitative T_2 and $T_{1\rho}$ relaxation times and diffusion maps were calculated by fitting the data voxel wise to standard single exponential formulae. The diffusion coefficient D was measured and calculated separately in three different orthogonal orientations (D_x, D_y and D_z) and the average of these three coefficients was determined as an orientation independent measure of water diffusion D_{av}. The data analysis was performed manually. The volumes of lesion and hippocampi were calculated as a sum of the voxels in the outlined regions in multi-slice T_2 weighted images. When analyzing the single slice maps the ROIs were first drawn into the corresponding slice of T_2 weighted images and overlaid thereafter to the maps. The *focal area* refers to the lesional cortex that was outlined based on hyperintensity in T_2 weighted images and using the visual aid of T_2 maps with standardized scaling 0-150 ms. *Perifocal area* refers to the ipsilateral parietal cortex that appears normal in T_2 weighted images excluding the focal lesion. In addition, we assessed the contralateral parietal cortex and the *hippocampus* bilaterally (Fig. 2A, **II**). When outlining the perifocal and hippocampal ROIs, the voxels overlapping with the enlarged ventricles were excluded to avoid partial volume effect, and to detect the possible degenerative process ongoing in the normal appearing tissue.

4.2.2.3 Study design and MRI methodology of CBV study IV

The last study aimed to characterize the CBV changes during two weeks frequent follow-up after TBI. The study design is shown in Fig.1. in **IV**. Briefly, rats were divided into 8 experimental TBI groups imaged at different time points: 1 hour (n=6), 2 hours (n=12), 4 hours (n=13), 1 day (n=6), 2 days (n=6), 3 days (n=6), 4 days (n=6), 7 days (n=6) and 2 weeks (n=14, repeated MRI for animals that had been previously imaged at days 1-3) post-injury. The neuroscore test was performed to a sub group of animals (n=29) repeatedly before and 2 days, 7 days and 14 days after the TBI induction to assess the impairment of motor functions post-injury. To monitor the level of CO_2 in blood a bench test was performed (additional n=6) with identical operation and anesthesia procedures and blood samples were taken 2 hours, 1 day, 4 days and 14 days post-injury.

For the intravenous administration of contrast agent the cannula was implanted into the right femoral vein. (The cannula was filled with saline to keep the line open prior to the actual contrast agent administration.) Animals were anesthetized by isoflurane (carrier gas of O_2 30% and N_2O 70%). After cannula implantation the animals were positioned into the stereotactics lying on their stomach, the leg position was stabilized and the head were stabilized using ear and bite bars. Upon imaging the breathing rate of the animals was continuously monitored with a pressure probe under them and the isofluorane level was adjusted accordingly (isoflurane between 1.3-1.7%). Animals were kept warm with water circulating heating bed under them and the bed temperature was maintained at +38.5ºC. Imaging was then performed prior and post the iron oxide contrast agent (ultrasmall superparamagnetic iron oxide, Sinerem, 3 mg/kg) injection into the femoral vein cannula (injection time was about one minute, after the injection 5 minutes delay before starting the post-contrast imaging sequence allowed the contrast agent to reach the target area; the animal was not moved in between pre and post measurements).

The MRI protocol was as follows. The RF coil setup used was the actively decoupled volume transmission coil and quadrature surface receiver coil (Rapid Biomedical, Germany). First, in addition to the CBV data, the multi-slice diffusion maps (D_{av}) were assessed using a spin echo sequence (b-values = 0, 700, 1000 $*10^{-3}$ mm^2/s, TE = 60 ms, TR = 2 s and 64*128 points), FOV = 4.0*4.0 cm^2, 17 coronal slices, slice thickness = 1.0 mm and 2 averages per phase encoding step. Then, to quantify the CBV, identical image acquisitions pre and post contrast agent consisted of T_2* weighted images measured using a gradient echo sequence (TE = 15 ms, TR = 1500 ms, flip = 70º, 128*256 points), and T_2 weighted images measured using spin echo sequence (TE = 70 ms, TR = 2500 ms, 128*256 points).

The ΔR2 and ΔR2* maps (**IV**) were calculated by subtracting images taken post and pre contrast agent administration and using a formula derived from the difference between T_2^{-1} with and without the contrast agent, where the T_2 decay is fitted to a standard mono-exponential decay function. The ΔR2 and ΔR2* are here assumed to be directly proportional to CBV (as previously described Wu et al. 2003) with a contribution of only small vessels (diameter 8-12 μm) or both large and small vessels, respectively. The ROIs were manually outlined in T_2 weighted images and overlaid on top of the quantitative maps thereafter. The lesion volume was determined through 17 slices. The CBV and diffusion values were quantified in the lesion, perifocal cortical area surrounding the lesion, both ipsilateral and contralateral hippocampus and contralateral cortex as an average of three consecutive 1mm-slices around the lesion epicenter (see Fig 2A, **IV**). The ΔR2 and ΔR2* were normalized animal by animal to a reference muscle area. This eliminated the effect of differences in the background contrast agent level. The reference area was a muscle area outlined in the most frontal slices distant from the operation site (visually corresponding the level of +1.00 mm from Bregma in Paxinos rat atlas (Paxinos and Watson 1986)) since it appeared to be unaffected by the impact. In this approach of CBV assessment the CO_2 level in blood is assumed to remain constant and within normal physiological limits and to verify this, the CO_2 level was measured in additional bench test in four different time points (2 hours, 1 day, 4 days and 2 weeks after CCI induction) and in each time twice during a procedure identical to the imaging setup (that is, identically operated and anesthetized animals, blood samples taken in time points corresponding the mid point of pre and post contrast imaging).

4.2.3 Magnetic resonance spectroscopy (MRS) measurements and analysis

In the study **II** *in vivo* single voxel spectroscopy data were obtained 5 and 10 months after TBI induction. Stimulated echo acquisition mode (STEAM) localization with a short echo time was used (Tkac et al., 1999) (TE = 2 ms , TR = 4 s , bandwidth of 2.5 kHz was covered with 3336 points, 512 averages were collected as a sum of 16 blocks of 32 averages each) and VAPOR water suppression scheme, after automatic FASTMAP shimming (Gruetter 1993) was incorporated. Typical achieved line width was around 13-15 Hz. Voxels (2.5*3*3 mm) were located around both the ipsilateral and contralateral hippocampus (Fig. 2B, **II**). The spectral analysis was performed using LC model and only results from metabolites with SD% < 20 were included in further analysis. All values were presented as relative concentrations to total creatine peak at 3.04 ppm consisting of creatine and phosphocreatine.

4.3 Behavioural testing

4.3.1 Cognitive test: Morris water maze

The Morris water maze tests hippocampal related spatial learning and memory functions. The water maze testing system was composed of a black pool of water (20 ± 2 °C), where the pool was surrounded with visual cues to enable the rats orient themselves. The pool diameter was 150 cm and it was divided into four quadrants. A platform (10 cm × 10 cm) was located in the middle of the northwest quadrant (25 cm from the pool rim) and it was hidden 1.5 cm below the water surface. When placed into the water the rats started to search a way out and eventually found the platform. The swimming pattern, speed and time of the rat were recorded using a video camera that was positioned above the pool and connected to a computerized image analysis system (HVS image, Imaging Research Inc., UK). The goal was to evaluate how the rats gradually learned the location of the platform. The rats were tested on three consecutive days, 5 trials in each day. There were four different starting positions for the rat (north, south, east and west) and the starting position of the rat was changed in each trial. The rat was allowed to swim for 70 s to find the platform and if it failed to find the hidden platform within 70 s, it was guided to the platform. After each trial, the rat was allowed to remain and rest on the platform for 10 s. Thereafter, it rested in the cage for 30 s (after trials 1, 2, and 4) or 1 min (after trials 3 and 5). On the third testing day, a sixth trial, so called probe trial, was performed without the platform. Four parameters were recorded: (a) latency to the platform (max 70 s), (b) length of the swimming path from the starting position to the end of the trial (cm), (c) mean swimming speed (cm/s), and (d) percent total time rat spent in the correct quadrant of the pool. (Karhunen et al., 2003)

4.3.2 Motor function test: neuroscore

The motor functions of the rats were tested by composite neuroscore procedure with small modifications to the previously described procedure (McIntosh et al., 1989; Okiyama et al., 1992;). Briefly, the rats were scored on a 0 (severely impaired) to 3-4 (normal) integral scale for several motor performance tasks. The test protocol was as follows: circling (scoring 0-4) and motility (scoring 0-3) when placed on the floor, general condition (scoring 0-3), paw placement back to the bench when taking each paw one by one over the edge of the bench (scoring 0-4), righting reflex when placed to lie on its back (score 1 for successful righting, 0 for failure), the ability to climb up when placed hanging on a ribbed horizontal bar by its forepaws (scoring 0-3), the ability to turn around on a 45º inclined plane when placed face 'downhill' (scoring 0-3), the ability to swivel around contralaterally to the rotation when rotated by the base of the tail clockwise and then counterclockwise (1 score for each side), visual forepaw reaching on suspension by the tail with vibrissae next to a bench top (score per paw if the animal arches and places forepaws on the bench), contralateral reflex when animal is held by the base of the tail (1 score for no reflex, 0 for a reflex), and finally, a grip strength onto bars on cage when dragged by the tail (score 0-2). Then the scores of each task were summed up to make a composite neuroscore (scoring 0–28).

4.3.3 Seizure activity: video-EEG recording

To detect the development of spontaneous seizures in study **I** and assess their possible effect on MEMRI signal, we performed continuous video-EEG monitoring for 2 weeks.

For electrode implantation the animals were anesthetized with a single i.p. injection (6 ml/kg) of a mixture containing sodium pentobarbital (58 mg/kg), chloral hydrate (60 mg/kg), magnesium sulfate (127.2 mg/kg), propylene glycol (42.8%), and absolute ethanol (11.6%).

The head of the rat was secured in a stereotaxics and the skull periosteum exposed by a midline skin incision. Two stainless steel cortical screw electrodes (E363/20 Plastics One Inc., Roanoke, VA, USA) were inserted one over the left and another over the right frontal cortex (2 mm lateral and 3 mm rostral to Bregma). Two additional screw electrodes were placed into the skull over the cerebellum bilaterally (10.3 mm caudal to Bregma, 2 mm lateral to the midline) and they served as indifferent and ground electrodes. Then all electrode pins were inserted into the plastic pedestal and the entire assembly was cemented to the calvarium with dental acrylic.
The continuous two weeks video-EEG monitoring was performed as described previously (Nissinen et al., 2000b). Briefly, electrical brain activity from the motor cortex was recorded with the Nervus EEG Recording System connected to a Nervus magnus 32/8 amplifier (Taugagreining, Iceland), and filtered with high-pass 0.3 Hz and low-pass 100 Hz cutoffs. The behaviour of the animals was monitored using the WV-BP330/GE video camera (Panasonic) that was positioned above the cages and allowed simultaneous videotaping of 8 animals. The camera was connected to a SVT-N72P time lapse VCR (Sony) and a PVM-145E video monitor (Sony). If the animal experienced a high amplitude rhythmic discharge with a clear onset, offset, and temporal evolution in wave morphology and amplitude, that lasted more than 5 seconds, it was defined to be an electrographic seizure. If such seizure was detected, its behavioural severity was assessed on video according to Racine's scale (Kharatishvili et al., 2006c; Racine 1972). Electrographic interictal discharge (ID) was defined to be a high amplitude rhythmic discharge containing spike-wave and/or polyspike-wave components and lasting less than 5 s.

4.4 Histology

Perfusion and fixation procedure
At the end of studies **I-III** rats were transcardially perfused according to the Timm fixation protocol (Nairismagi et al., 2004). After perfusion the brains were removed, postfixed in 4% PFA for 4 hours, cryoprotected in a solution containing 20% glycerol in 0.02 M KPBS (pH 7.4) for 48 hours and then frozed in dry ice in -70 ºC. The frozen brains were cut with a sliding microtome (30 µm thick coronal sections, 1-in-5 series) and sections were stored in tissue collecting solution (30% ethylene glycol, 25% glycerol at -20 ºC).

Nissl staining for neuronal loss
Every fifth section (1-in-5 series) was stained for thionin or cresyl violet to identify the cytoarchitectonic boundaries and to locate and quantify the neuronal damage. The severity of neurodegeneration in the hippocampus was evaluated either by calculating the hilar neuron cells (**III**) or using a semi-quantitative scoring system evaluating the percentual damage in each sub areas of interest, that is CA1, CA3 or hilus (**I** and **III**): 0 = no damage, 1 < 20% damage, 2 = 20-50% damage, 3 > 50% damage as described before (Nissinen et al., 2004). The mean scores were calculated from consecutive sections corresponding to the coverage of single slice MRI map, 6 sections in study **I** and 9 sections in study **III**.

Fluoro Jade B staining for recent cell death
Another series of every fifth section (1-in-5 series) was stained for Fluoro-Jade B to detect ongoing neurodegeneration and recent cell death (in study **I**). Staining was performed according to Schmued et al. (Schmued, Albertson, Slikker 1997). Briefly, sections were washed three times for 10 min with phosphate buffer, then mounted on glass slides and dried

overnight at +37 ºC. In the next day the sections were then first rehydrated in absolute ethanol (3 min), 70% ethanol (2 min) and dH_2O (2 min), then incubated in 0.06% potassium permanganate for 15 min, rinsed briefly in dH_2O (2 min) and finally incubated for 30 min in a solution containing 0.001% Fluoro-Jade B (Histo-Chem, Jefferson, AR, USA) and 0.1% acetic acid. Thereafter the sections were washed with dH_2O, dried, dehydrated in a series of xylenes and coverslipped. One representative brain section per animal was analyzed in study **I**, and fluorescence microscopy was used for image capturing. Semi-quantitative scoring from 0-3 described both the amount and coverage of Fluoro Jade positive cells.

Immunhistochemical staining for astroglia and microglia

In study I the degree and distribution of both astrogliosis and microgliosis was assessed by immunostaining. Astrogliosis was analyzed from sections stained with an astroglial marker GFAP (glial fibrillary acidic protein) and microgliosis from sections stained with Ox-42 microglia marker. Free floating sections were immunohistochemically stained with monoclonal mouse anti-mouse GFAP antibody (Boehringer Mannheim #814369) or with monoclonal mouse anti-rat Ox-42 antibody (Serotec MCA275G). Procedure was similar for both antibodies and the method described below is the method when using GFAP antibody. Briefly, the free floating sections were treated with 1% hydrogen peroxide to remove endogenous peroxidase, and washed in 0.02M KPBS, pH 7.4 before blocking in 10% normal horse serum (NHS) and 0.5% TritonX-100 in KPBS. Then, sections were incubated for 2 days (+4 ºC) in primary antibody (1:40 000) in 1% NHS and 0.5% TritonX-100 in KPBS. Sections were then washed three times (2% NHS in KPBS), and incubated for 60 minutes in biotinylated anti-mouse IgG (1:200, #BA-2000; Vector Laboratories, Burlingame, CA) diluted in 1% NHS, 0.3% TritonX-100 in KBPS. Thereafter, the sections were incubated for 45 minutes in avidin-biotin-peroxidase complex according to manufacturer's instructions (Standard ABCkit; #PK-4000, Vector Laboratories). The incubations in the secondary antibody and in the avidin-biotin solution were repeated. At the end the peroxidase activity was visualized with 0.05% 3,3' -diaminobenzidine (DAB; Pierce Chemical Company, Rockford, IL) and 0.08% H_2O_2 in KBPS. Finally, the sections were mounted in gelatin-coated glass slides, dried, and intensified with osmium tetroxide and thiocarbohydrazine according to the method of Lewis et al. (1986).

In the analysis both the GFAP and Ox-42 immunostainings were semiquantitatively scored in the hippocampal subfields CA1, CA3b, CA3c, and the hilus of the dentate gyrus: Score 0, no GFAP/Ox-42 immunorective cells present; Score 1, light; Score 2, moderate; Score 3 high number of immunoreactive cells present (Fig. 4 in **I** shows representative photomicrograph with gliosis Scores 1-3). For the final analysis, we summed the scores of the CA3c and the hilus to match the histologic analysis with the ROI drawn onto the MRI images.

Timm staining for mossy fiber sprouting

To detect abnormal growth of granule cell axons (mossy fiber sprouting) one series of sections was stained with the Timm sulfide/silver method (Sloviter 1982). The density of mossy fiber sprouting was evaluated separately in the tip, mid, and crest portions of the granule cell layer of the hippocampus. The density of sprouting was scored from 0 (no sprouting) to 5 (entire inner molecular layer covered with sprouted mossy fibers) according to Cavazos et al. (Cavazos, Golarai, Sutula 1991). The density of sprouting in each animal was assessed. First the mean sprouting score for each section (mean of the scores in the tip, mid, and crest portions) was calculated, and then the scores in 5 to 8 sections were averaged. The set of histological sections included corresponded to the region of the MRI analysis.

4.5 Statistics

Statistical analysis was done using SPSS for Windows software (Chicago, IL, version 14.0). Differences between groups were analyzed with Student's t-test for MRI data and with Kruskal-Wallis followed by *post hoc* analysis with Mann Whitney *U* test for non-parametric behavioural or histological data or MRI data with low animal number. All values are expressed as mean ± standard error of mean (SEM). *Spearman rank* correlation coefficient was used to assess correlations between MRI and functional or histological results.

5 Results

5.1 MEMRI detects axonal sprouting

The first aim was to demonstrate the ability of systemic MEMRI to detect structural axonal plasticity during epileptogenesis. To induce epileptogenesis and mossy fiber sprouting rats were treated with kainate and then later, to visualize the axonal sprouting, they were imaged after contrast agent $MnCl_2$ administration. The first major finding was that the chronic kainate-treated animals showed a remarkably enhanced MEMRI signal both in the DG and CA1 sub regions of the hippocampus as compared to controls. MEMRI signal of the DG differed from that in controls in 9/11 rats in Group 1 showing hyperintensity and/or shape alterations. An average relative signal intensity in the DG in those rats with hyperintense DG was 1.37 ± 0.02 and in controls (Group 2) 1.25 ± 0.02 ($p<0.05$). When quantifying the alterations in the shape of the DG (i.e., in the spread of the MEMRI signal), we found that the thickness of the signal from the CA3 region was increased to 260 ± 40% of that in controls (Group 1 versus Group 2, $p<0.05$). Interestingly, there was also increased MEMRI signal in the CA1 in 8/11 of the chronic KA-injected animals suggesting accumulation of Mn^{2+} in that layer. Relative signal intensities were 1.33 ± 0.03 in these 8 animals in Group1 and 1.13 ± 0.02 in the controls in Group 2 ($p<0.01$). Analysis of T_1 profiles revealed this same manganese accumulation in the CA1 as a drop of absolute T_1 relaxation time in the CA1 below the control level (Fig. 3. in **I,** right panel).

To investigate the cause for the signal enhancement and manganese accumulation, groups with different cellular level pathology were added and detailed histologic analyzes were performed. The second major finding, based on the series of histological stainings, was that the observed MEMRI hyperintensity was associated with axonal sprouting rather than other ongoing histopathologic alterations, such as neurodegeneration, astrogliosis, or microgliosis (Fig. 4 and 5 in **I**). The inter animal variation and individual analysis of each animal led to elimination of neurodegeneration, astrogliosis and microgliosis as the primary sources of signal enhancement in systemic MEMRI (Tables 1-2, Figs. 3-4, **I**). Furthermore, the observed enhanced MEMRI signal in DG and CA1 were found not to be associated with local BBB leakage either, since the Group 5 receiving intravenous Gd contrast agent at corresponding time points post-SE did not display similar signal enhancement pattern in the hippocampus (Fig.6, **I**).

The third major finding was that MEMRI hyperintensity was not associated with seizure activity. Because the neuronal activity is one possible factor causing accumulation of manganese and contributing to MEMRI signal, this had to be addressed as well. The emergence of spontaneous seizures in the chronic phase was studied by video-EEG (the electroencephalograph was recorded from 6 rats of Group 3 and 4 rats in Group 1) and 75% of the recorded rats in both groups had epileptiform activity or spontaneous seizures in EEG (no difference between the groups). But the seizure frequency in epileptic animals and MEMRI hyperintensity did not correlate (Table 1 and 2). Another approach was the imaging acutely after KA induced SE, which was done to examine how the ongoing generalized seizure would affect the manganese accumulation. $MnCl_2$ injection was given prior to the seizure induction, hence manganese was available during SE. No MEMRI hyperintensity in the DG or CA1 during SE (i.e. 3 hours post-KA or 25 hours post-Ka in Group 1) was found. Rather, we found that during SE (i.e., 15 h after $MnCl_2$ and 3 h after KA injection) T_1 was longer in the hippocampus of Group 1 (receiving both KA and $MnCl_2$) as compared to control Group 2 receiving only $MnCl_2$ (DG 1117 ± 16 ms and 1042 ± 21 ms, respectively, $p<0.05$;

CA1 1178 ± 11 ms and 1120 ± 27 ms, respectively, $p<0.05$). The slight increase of T_1 relaxation time could be due to edema formation during and after SE. In other studied brain areas there were no T_1 differences between the post-SE and control groups. This data showed that seizure activity does not lead enhanced Mn^{2+} accumulation *per se* even though Mn^{2+} is present in the brain. (Fig. 5, **I**)

One more result to report was that the data from control group 2 receiving only $MnCl_2$ demonstrated that Mn^{2+} did not influence the histologic outcome or epilepsy phenotype.

After summing up and cross comparing all these findings it was demonstrated that MEMRI, after systemic administration of $MnCl_2$, actually detects the axonal sprouting. According to this data the density of mossy fiber sprouting had to be high enough to be detectable, a density of score 1.19 did not cause detectable signal enhancement (table 1, **I**)).

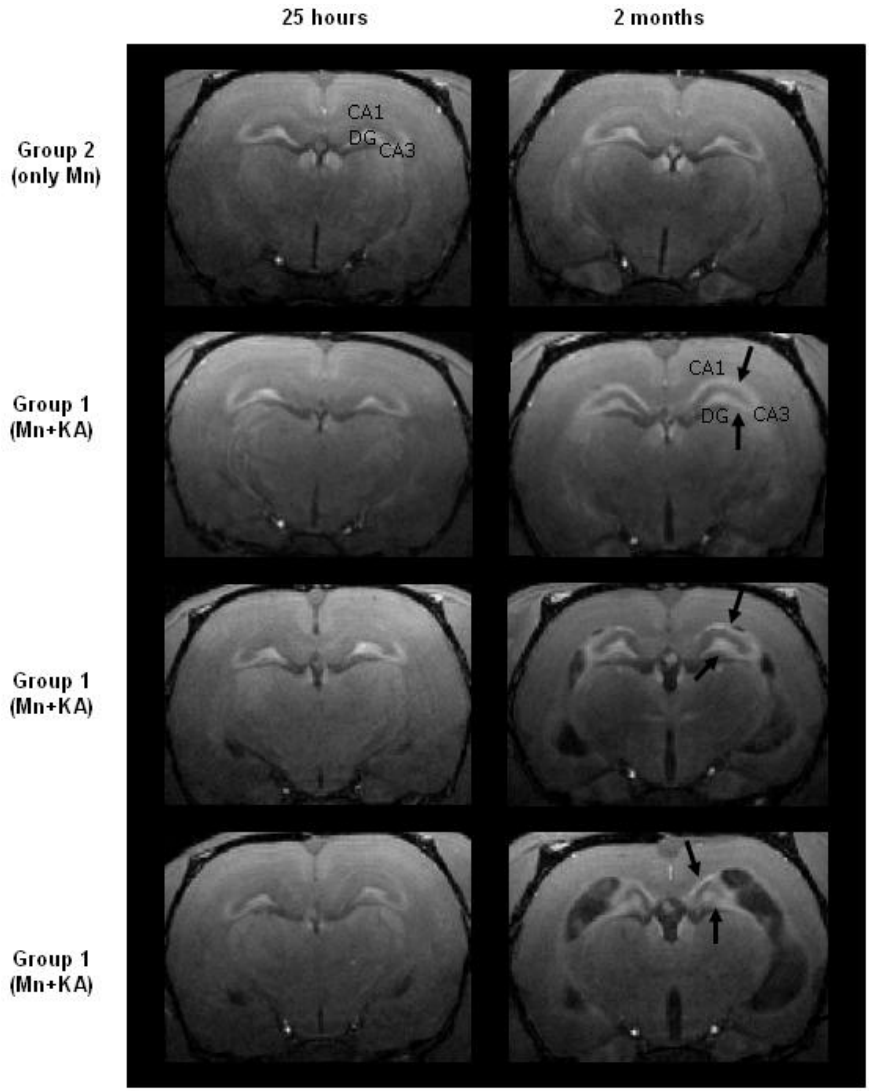

Figure 1. Manganese enhanced T_1 weighted images of a control animal (top row) and three representative kainate treated (and therefore epileptogenic) animals (second, third and fourth rows). The left column shows the images taken at the acute stage 25 hours after KA administration and status epilepticus (that is, 37 hours after $MnCl_2$ administration) and the right column shows the same animals at chronic stage, 2 months after the status epilepticus with a manganese contrast agent given 24 hours prior to the imaging. Chronic animals displayed hyperintensity in the CA1 region and shape and intensity changes in the CA3 and DG regions (arrows). Some chronic animals had also atrophy and enlarged ventricles (see the chronic case at bottom row as an example).

5.2 Quantitative MRI after TBI detects distinct temporal damage progression in different brain regions

The second major aim was to explore the potential of different MRI methodologies to detect, follow and characterize brain pathology after traumatic brain injury. The fluid percussion impact generated local contusion and hyperintense primary lesion was detected in the cortex immediately in the T_2 weighted images (Figure 2A, below). In addition, intracerebral hemorrhage was detected adjacent to the lesion and also more distantly (Figure 2B, below). The first major finding was that the MRI detectable tissue alterations continued for several months. The volume of the primary focal lesion continued to expand for 3 months, and quantitative MRI observations showed progressive changes at the primary cortical lesion site for 6 months. In the perifocal region and in the hippocampus the slow secondary increase in quantitative D_{av}, T_2 and $T_{1\rho}$ continued steadily for the first 2-3 months (significant further increase in the hippocampus until 3 months and in the perifocal area until 2 months).

The second major finding was that in the primary lesion site and in the perilesional areas the MRI contrast parameter alterations differed evidently. In the lesion the drastic increase of all T_2, $T_{1\rho}$ and D_{av}, which was detectable already 3 hours or 3 days post-injury and rapidly increasing henceforth, was several fold in magnitude as compared to the more subtle alterations detected in the perilesional regions. For example, when considering the situation 9 days after injury, the observed changes at that time in the perilesional regions were maximally +8% (for $T_{1\rho}$) or even undetectable (for T_2 and D_{av}) while in the primary lesion the irreversible damage was revealed by 70% increase in diffusion, 54% increase in T_2 and 80% increase in $T_{1\rho}$. Thereafter the lesion values rose up to the values equal to those in CSF, that is, the tissue was absorbed and the cavity filled with CSF was generated (Fig.3B, in **II**). In addition to the magnitude differences the temporal pattern of MRI changes differed between lesion and surroundings. In the primary lesion the T_2, $T_{1\rho}$ and D_{av} values simply shot up, continuing the rapid irreversible increase, while in the perilesional regions (the perifocal cortical area and the hippocampus) the values first displayed acute edema related increase and recovery and then begun a delayed, slow, persistent secondary increase. The magnitude of quantitative MRI contrast parameter deviations during the delayed secondary increase remained around 10-13% for the relaxation times in the ipsilateral hippocampus (4-7% in the contralateral hippocampus and 3-9% in the perifocal area) and around 7-15% for the diffusion in the ipsilateral hippocampus (6-8% in the contralateral hippocampus and 4-6% in the perifocal area). [See Figure 3 shown below, and Figs. 5, 6 and 7 in **II.**] Taken together, both the magnitude and the temporal pattern of the observed MRI changes differ between the primary lesion site and in the perilesional regions around it. This feature enables the distinction of the irreversible damaged tissue region from the more mildly damaged, potentially salvageable region.

Furthermore, the results demonstrated that quantitative MRI values in the perilesional tissue are direct measures of the current severity of damage in that area, while the size of the nearby lesion is not. The lesion volume 23 days post-injury did not correlate with the tissue MRI parameters in the perifocal or hippocampal region at that same time point. (See Fig.8 in **II**)

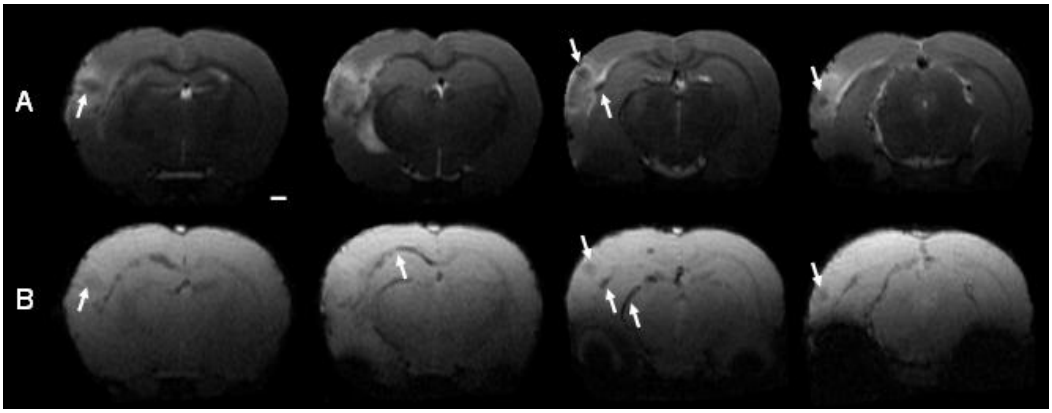

Figure 2. A representative animal 3 days after fluid percussion induced TBI. Rows **A** and **B** are showing the same four 0.75 mm thick slices (with 0.75 mm gap between them, arranged in rostral to caudal direction) imaged with spin echo and gradient echo techniques, respectively. **(A)** T_2 weighted signal intensity images showing the cortical hyperintense primary lesion (contusion) in the impact site and adjacent hypointense spots (arrows). **(B)** T_2* weighted signal intensity images showing intracerebral hemorrhages as signal void areas. Arrows in row **B** are pointing at the hemorrhagic spots that can also be seen in T_2 weighted images above.

5.3 Quantitative MRI findings early after TBI correlated with the long-term outcome

Since quantitative MRI was able to provide multifaceted information about the brain damage after traumatic brain injury, the next question was if it could help to predict the long-term outcome. Therefore, in the long follow-up studies the associations between the MRI findings already at the acute (3 hours) to sub acute (3-23 days) phases after initial impact and the long-term outcome 6 to 12 months later were the major interests. As outcome measures the final atrophy extent 6 months post-injury, memory and learning ability tested in Morris Water maze 7 months post-injury, and histopathological neuronal loss 12 months post-injury were assessed. At the chronic phase after TBI the animals displayed largely expanded lesion cavity, the ipsilateral hippocampal volume was decreased by 21%, the number of hilar neurons was decreased by 63% and the hippocampus related learning and memory performance was impaired in trauma animals (Fig. 5, in **III**). Several correlations were found between the early MRI data and these chronic measures supporting the hypothesis that early MRI findings could predict the long-term outcome. Table 1 summarizes the found correlations.

The lesion volume measured and the amount of intracerebral hemorrhage in the acute and sub acute phases after injury correlated with the final lesion extent 6 months later. The increased $T_{1\rho}$ in the focal cortical lesion at 23 days post-injury and the $T_{1\rho}$ increase in the perifocal area surrounding the lesion at 9 days post-injury both correlated with the final cortical lesion volume. The edema related transient increase in $T_{1\rho}$ and T_2 in the ipsilateral hippocampus 3 days post-injury (Figure 1, above) correlated with the chronic volume reduction of the ipsilateral hippocampus and with the hilar neuron loss - and so did the $T_{1\rho}$ increase 9 days post-injury. The delayed secondary increase 23 days post-injury in $T_{1\rho}$, T_2 and D_{av} in the ipsilateral hippocampus, which was already an indicator of the severity of the secondary injury cascades, correlated with the later hippocampal volume decrease at 6 months and with the final hilar neuron loss. This same delayed diffusion increase (in the ipsilateral hippocampus 23 days post-injury) correlated also with the long-term learning impairment. Also, the severity of hemorrhage at the sub acute phase was indicative of the long-term learning impairment. (See **III** results chapter for more details.)

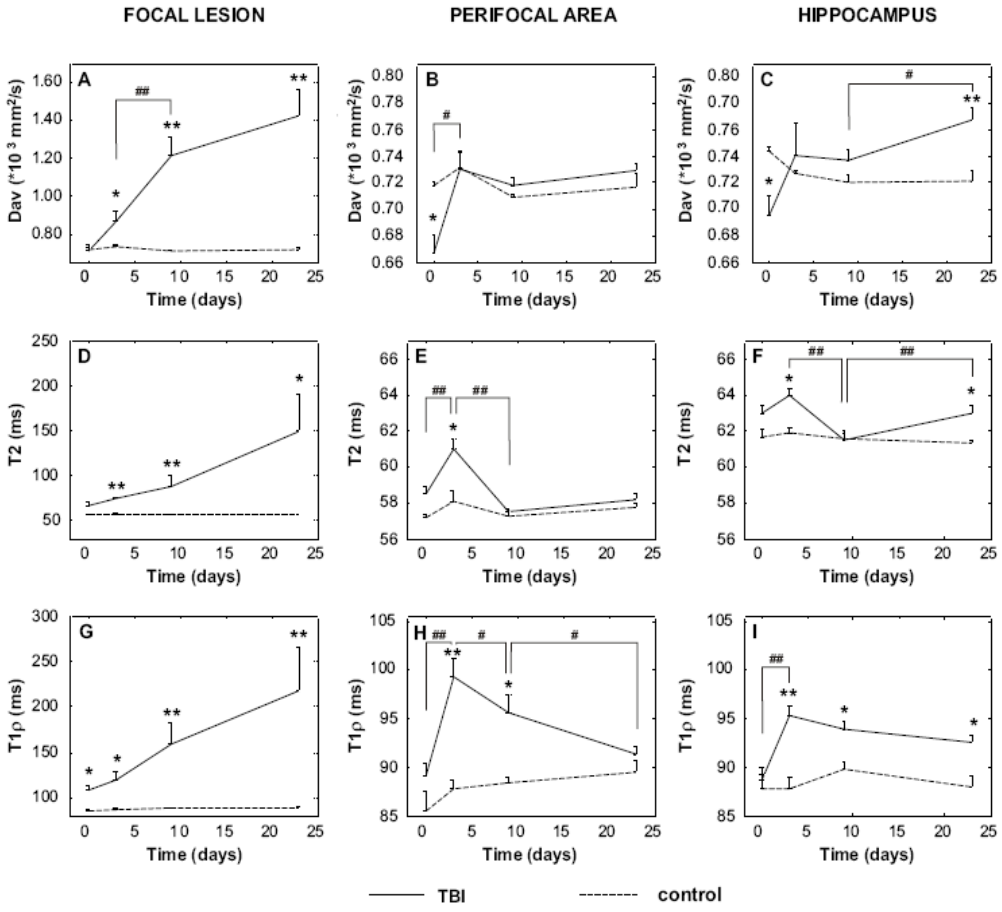

Figure 3. Early progression of D_{av}, T_2 and $T_{1\rho}$ in the lesion (left column), in the perifocal area (middle column) and in the ipsilateral hippocampus (right column). Data from TBI and sham groups at 3 hours, 3 days, 9 days and 23 days after TBI induction are shown. **The lesion:** D_{av} increased rapidly in the lesion area starting from day 3. Both T_2 and $T_{1\rho}$ also increased steadily, and $T_{1\rho}$ was significantly elevated already at 3 hours after TBI induction. **The perifocal area** (*i.e.* ipsilateral cortex excluding the lesion): D_{av} dropped acutely (3 hours) after TBI. T_2 and $T_{1\rho}$ show transient peak at day 3 post TBI, but unlike T_2, $T_{1\rho}$ remained elevated still at day 9. **The ipsilateral hippocampus**: D_{av} dropped acutely (3 hours) after TBI and increased 23 days later. Both T_2 and $T_{1\rho}$ peaked at day 3 post TBI and were elevated at day 23, but T_2 recovered at day 9 while $T_{1\rho}$ remained elevated. Differences between groups are indicated as **, $p<0.01$ and *, $p<0.05$ (Mann Whitney *post hoc* test), and the differences between time points as #, $p<0.05$ and ##, $p<0.01$ (Wilcoxon *post hoc* test). Note that the scaling of the lesion graphs differ from the scaling of perifocal and hippocampus graphs.

Table 1. The found correlations between the acute and sub acute MRI findings and the long-term outcome measures.

CORRELATIONS			LONG-TERM OUTCOME			
			Cortical atrophy	Functional	Hippocampal atrophy	
			Lesion volume	WM correct Quadrant %	ipsi HC volume	neuronal loss
ACUTE / SUB ACUTE MRI FINDINGS						
Hemorrhage		3 h - 9 d	r=0.664 *	r=-0.643 **	r=-0.824 **	-
Lesion volume	3 d	3 d	r=0.811 **	-	-	-
	9 d	9 d	r=0.864 **	-	-	-
	23 d	23 d	r=0.956 **	-	-	-
T_2	hippocampus	3 d	-	-	r=-0.642 **	r=-0.580 *
		23d	-	-	r=-0.555 *	r=-0.715 **
	perifocal	3 d	r=0.720 **	-		
$T_{1\rho}$	hippocampus	3 d	-	-	r=-0.755 **	r=-0.612 *
		9 d	-	-	r=-0.707 **	r=-0.739 **
		23 d	-	-	r=-0.650 **	r=-0.652 **
	perifocal lesion	9 d	r=0.748 **	-	-	-
		23 d	r=0.560 *	-	-	-
D_{av}	hippocampus	3 h	-	-	-	-
		23d	-	r=-0.512 *	r=-0.807 **	r=-0.665 **

*, $p<0.05$; **, $p<0.01$; only the found correlations are shown, both TBI animals and controls are included (n=17) in the correlations regarding the hippocampal atrophy, hippocampal (hilar) neuron number and water maze performance, while in the correlations regarding the lesion volume and hemorrhage score only the TBI animals were included (n=14)

5.4 CBV changes in the acute and sub acute phase after TBI and their association with the recovery of the motor functions

Upon contemplating the role of hemodynamic alterations in the secondary damage and repair processes after traumatic brain injury, a study about CBV changes in the acute and sub acute time points was conducted. Distinct CBV alterations were found and their nature changed over time and between brain regions. The first phenomena in all regions was the acute decrease in CBV, probably reflecting the initial hypoperfusion, but thereafter the different brain regions displayed different CBV patterns. In the primary lesion site (where the tissue appeared to be very severely damaged based on T_2 weighted anatomical images) the CBV in both large and small vessels was decreased during the first day, then the values seemed to

recover (ΔR2* still had a trend of reduced values but ΔR2 seemed to return to control level) until they dropped again at 2 weeks post-injury (47% decrease in ΔR2* and 61% decrease in ΔR2). In the cortical perifocal region the CBV values were decreased until day 4 post-injury and then the values slowly recovered towards the control level during the 2 weeks follow-up. Interestingly, this recovery happened in parallel with the recovery of motor functions, which were evaluated by repeated composite neuroscore behavioural tests. (Fig. 3 shows the CBV recovery and Fig. 6 the motor function recovery, in **IV**). According to the neuroscore the animals had 33 % worse performance 2 days after TBI than they had before the TBI. Then the impairment alleviated and 7 days post-injury the performance was 16% below the healthy level and 2 weeks post injury only 8% below the healthy level (all $p<0.01$).

In the hippocampus the CBV changes were different from the changes in the cortical regions. The acute drop in CBV was seen also in the hippocampi, but in the ipsilateral hippocampus there was persistent increase in capillary level CBV after day 1 post-injury (Fig. 4 in **IV**). The CBV values in the contralateral hippocampus showed only a small increase in the capillary level 2 weeks post-injury.

Acute diffusion drop within hours was seen in all brain regions. In this CCI trauma model diffusion drop revealed physiological disturbances even in the contralateral cortex, and therefore a distant muscle area was chosen as a reference area. The rate of diffusion increase in the following two weeks was very different between primary lesion and perifocal areas, again highlighting the ability of MRI to differentiate between irreversibly damaged and more mildly damaged tissue. In the sub acute phase the diffusion values were elevated in the perifocal region (only at day 4, $p<0.05$) and in the ipsilateral hippocampus (significant increase at day 2 and at 2 weeks post-injury, $p<0.05$). The contralateral cortex and hippocampus displayed a trend of low diffusion. (Figs. 3C and 4C in **IV**)

5.5 Metabolic findings in the hippocampus of chronic TBI animals

Metabolic changes preceed the structural changes and the spectroscopic methods could therefore provide a more sensitive measure of brain damage than MRI. Five months after the TBI induction the metabolic alterations detectable by ^{1}H-MRS in both the ipsilateral and in the contralateral hippocampus were studied. The relative concentration (relative to total creatine) changes as compared to controls were reported. We found decreased γ-aminobutyric acid (GABA), glutamate (Glu), N-acetylaspartylglutamate (NAAG), N-acetylaspartate + N-acetylaspartylglutamate (NAA+NAAG) and glutamate+glutamine (Glu+Gln) levels in the ipsilateral hippocampus ($p<0.05$, Figs. 9-10, in **II**), and increased level of *myo*-inositol (Ins). No significant metabolic alterations were detected in the contralateral hippocampus. The only progressive change from 5 months to 10 months was the further decrease in Glu level.

6 Discussion and conclusions

6.1 MRI read out for epileptogenesis - detection of axonal plasticity

The first major aim of the thesis was to test if systemic MEMRI can detect the axonal sprouting in the epileptogenic hippocampus and can the MEMRI findings therefore function as a potential surrogate marker for the epileptogenesis and epilepsy (regarding the plausible role of axonal plasticity in the hippocampal circuitry reorganization leading to epilepsy). Several groups were included to test if systemic injection of $MnCl_2$ can label axons and reveal axonal sprouting and what are the contributions of other cellular phenomena, seizure activity and the possible leakage of BBB to the MEMRI signal.

We demonstrated that systemic MEMRI indeed can detect structural axonal plasticity during epileptogenesis. Systemic administration of the $MnCl_2$ contrast agent two months after KA induced status epilepticus and epileptogenesis led to manganese accumulation into the CA1 and dentate gyrus sub regions of the hippocampus and caused them to be highlighted in T_1 weighted signal intensity images (corresponding to the T_1 relaxation time decrease quantified in T_1 maps). Alterations in the signal intensity, thickness and shape of the DG could be attributed to mossy fiber sprouting, since the neurodegeneration, astrogliosis and microgliosis could be eliminated as a primary cause of the observed contrast enhancement. Histological stainings and individual analysis pointed out the density of mossy fiber sprouting needed for an observable change in MEMRI. Interestingly, the CA1 region in several epileptic animals appeared hyperintense, indicating possible plasticity manifestation there as well. However, the underlying reason could not be determined since our zinc-based histological staining procedures were not able to stain axonal alterations in the CA1. Still, previous cellular studies have reported axonal plasticity triggered by kainate treatment also in the CA1 (Cavazos, Jones, Cross 2004; Smith and Dudek 2001). The manganese administration systemically led to the detection of mossy fiber sprouting in the DG of epileptic and epileptogenic animals. This means that systemic MEMRI can be utilized in experimental epilepsy studies as well as in studies of other nervous system diseases with potential axonal damage present.

It is important to note that generally the contribution of other neurobiologic changes to MEMRI signal can not be excluded. Glia cells, both astroglia and microglia can take up manganese. In a different context, particularly in situations with significant neurodegeneration and glial hypertrophy during aggressive inflammation etc. manganese accumulation and consequent signal enhancement can be largely due to the gliosis (Haapanen et al., 2007). Phagocytosis can also lead to manganese accumulation into the macrophages. The dominant reason for the manganese accumulation in most of the situations, however, is the neural uptake and the axonal transport thereafter. The latest MEMRI applications have concentrated on studies of neural circuits, integrity of axons and fiber bundles as well as stimulated neuronal activation related manganese uptake (Chuang et al., 2008; Serrano et al., 2008; Tucciarone et al., 2008; Van der Linden et al., 2004b).

Based on this study the role of seizure activity to the manganese accumulation is either non existent or negligible. We did not find any T_1 decrease (that is, no hyperintensity in T_1 weighted images) acutely after *status epilepticus*, rather we found a T_1 increase. This indicates that there is no detectable Mn^{2+} accumulation caused by prolonged seizure activity. The control data of the animals receiving only KA but no manganese showed that the effect of

only *status epilepticus* to the T_1 values (i.e. the pathological findings not related to manganese or its properties) was elevating [the animals suffering status showed elevated T_1 values 3 hours post KA as compared to naive rats, unpublished data]. This suggests that counteracting T_1 increasing physiological processes may also mask potential manganese accumulation related T_1 decrease. Kainic acid causes a sub group of neurons to die very rapidly, only hours after insult (Fujikawa, Shinmei, Cai 2000; Tuunanen et al., 1999). Hippocampal CA3 pyramidal neurons and interneurons in the hilus are particularly vulnerable to kainate and CA1 pyramidal neurons degenerate as well (Ben-Ari 1985; Covolan and Mello 2000; Covolan et al., 2000).

Because the manganese was administered systemically the availability of manganese in the brain tissue, that is inside the BBB, is of course one key question. To make sure that the lack of MEMRI enhancement in the most acute 3 hours post status (15 hours post $MnCl_2$) was not because of lack of available manganese, we repeated the imaging 22 hours later (37 hours from $MnCl_2$, 25 hours from KA). We found that in the control animals (receiving only manganese) Mn^{2+} accumulation and consequent T_1 decrease continued from 15 hours to 37 hours time point after $MnCl_2$ administration both in the cortex and the hippocampus. Similarly, further decrease was also observed in rats suffering status epilepticus. Actually, there were no significant differences in the cortical or hippocampal T_1 relaxation times between the SE and control groups at either of the two time points analyzed. This all suggests that there indeed is no manganese accumulation due to the seizure activity. The manganese accumulation due to long lasting stimulus activity has been reported in several studies, but the nature of activity during seizures differs drastically to that during for example, sound or scent stimuli. Furthermore, considering the neural activity during seizures there are studies suggesting that the granule cells of the DG there might not even be activated ((Fernandes et al., 1999) and personal communication with Dr. Astrid Nehlig).

6.2 The MRI detectable alterations after TBI are distinctively different in different brain regions, reveal the tissue at risk and may help to predict the outcome

The second major effort in this thesis work was the MRI characterization of brain changes after traumatic brain injury. Several MRI techniques were harnessed to answer questions about the tissue damage in different brain regions and about the progression of the damage. A main objective was to find out if the MRI performed shortly after injury could predict the long-term outcome and if it would reflect the concurrent functional impairment. The multifaceted approach included determination of quantitative T_2, $T_{1\rho}$, D_{av} and evaluation of the hemodynamic changes in the acute and sub acute phases post-injury.

In order to understand the dynamics of brain damage after TBI, the status of the brain tissue by quantitative *in vivo* MRI and MRS after fluid percussion induced TBI was followed for 11 months. There is a variety of cognitive and functional ramifications for head injury and some of these were evaluated by behavioral tests at the chronic stage of the disease. Also the structural pathology and cellular changes were quantified about a year after the injury. Only the use of animal models and totally non-invasive techniques, such as MRI, enable this intensive follow-up without any interference with the disease progression, and finally the access to the histological outcome. The rat model of lateral fluid percussion induced TBI is the most widely used experimental model of human closed head injury (Thompson et al.,

2005). The long-term outcome measures assessed 6-12 months post-injury in rat could temporally correspond to the outcome of patients several years post-injury.

Here, the focus of analysis were the areas of injured cortex, the perifocal area and the hippocampus, which are reported to suffer most as a consequence of an impact injury (Hallam et al., 2004; Sato et al., 2001). The role of these brain structures in the impairment of a patient is undoubtedly essential, but one must recognize that they do not provide a complete picture of the brain damage since there are other brain regions involved as well. For example, the thalamus and amygdala are known to undergo histopathologic changes after experimental TBI (Abrous et al., 1999; Rodriguez-Paez, Brunschwig, Bramlett 2005).

The temporal pattern and magnitude of measured T_2, $T_{1\rho}$, D_{av}, $\Delta R2$ and $\Delta R2^*$ changes varied substantially between the different brain areas revealing different types of tissue damage. The focal lesion area displayed values of irreversible tissue loss, the adjacent perifocal area displayed initially milder damage with delayed start but progressive nature, the ipsilateral hippocampus displayed also delayed progressive changes but with distinct hemodynamic alterations, and remote areas including the contralateral hippocampus and the contralateral cortex were affected as well to some extent. This means that quantitative MRI can be used to differentiate the regions with risk of delayed secondary damage from those of continuously progressing irreversible damage or from the intact areas. Importantly, quantitative MRI could also identify how far advanced are the pathological processes in each region, which is a major advantage in targeting treatments and following the treatment response.

6.2.1 The slowly progressive nature of the brain damage provides a wide window of opportunity for interventions

This data showed that the brain damage after TBI continues to progress for several months in rats, which corresponds to several years in humans. In rats the MRI detected further progression up to 6 months in the lesion site and up to 3 months in the hippocampus. After this all of the values remained elevated and some of them even showed a trend of further increase. These observations are in line with the previous cross-sectional histological studies demonstrating ongoing pathology for up to 1 year, including chronic inflammation, neurodegeneration, and axonal injury (Bramlett et al., 1997; Lenzlinger et al., 2001; Morganti-Kossmann et al., 2002; Philips et al., 2001; Pierce et al., 1998; Rodriguez-Paez, Brunschwig, Bramlett 2005; Smith et al., 1997; Soares et al., 1995; Toulmond and Rothwell 1995). The facts that the state of the tissue does not seem to stabilize for a long time after the impact, and that *in vivo* MRI can detect even the late progression, may promote the use of MRI in patients with old-established TBI diagnosis but possibly still with deteriorating status. Furthermore, this data reveals the long temporal window of opportunity for interventions, particularly those that aim to alleviate or stop the destructive molecular cascades in hippocampal and perifocal regions.

6.2.2 Primary lesion and irreversible damage

The primary contusion site could be easily detected by MRI, even with just T_2 weighted anatomical images. Lesion was seen as a hyperintense region, which appeared transiently larger around day 3 due to a strong edematic effect, became brighter with sharp edges at 23 days post-injury and thereafter started to slowly expand. Only after 6 months was the lesion

growth seized. The magnitude of the increase in relaxation times and diffusion values just days after injury revealed the drastic cellular degeneration and irreversible destruction. This was followed by tissue absorption and possibly by formation of a glia envelope around the lesion. Even though after this the border between primary lesion and the perifocal area was easy to detect, determining that border during the first week after injury was ambiguous. During this period only the quantitative MRI could differentiate the voxels with changes exceeding alarming thresholds. Some of the early MRI findings predicted the later lesion development. Initial lesion volume and amount of hemorrhages correlated with the final lesion size.

The hemodynamic disturbances were studied in CCI model and assessed as $\Delta R2$ and $\Delta R2^*$. The changes were found to be close to the same magnitude in the lesion and in the perifocal area. The CBV pattern also proceeded quite similarly in both regions (acute hypoperfusion followed by partial recovery), except for the sudden decrease in CBV values at 2 weeks post-injury in the lesion site. This drop at 2 weeks could represent dramatically reduced circulation in the capillary bed consistent with the vasospasm phase, which is seen in humans 4-15 days post-injury (Martin et al., 1997). Even though the CBV values did not seem to differ much between lesion and perifocal region, the big difference arose from the diffusion values, which in the sub acute phase were several fold higher in the lesion than elsewhere. It can be concluded that CBV measurements are able to detect circulation deficits in the perifocal region as well, but can not differentiate perifocal area from the primary lesion. This resembles the situation in ischemic brain injury. In the case of cerebral ischemia the perfusion reduction expands over the lesion to cover also the ischemic penumbra, while the diffusion abnormalities (decreased diffusion due to cytotoxic edema) are present only in the ischemic core region. In spite of the plausible appearing CBV results inside the primary lesion, a question remains how to interpret the results obtained by utilizing intravenous contrast agent when the vasculature inside the primary lesion is most likely leaking. Histological studies confirm vascular ruptures and BBB leakage in the lesion site after TBI (Beaumont et al., 2000; Whalen et al., 1998).

6.3.3 Perifocal cortical area - tissue at risk but potentially salvageable

One potentially clinically relevant observation was that the viability of the perifocal tissue did not depend on the size of the focal lesion. The perifocal tissue surrounding the lesion was displaying only mild MRI changes in the sub acute phase and the severity of these sub acute MRI changes did not correlate with the current lesion size. That is, large lesion size in the sub acute phase after TBI should not be thought as an indicator of severe perifocal tissue damage. Even in cases with very large initial focal hyperintense lesion the tissue surrounding the lesion can be viable and thus a potential target for interventions. On the other hand, the severity of the observed MRI changes in the perifocal tissue in the sub acute phase does seem to indicate the later fate of that tissue if no actions are taken. The magnitude of $T_{1\rho}$ increase in the perifocal area surrounding the lesion at 9 days post-injury correlated with the final lesion extent and thereby already predicted whether the perifocal tissue shall be later absorbed and merged into the lesion cavity.

The perifocal tissue displayed transient edema related changes in T_2, $T_{1\rho}$ and D_{av} during the first days after injury and then a delayed secondary increase after 23 days. In the course of the following months the relaxation time values obtained from ROI analysis remained increased by 3-9% and diffusion values by 4-6%. The increases appear small, but they are significant.

The corresponding values in healthy tissue can vary even ~2% over time. However, when taking into account that the perifocal ROI includes also healthy voxels that (when calculating an average over the whole ROI) causes the observed abnormality to attenuate, these small but still significant increases can be regarded as a true pathological change.

The hemodynamic study revealed association between the CBV drop and recovery in the perifocal cortical area, and the simultaneous loss and recovery of motor functionality. These phenomena seemed to happen in parallel and may have a direct causal relation, since the motor cortex and somatosensory cortex were included into the perifocal ROI (if they were not within the primary lesion). This indicates that hemodynamics, and thereby indirectly the underlying reason for the dysfunction of motor cortex, can be potentially evaluated by MRI measurement of CBV changes.

One aspect to discuss is the interrelationship between oedema and CBV changes. The oedema (vasogenic or cytotoxic) may compress microvessels and hence impair perfusion. Thus the detected strong oedematic increase of tissue water around 3 to 9 days post-injury can interfere with the tissue perfusion pressure and the tissue perfusion particularly in the perifocal area as well as inside the primary contusion area and in the ipsilateral hippocampus.

6.3.4 The MRI findings in the hippocampus, underlying cellular alterations and the interrelation with the cognitive impairment

The hippocampus has a complex role in the function of brain and mind. The significance of hippocampal integrity has been shown in relation to cognitive spatial learning and memory functionality, and in the temporal lobe epilepsy. After the primary contusion site, the hippocampus ipsilaterally to the impact site suffers second most severe consequences. This was detected by MRI as 10-13% increase in relaxation times, 7-15% increase in average diffusivity, volumetric atrophy (hippocampal sclerosis) and metabolic changes detected at the chronic stage by MRS. Decreased NAA indicated decreased neuronal number, which was perfectly in line with histological findings, that is, massive neuronal loss in hilus. Increased Ins is an indicator of inflammation and gliosis, which have both been shown to be present in previous cellular studies of TBI (Lenzlinger et al., 2001; Philips et al., 2001; Soares et al., 1995). Decreased GABA is associated with loss of inhibitory tone and might have a role in the epilepsy development after TBI.

Histological studies have shown that the hippocampus is very sensitive to several types of brain insults. For example, kainic acid causes primarily hippocampal and amygdala neurodegeneration, TBI causes cortical and hippocampal damage (Kharatishvili et al., 2006a) and febrile seizures cause hippocampal axonal plasticity (Bender et al., 2003; Jansen et al., 2008). After lateral fluid percussion TBI, neuronal degeneration begins in the parieto-occipital cortex and the hippocampus of injured hemisphere 1-24 hours after impact and leads to significant neuronal loss in these areas 1-4 weeks post-injury (Cortez, McIntosh, Noble 1989b). This time frame is congruent with the presented results of the delayed increase of MRI parameters in the hippocampus. Reactive astrogliosis has also been reported to be present throughout the injured hemisphere, most densely around the lesion (Cortez, McIntosh, Noble 1989b). This may explain the clear sharp edges of the lesion seen in the MRI.

In unilateral head injury the hippocampus ipsilateral to the impact is the first to be injured, however, the delayed damage was now detected in the contralateral hippocampus as well by

quantitative MRI. In the investigation about the hemodynamic disturbances in the hippocampus, the ipsilateral and contralateral hippocampus both showed similar trends of altered CBV, but ipsilaterally the observed changes were much more pronounced. The found quantitative T_2, $T_{1\rho}$ and D_{av} abnormalities contralaterally were also much milder than ipsilaterally, but they were significant. In the histological analysis performed in the chronic stage no neuronal loss in the contralateral hippocampus was found, nor was any volumetric atrophy present in that side. Moreover, the MRS of the contralateral hippocampus did not show any significant metabolic abnormalities in the chronic phase either. There are several possible pathological processes and cellular changes that we did not directly test for, that could be the underlying cause of the contralateral T_2, $T_{1\rho}$ and D_{av} observations. When speculating possible reasons for the bilateral damage, one could be that some mechanical shear forces of the impact extended to the contralateral side, and even though in the LFP model there was no damage in the contralateral cortex, the hippocampus might be more sensitive to the disturbances. Another explanation could be the interconnectivity of left and right hippocampi and that the damage then progresses from the ipsilateral side to the contralateral side through some signalling cascades. In any case, the fact that *in vivo* MRI was able to detect the subtle contralateral hippocampal damage is a further demonstration of the sensitivity of quantitative MRI.

Considering the prognostic value of early hippocampal MRI findings we found that the acute and sub acute increase of $T_{1\rho}$, T_2 and diffusion in the hippocampus already correlated with the severity of long-term hippocampal atrophy and hilar neurodegeneration. This is logical since the relaxation and diffusion properties of the hippocampal tissue are indicators of the cell density and if notable cell loss is found in the hippocampus already at early stage, the neurodegenerative processes are most likely to continue and the severity of the final situation mirrors the severity of the initial starting status. In line with the hippocampal atrophy and neuron loss, the cognitive test revealed chronic learning impairment indicating deteriorated hippocampal function. The learning impairment was most severe in those animals with most severe sub acute increase in water diffusion in the ipsilateral hippocampus. The amount of intracerebral hemorrhage appeared to be associated with the performance in water maze as well. This indicates that early MRI (D_{av} and hemorrhage) could have predictive value for chronic learning impairment.

The hippocampus seemed to have a distinct pattern of T_2, $T_{1\rho}$ and D_{av} during the progression of TBI, reflecting the unique role of the hippocampus as a ground for destructive and restructive biological processes. This was seen also in CBV findings. In the ipsilateral hippocampus the CBV in capillaries was increased from day 1 onwards indicating local hyperemia, which in turn could be a sign of angiogenesis (Dunn et al., 2004). However, previous studies have also reported BBB leakage after experimental TBI both in the ipsilateral cortex and in the ipsilateral hippocampus (Schmidt and Grady 1993) which must be accounted for when interpreting the CBV data. The novel hippocampal observations of the CBV approach supports the usefulness of MRI in detecting different brain injury related processes and speaks for the benefits of monitoring also CBV alterations after TBI.

6.3.5 Which MRI approaches should be used after head trauma?

Based on the experiences built up by this thesis work, what would then be the optimal MRI method to use after traumatic brain injury? Time to perform the imaging is limited, so the number of techniques used is limited as well. The palette for imaging TBI should include

standard anatomical T_2 weighted (or T_1 weighted) signal intensity image set covering the whole brain to detect hyperintense lesion and atrophy and to perform volumetric analysis. T_2* weighted scanning is fast and would be required to detect the hemorrhages. Collecting the data for quantitative maps takes slightly more time, and therefore only two are chosen here. Considering the sensitivity and accuracy, the combination of $T_{1\rho}$ and D_{av} appeared to be the most sensitive measure for detecting both acute and sub acute as well as chronic progressive damage. $T_{1\rho}$ was elevated in the lesion region already 3 hours post-injury while acute D_{av} drop revealed perilesional milder damage at the same time point. In the primary lesion all T_2, $T_{1\rho}$ and D_{av} easily detected the tissue degradation from day 3 onwards, but D_{av} was the most sensitive to the chronic progression even after 6 months post-injury. Similarly in the perifocal and the hippocampal regions D_{av} was the most sensitive to the continuous progression from 2 to 3 months. In the sub acute phase, around 9 days post-injury, $T_{1\rho}$ was the only parameter to detect the pathological state of tissue while T_2 and D_{av} appeared misleadingly normal. These findings highlight the need to use multimodal approach when imaging progressive brain diseases. Combining of different MRI contrasts both aids to eliminate false negative findings and brings out more subtle changes than a simplified approach with just one contrast parameter would bring. Adding a imaging modality of tissue perfusion or CBV may not be feasible in every case, but should be considered at least in cases where ischemic condition is suspected or functional deficits are present that are not explained by the location of the primary lesion.

6.3 Methodological considerations

In the case of different MRI techniques it is essential to recognize the challenges in the interpretation of the findings, but equally important is to realise the vast range of applications and targets of MRI probes. With the *a priori* knowledge about the neuropathology and the symptoms, the boundary conditions can be set to aid the interpretation of NMR data. The results presented in this thesis work are based on TBI and epileptogenesis but can be to some extent extrapolated to other neurodegenerative diseases as well. The similar underlying biophysiological processes are present in characteristic form and in characteristic brain regions in several brain pathologies. The introduced MRI methods are equally equipped to probe these other disease processes as well. The sensitivity of diffusion to several type of cellular changes has been reported both in the context of TBI (Graham et al., 2000b; Iwamoto et al., 1997) and epilepsy (Grohn and Pitkanen 2007) as well as in the context of other neurodegenerative diseases such as hippocampal sclerosis (Bote et al., 2008), ischemic stroke (Aronen et al., 2007; van der Zijden et al., 2008), multiple system atrophy (Ito et al., 2007), Parkinson's disease (Au et al., 2006) and Alzheimer's disease(Lehericy et al., 2007). The sensitivity of $T_{1\rho}$ has been previously demonstrated in experimental stroke studies (Grohn et al., 2003; Grohn et al., 2000), in experimental glioma studies (Sierra et al., 2008), and recently in Parkinson's (Michaeli et al., 2007) as well as in Alzheimer's patients (Borthakur et al., 2008), but not in the case of TBI. Our results, however, strongly advocates the potential of $T_{1\rho}$ in the context of TBI and other neurodegenerative diseases as well.

In this thesis work the biggest methodological question rose from the interpretation of CBV data. The obtained values of $\Delta R2$ and $\Delta R2$* are indirect measures of change in the susceptibility contrast agent amount. Drawing conclusions about the actual tissue perfusion based on $\Delta R2$ and $\Delta R2$* is at its best a crude approximation and relying on the assumption that the intravascular contrast agent is indeed remaining inside the vasculature. The interpretation of the situation gets more difficult when head injury is introduced causing

disturbances in autoregulation, mechanical damage to the vasculature and leaking of the BBB. Supported by several cerebral blood flow studies, the acute observed CBV decrease can be linked to hypoperfusion. Since the CO_2 levels in blood do not seem to increase too much after the TBI and during the imaging related anesthesia, the CO_2 can be ruled out as a cause of the observed CBV changes. However, the results about the increase of CBV in the hippocampus must be taken with caution, while the contribution of BBB leakage is not determined. Generally, in this frequent and 2 weeks lasting follow-up the persistent type of CBV increase or decrease most likely reflects a corresponding CBF increase or decrease, of some amount.

The animal models can never completely correspond to the human condition, yet they have provided indispensable information about the underlying processes of the neuropathologies, and about the effects of different interventions. Particularly the complex interactions and progression of neurodegenerative processes can not be studied without the involvement of the complete biological system, and therefore animal models are still needed in the attempt to uncover the molecular biology behind the brain pathologies. In the case of TBI and epilepsy the disease mechanisms are largely not known. The *status epilepticus* animal model used in the epileptogenesis study was chosen because it develops dense mossy fiber sprouting, which is seen also in epilepsy patients, and which may have an important role in seizure generation. Traumatic brain injury was studied in two different models that complement each other. The CCI injury causes larger initial contusion than the LFP model, and is not as reproducable as the LFP, where the pressure impact is mediated by saline rather that by mechanical tip. Both models are widely used and for both histological and behavioural data are available for both. LFP model has been said to mimic human closed head injury with a rather confined lesion, while CCI represents perhaps more penetrating head injury with more frequent intracortical hemorrhages. The MRI results obtained from these models are in line with each other and can be regarded to describe some common alterations taking place after the impact injury.

7 Summary

This thesis work has extensively studied the potential of multimodal MRI to *in vivo* characterize and identify the progression and status of the complex pathological processes during epileptogenesis and traumatic brain injury. The results support the potential role of multimodal MRI in detecting surrogate markers and predicting the long-term outcomes.

The novel information provided by this thesis is straightforwardly applicable to animal studies. The researchers of these same diseases have to take into account the spatio-temporal development of tissue damage when planning and testing the interventions. On the other hand, similar promising MRI procedures should now be applied to several other neurodegenerative diseases in experimental settings. Importantly, most of these MRI techniques can be readily transferred into clinics. If the prognostic value of early *in vivo* MRI can be established with further experimental studies, quantitative multimodal MRI could potentially be integrated into the standard clinical practise after brain insult.

Furthermore, this thesis sheds light on the interpretation of alterations in different MRI contrast parameters by providing an example of the combined and interrelated behaviour of D_{av}, T_2 and $T_{1\rho}$ (as well as T_1 and $\Delta R2$ and $\Delta R2^*$) in the case of traumatic brain injury (and epilepsy) in different states of the disease.

The key findings and conclusions of this thesis work are as follows:

1. The manganese enhanced MRI even after systemic administration was able to detect axonal plasticity in the hippocampus of the epileptic rat, and thereby MEMRI can potentially function as a surrogate marker for epileptogenesis in the experimental setting.

2. Quantitative MRI was able to detect the tissue at risk after traumatic brain injury and revealed a distinct pattern of damage progression in the primary lesion site, perifocal region and in the hippocampus. The ability to non-invasively monitor the long-lasting pathological processes after TBI is of great interest when developing and applying treatments first in pre-clinical and thereafter in clinical studies.

3. The multimodal quantitative MRI measured in the acute (3 hours) and sub acute (3 to 23 days) phases after TBI correlated with the long-term (6 months to 1 year) histopathological and functional outcome. This means that the early MRI assessment may aid to predict the long-term impairment and thereby help with diagnosis and treatment strategy.

4. The iron-oxide contrast enhanced measurement of relaxation rate changes yielded information about the CBV changes after TBI during two weeks follow-up. Regional differences of CBV deviations were revealed and the drop and recovery of CBV in the perifocal cortical region was found to be associated with the parallel drop and recovery of motor functions.

8 References

Abrous, D.N., Rodriguez, J., le Moal, M., Moser, P.C., and Barneoud, P. (1999). Effects of mild traumatic brain injury on immunoreactivity for the inducible transcription factors c-Fos, c-Jun, JunB, and Krox-24 in cerebral regions associated with conditioned fear responding. Brain Res. *826,* 181-192.

Albensi, B.C., Knoblach, S.M., Chew, B.G., O'Reilly, M.P., Faden, A.I., and Pekar, J.J. (2000). Diffusion and high resolution MRI of traumatic brain injury in rats: time course and correlation with histology. Exp. Neurol. *162,* 61-72.

Allen, K.L., Busza, A.L., Proctor, E., King, M.D., Williams, S.R., Crockard, H.A., and Gadian, D.G. (1993). Controllable graded cerebral ischaemia in the gerbil: studies of cerebral blood flow and energy metabolism by hydrogen clearance and 31P NMR spectroscopy. NMR Biomed. *6,* 181-186.

Annegers, J.F., Rocca, W.A., and Hauser, W.A. (1996). Causes of epilepsy: contributions of the Rochester epidemiology project. Mayo Clin. Proc. *71,* 570-575.

Aoki, I., Tanaka, C., Takegami, T., Ebisu, T., Umeda, M., Fukunaga, M., Fukuda, K., Silva, A.C., Koretsky, A.P., Naruse, S. (2002). Dynamic activity-induced manganese-dependent contrast magnetic resonance imaging (DAIM MRI). Magn Reson Med. *48,* 927-33.

Aronen, H.J., Laakso, M.P., Moser, M., and Perkio, J. (2007). Diffusion and perfusion-weighted magnetic resonance imaging techniques in stroke recovery. Eura Medicophys *43,* 271-284.

Aschner, M., Aschner, J.L. (1991). Manganese neurotoxicity: cellular effects and blood-brain barrier transport. Neurosci Biobehav Rev. *15*, 333-40.

Ashwal, S., Holshouser, B., Tong, K., Serna, T., Osterdock, R., Gross, M., and Kido, D. (2004). Proton spectroscopy detected myoinositol in children with traumatic brain injury. Pediatr. Res. *56,* 630-638.

Au, W.L., Adams, J.R., Troiano, A., and Stoessl, A.J. (2006). Neuroimaging in Parkinson's disease. J. Neural Transm. Suppl. *70,* 241-248.

Babb, T.L., Pretorius, J.K., Mello, L.E., Mathern, G.W., and Levesque, M.F. (1992). Synaptic reorganizations in epileptic human and rat kainate hippocampus may contribute to feedback and feedforward excitation. Epilepsy Res. Suppl. *9,* 193-202; discussion 203.

Baird, A.E., Benfield, A., Schlaug, G., Siewert, B., Lovblad, K.O., Edelman, R.R., and Warach, S. (1997). Enlargement of human cerebral ischemic lesion volumes measured by diffusion-weighted magnetic resonance imaging. Ann. Neurol. *41,* 581-589.

Baron, J.C. (2001). Perfusion thresholds in human cerebral ischemia: historical perspective and therapeutic implications. Cerebrovasc. Dis. *11 Suppl 1,* 2-8.

Basser, B.J., Mattiello, J., and Le Bihan, D. (1994). MR diffusion tensor spectroscopy and imaging. Biophys J *66,* 259-267.

Beaumont, A., Marmarou, A., Hayasaki, K., Barzo, P., Fatouros, P., Corwin, F., Marmarou, C., and Dunbar, J. (2000). The permissive nature of blood brain barrier (BBB) opening in edema formation following traumatic brain injury. Acta Neurochir. Suppl. *76,* 125-129.

Behar, K.L., and Ogino, T. (1993). Characterization of macromolecule resonances in the 1H NMR spectrum of rat brain. Magn. Reson. Med. *30,* 38-44.

Belanger, H.G., Vanderploeg, R.D., Curtiss, G., and Warden, D.L. (2007). Recent neuroimaging techniques in mild traumatic brain injury. J. Neuropsychiatry Clin. Neurosci. *19,* 5-20.

Ben-Ari, Y. (1985). Limbic seizure and brain damage produced by kainic acid: mechanisms and relevance to human temporal lobe epilepsy. Neuroscience *14,* 375-403.

Ben-Ari, Y., and Holmes, G.L. (2005). The multiple facets of gamma-aminobutyric acid dysfunction in epilepsy. Curr. Opin. Neurol. *18,* 141-145.

Bender, R.A., Dube, C., Gonzalez-Vega, R., Mina, E.W., and Baram, T.Z. (2003). Mossy fiber plasticity and enhanced hippocampal excitability, without hippocampal cell loss or altered neurogenesis, in an animal model of prolonged febrile seizures. Hippocampus *13,* 399-412.

Berry, I., Moseley, M., Germano, I.M., Ishige, N., Nishimura, M.C., Bartkowski, H.M., Pitts, L.H., and Brant-Zawadzki, M. (1986). Combined magnetic resonance imaging and spectroscopy in experimental regional injury of the brain. Ischemia and impact trauma. Acta Radiol. Suppl. *369,* 338-349.

Bonne, O., Gilboa, A., Louzoun, Y., Kempf-Sherf, O., Katz, M., Fishman, Y., Ben-Nahum, Z., Krausz, Y., Bocher, M., Lester, H., Chisin, R., and Lerer, B. (2003). Cerebral blood flow in chronic symptomatic mild traumatic brain injury. Psychiatry Res. *124,* 141-152.

Borthakur, A., Sochor, M., Davatzikos, C., Trojanowski, J.Q., and Clark, C.M. (2008). T1rho MRI of Alzheimer's disease. Neuroimage *41,* 1199-1205.

Bote, R.P., Blazquez-Llorca, L., Fernandez-Gil, M.A., Alonso-Nanclares, L., Munoz, A., and De Felipe, J. (2008). Hippocampal sclerosis: histopathology substrate and magnetic resonance imaging. Semin. Ultrasound CT MR *29,* 2-14.

Bouma, G.J., and Muizelaar, J.P. (1990). Relationship between cardiac output and cerebral blood flow in patients with intact and with impaired autoregulation. J. Neurosurg. *73,* 368-374.

Bramlett, H.M., Kraydieh, S., Green, E.J., and Dietrich, W.D. (1997). Temporal and regional patterns of axonal damage following traumatic brain injury: a beta-amyloid precursor protein immunocytochemical study in rats. J. Neuropathol. Exp. Neurol. *56,* 1132-1141.

Brand, A., Richter-Landsberg, C., and Leibfritz, D. (1993). Multinuclear NMR studies on the energy metabolism of glial and neuronal cells. Dev. Neurosci. *15,* 289-298.

Brulatout, S., Meric, P., Loubinoux, I., Borredon, J., Correze, J.L., Roucher, P., Gillet, B., Berenger, G., Beloeil, J.C., Tiffon, B., Mispelter, J., and Seylaz, J. (1996). A one-dimensional (proton and phosphorus) and two-dimensional (proton) in vivo NMR spectroscopic study of reversible global cerebral ischemia. J. Neurochem. *66,* 2491-2499.

Caroli, M., Locatelli, M., Campanella, R., Balbi, S., Martinelli, F., and Arienta, C. (2001). Multiple intracranial lesions in head injury: clinical considerations, prognostic factors, management, and results in 95 patients. Surg. Neurol. *56,* 82-88.

Catroppa, C., Anderson, V., Ditchfield, M., and Coleman, L. (2008). Using magnetic resonance imaging to predict new learning outcome at 5 years after childhood traumatic brain injury. J. Child Neurol. *23,* 486-496.

Cavazos, J.E., Golarai, G., and Sutula, T.P. (1991). Mossy fiber synaptic reorganization induced by kindling: time course of development, progression, and permanence. J. Neurosci. *11,* 2795-2803.

Cavazos, J.E., Jones, S.M., and Cross, D.J. (2004). Sprouting and synaptic reorganization in the subiculum and CA1 region of the hippocampus in acute and chronic models of partial-onset epilepsy. Neuroscience *126,* 677-688.

Chieregato, A., Fainardi, E., Morselli-Labate, A.M., Antonelli, V., Compagnone, C., Targa, L., Kraus, J., and Servadei, F. (2005). Factors associated with neurological outcome and lesion progression in traumatic subarachnoid hemorrhage patients. Neurosurgery *56,* 671-80; discussion 671-80.

Choi, C.B., Kim, H.Y., Han, D.Y., Kang, Y.W., Han, Y.M., Jeun, S.S., and Choe, B.Y. (2005). In vivo 1H MR spectroscopic findings in traumatic contusion of ICR mouse brain induced by fluid percussion injury. Eur. J. Radiol. *55,* 96-101.

Chuang, K.H., Lee, J.H., Silva, A.C., Belluscio, L., and Koretsky, A.P. (2008). Manganese enhanced MRI reveals functional circuitry in response to odorant stimuli. Neuroimage

Cohen, A.S., Pfister, B.J., Schwarzbach, E., Grady, M.S., Goforth, P.B., and Satin, L.S. (2007). Injury-induced alterations in CNS electrophysiology. Prog. Brain Res. *161,* 143-169.

Connelly, A., Jackson, G.D., Duncan, J.S., King, M.D., and Gadian, D.G. (1994). Magnetic resonance spectroscopy in temporal lobe epilepsy. Neurology *44,* 1411-1417.

Conti, A.C., Raghupathi, R., Trojanowski, J.Q., and McIntosh, T.K. (1998). Experimental brain injury induces regionally distinct apoptosis during the acute and delayed post-traumatic period. J. Neurosci. *18,* 5663-5672.

Cortez, S.C., McIntosh, T.K., and Noble, L.J. (1989a). Experimental fluid percussion brain injury: vascular disruption and neuronal and glial alterations. Brain Res. *482,* 271-282.

Cortez, S.C., McIntosh, T.K., and Noble, L.J. (1989b). Experimental fluid percussion brain injury: vascular disruption and neuronal and glial alterations. Brain Res. *482,* 271-282.

Covolan, L., and Mello, L.E. (2000). Temporal profile of neuronal injury following pilocarpine or kainic acid-induced status epilepticus. Epilepsy Res. *39,* 133-152.

Covolan, L., Ribeiro, L.T., Longo, B.M., and Mello, L.E. (2000). Cell damage and neurogenesis in the dentate granule cell layer of adult rats after pilocarpine- or kainate-induced status epilepticus. Hippocampus *10,* 169-180.

de Graaf, R.A. (2007). *in vivo* NMR Spectroscopy, Principles and Techniques.

de Graaf, R.A., Braun, K.P., and Nicolay, K. (2001). Single-shot diffusion trace (1)H NMR spectroscopy. Magn. Reson. Med. *45,* 741-748.

De Stefano, N., Matthews, P.M., and Arnold, D.L. (1995). Reversible decreases in N-acetylaspartate after acute brain injury. Magn. Reson. Med. *34,* 721-727.

Dennie, J., Mandeville, J.B., Boxerman, J.L., Packard, S.D., Rosen, B.R., and Weisskoff, R.M. (1998). NMR imaging of changes in vascular morphology due to tumor angiogenesis. Magn. Reson. Med. *40,* 793-799.

Dietrich, W.D., Alonso, O., Busto, R., and Ginsberg, M.D. (1994). Widespread metabolic depression and reduced somatosensory circuit activation following traumatic brain injury in rats. J. Neurotrauma *11,* 629-640.

Dietrich, W.D., Alonso, O., Busto, R., Prado, R., Zhao, W., Dewanjee, M.K., and Ginsberg, M.D. (1998). Posttraumatic cerebral ischemia after fluid percussion brain injury: an autoradiographic and histopathological study in rats. Neurosurgery *43,* 585-93; discussion 593-4.

Dietrich, W.D., Alonso, O., and Halley, M. (1994a). Early microvascular and neuronal consequences of traumatic brain injury: a light and electron microscopic study in rats. J. Neurotrauma *11,* 289-301.

Dietrich, W.D., Alonso, O., and Halley, M. (1994b). Early microvascular and neuronal consequences of traumatic brain injury: a light and electron microscopic study in rats. J. Neurotrauma *11,* 289-301.

Dixon, C.E., Clifton, G.L., Lighthall, J.W., Yaghmai, A.A., and Hayes, R.L. (1991). A controlled cortical impact model of traumatic brain injury in the rat. J. Neurosci. Methods *39,* 253-262.

Dube, C., Boyet, S., Marescaux, C., and Nehlig, A. (2001). Relationship between neuronal loss and interictal glucose metabolism during the chronic phase of the lithium-pilocarpine model of epilepsy in the immature and adult rat. Exp. Neurol. *167,* 227-241.

Dube, C., Yu, H., Nalcioglu, O., and Baram, T.Z. (2004). Serial MRI after experimental febrile seizures: altered T2 signal without neuronal death. Ann. Neurol. *56,* 709-714.

Dunn, J.F., Roche, M.A., Springett, R., Abajian, M., Merlis, J., Daghlian, C.P., Lu, S.Y., and Makki, M. (2004). Monitoring angiogenesis in brain using steady-state quantification of DeltaR2 with MION infusion. Magn. Reson. Med. *51,* 55-61.

Engel, J.,Jr. (1996). Introduction to temporal lobe epilepsy. Epilepsy Res. *26,* 141-150.

Engel, J.,Jr. (1989). Seizures and epilepsy.

Erecinska, M., and Silver, I.A. (1990). Metabolism and role of glutamate in mammalian brain. Prog. Neurobiol. *35,* 245-296.

Faden, A.I., Demediuk, P., Panter, S.S., and Vink, R. (1989). The role of excitatory amino acids and NMDA receptors in traumatic brain injury. Science *244,* 798-800.

Federico, F., Conte, C., Simone, I.L., Giannini, P., Liguori, M., Picciola, E., Tortorella, C., and Ferrari, E. (1994). Proton magnetic resonance spectroscopy in patients with ischemic stroke. Ital. J. Neurol. Sci. *15,* 413-420.

Fenstermacher, M.J., and Narayana, P.A. (1990). Serial proton magnetic resonance spectroscopy of ischemic brain injury in humans. Invest. Radiol. *25,* 1034-1039.

Fernandes, M.J., Dube, C., Boyet, S., Marescaux, C., and Nehlig, A. (1999). Correlation between hypermetabolism and neuronal damage during status epilepticus induced by lithium and pilocarpine in immature and adult rats. J. Cereb. Blood Flow Metab. *19,* 195-209.

Finelli, D.A., Hopkins, A.L., Selman, W.R., Crumrine, R.C., Bhatti, S.U., and Lust, W.D. (1992). Evaluation of experimental early acute cerebral ischemia before the development of edema: use of dynamic, contrast-enhanced and diffusion-weighted MR scanning. Magn. Reson. Med. *27,* 189-197.

Firbank, M.J., Harrison, R.M., and O'Brien, J.T. (2002). A comprehensive review of proton magnetic resonance spectroscopy studies in dementia and Parkinson's disease. Dement. Geriatr. Cogn. Disord. *14,* 64-76.

Frahm, J., Bruhn, H., Gyngell, M.L., Merboldt, K.D., Hanicke, W., and Sauter, R. (1989). Localized high-resolution proton NMR spectroscopy using stimulated echoes: initial applications to human brain in vivo. Magn. Reson. Med. *9,* 79-93.

Fujikawa, D.G., Shinmei, S.S., and Cai, B. (2000). Kainic acid-induced seizures produce necrotic, not apoptotic, neurons with internucleosomal DNA cleavage: implications for programmed cell death mechanisms. Neuroscience *98,* 41-53.

Gadian, D.G. (1995). NMR and its applications to living systems.

Gallagher, C.N., Hutchinson, P.J., and Pickard, J.D. (2007). Neuroimaging in trauma. Curr. Opin. Neurol. *20,* 403-409.

Garcia, J.H., Wagner, S., Liu, K.F., and Hu, X.J. (1995). Neurological deficit and extent of neuronal necrosis attributable to middle cerebral artery occlusion in rats. Statistical validation. Stroke *26,* 627-34; discussion 635.

Garnett, M.R., Blamire, A.M., Corkill, R.G., Cadoux-Hudson, T.A., Rajagopalan, B., and Styles, P. (2000). Early proton magnetic resonance spectroscopy in normal-appearing brain correlates with outcome in patients following traumatic brain injury. Brain *123 (Pt 10),* 2046-2054.

Gennarelli, T.A., and Graham, D.I. (1998). Neuropathology of the Head Injuries. Semin. Clin. Neuropsychiatry *3,* 160-175.

Gillies, R.J., and Morse, D.L. (2005). In vivo magnetic resonance spectroscopy in cancer. Annu. Rev. Biomed. Eng. *7,* 287-326.

Ginsberg, M.D., Zhao, W., Alonso, O.F., Loor-Estades, J.Y., Dietrich, W.D., and Busto, R. (1997). Uncoupling of local cerebral glucose metabolism and blood flow after acute fluid-percussion injury in rats. Am. J. Physiol. *272,* H2859-68.

Goddard, A.W., Mason, G.F., Almai, A., Rothman, D.L., Behar, K.L., Petroff, O.A., Charney, D.S., and Krystal, J.H. (2001). Reductions in occipital cortex GABA levels in panic disorder detected with 1h-magnetic resonance spectroscopy. Arch. Gen. Psychiatry *58,* 556-561.

Godfrey, D.A., Hallcher, L.M., Laird, M.H., Matschinsky, F.M., and Sherman, W.R. (1982). Distribution of myo-inositol in the cat cochlear nucleus. J. Neurochem. *38,* 939-947.

Golding, E.M., Robertson, C.S., and Bryan, R.M.,Jr. (1999). The consequences of traumatic brain injury on cerebral blood flow and autoregulation: a review. Clin. Exp. Hypertens. *21,* 299-332.

Graham, D.I., McIntosh, T.K., Maxwell, W.L., and Nicoll, J.A. (2000). Recent advances in neurotrauma. J. Neuropathol. Exp. Neurol. *59,* 641-651.

Graham, D.I., Raghupathi, R., Saatman, K.E., Meaney, D., and McIntosh, T.K. (2000). Tissue tears in the white matter after lateral fluid percussion brain injury in the rat: relevance to human brain injury. Acta Neuropathol. *99,* 117-124.

Graham, G.D., Hwang, J.H., Rothman, D.L., and Prichard, J.W. (2001). Spectroscopic assessment of alterations in macromolecule and small-molecule metabolites in human brain after stroke. Stroke *32,* 2797-2802.

Griffiths, D.J. (1995). Introduction to Quantum Mechanics.

Grohn, H.I., Michaeli, S., Garwood, M., Kauppinen, R.A., and Grohn, O.H. (2005). Quantitative T(1rho) and adiabatic Carr-Purcell T2 magnetic resonance imaging of human occipital lobe at 4 T. Magn. Reson. Med. *54,* 14-19.

Grohn, O., and Pitkanen, A. (2007). Magnetic resonance imaging in animal models of epilepsy-noninvasive detection of structural alterations. Epilepsia *48 Suppl 4,* 3-10.

Grohn, O.H., Makela, H.I., Lukkarinen, J.A., DelaBarre, L., Lin, J., Garwood, M., and Kauppinen, R.A. (2003). On- and off-resonance T(1rho) MRI in acute cerebral ischemia of the rat. Magn. Reson. Med. *49,* 172-176.

Grohn, O.H.J., Kettunen, M.I., Makela, H.I., Penttonen, M., Pitkanen, A., Lukkarinen, J.A., and Kauppinen, R.A. (2000). Early detection of irreversible cerebral ischemia in the rat using dispersion of the magnetic resonance imaging relaxation time, T1rho. J. Cereb. Blood Flow Metab. *20,* 1457-1466.

Haacke, E.M. (1999). Magnetic Resonance Imaging Physical Principles and Sequence Design.

Haapanen, A., Ramadan, U.A., Autti, T., Joensuu, R., and Tyynela, J. (2007). In vivo MRI reveals the dynamics of pathological changes in the brains of cathepsin D-deficient mice and correlates changes in manganese-enhanced MRI with microglial activation. Magn. Reson. Imaging *25*, 1024-31

Hahn, E.L. (1950). Spin-echoes. Physical Rev *80,* 580-594.

Hallam, T.M., Floyd, C.L., Folkerts, M.M., Lee, L.L., Gong, Q.Z., Lyeth, B.G., Muizelaar, J.P., and Berman, R.F. (2004). Comparison of behavioral deficits and acute neuronal degeneration in rat lateral fluid percussion and weight-drop brain injury models. J. Neurotrauma *21,* 521-539.

Hammen, T., Stefan, H., Eberhardt, K.E., W-Huk, B.H., and Tomandl, B.F. (2003). Clinical applications of 1H-MR spectroscopy in the evaluation of epilepsies--what do pathological spectra stand for with regard to current results and what answers do they give to common clinical questions concerning the treatment of epilepsies? Acta Neurol. Scand. *108,* 223-238.

Hoehn-Berlage, M., Norris, D.G., Kohno, K., Mies, G., Leibfritz, D., and Hossmann, K.A. (1995). Evolution of regional changes in apparent diffusion coefficient during focal ischemia of rat brain: the relationship of

quantitative diffusion NMR imaging to reduction in cerebral blood flow and metabolic disturbances. J. Cereb. Blood Flow Metab. *15,* 1002-1011.

Hossmann, K.A., and Schuier, F.J. (1980). Experimental brain infarcts in cats. I. Pathophysiological observations. Stroke *11,* 583-592.

Houser, C.R. (1990). Granule cell dispersion in the dentate gyrus of humans with temporal lobe epilepsy. Brain Res. *535,* 195-204.

Houser, C.R., Miyashiro, J.E., Swartz, B.E., Walsh, G.O., Rich, J.R., and Delgado-Escueta, A.V. (1990). Altered patterns of dynorphin immunoreactivity suggest mossy fiber reorganization in human hippocampal epilepsy. J. Neurosci. *10,* 267-282.

Howe, F.A., Barton, S.J., Cudlip, S.A., Stubbs, M., Saunders, D.E., Murphy, M., Wilkins, P., Opstad, K.S., Doyle, V.L., McLean, M.A., Bell, B.A., and Griffiths, J.R. (2003). Metabolic profiles of human brain tumors using quantitative in vivo 1H magnetic resonance spectroscopy. Magn. Reson. Med. *49,* 223-232.

Isokawa, M., Levesque, M.F., Babb, T.L., and Engel, J.,Jr. (1993). Single mossy fiber axonal systems of human dentate granule cells studied in hippocampal slices from patients with temporal lobe epilepsy. J. Neurosci. *13,* 1511-1522.

Ito, M., Watanabe, H., Kawai, Y., Atsuta, N., Tanaka, F., Naganawa, S., Fukatsu, H., and Sobue, G. (2007). Usefulness of combined fractional anisotropy and apparent diffusion coefficient values for detection of involvement in multiple system atrophy. J. Neurol. Neurosurg. Psychiatry. *78,* 722-728.

Iwamoto, Y., Yamaki, T., Murakami, N., Umeda, M., Tanaka, C., Higuchi, T., Aoki, I., Naruse, S., and Ueda, S. (1997). Investigation of morphological change of lateral and midline fluid percussion injury in rats, using magnetic resonance imaging. Neurosurgery *40,* 163-167.

Jansen, J.F., Lemmens, E.M., Strijkers, G.J., Prompers, J.J., Schijns, O.E., Kooi, M.E., Beuls, E.A., Nicolay, K., Backes, W.H., and Hoogland, G. (2008). Short- and long-term limbic abnormalities after experimental febrile seizures. Neurobiol. Dis.

Jutila, L., Immonen, A., Partanen, K., Partanen, J., Mervaala, E., Ylinen, A., Alafuzoff, I., Paljarvi, L., Karkola, K., Vapalahti, M., and Pitkanen, A. (2002). Neurobiology of epileptogenesis in the temporal lobe. Adv. Tech. Stand. Neurosurg. *27,* 5-22.

Karhunen, H., Jolkkonen, J., Sivenius, J., and Pitkanen, A. (2005). Epileptogenesis after experimental focal cerebral ischemia. Neurochem. Res. *30,* 1529-1542.

Karhunen, H., Pitkanen, A., Virtanen, T., Gureviciene, I., Pussinen, R., Ylinen, A., Sivenius, J., Nissinen, J., and Jolkkonen, J. (2003). Long-term functional consequences of transient occlusion of the middle cerebral artery in rats: a 1-year follow-up of the development of epileptogenesis and memory impairment in relation to sensorimotor deficits. Epilepsy Res. *54,* 1-10.

Katayama, Y., Becker, D.P., Tamura, T., and Hovda, D.A. (1990). Massive increases in extracellular potassium and the indiscriminate release of glutamate following concussive brain injury. J. Neurosurg. *73,* 889-900.

Kauppinen, R.A., Kokko, H., and Williams, S.R. (1992). Detection of mobile proteins by proton nuclear magnetic resonance spectroscopy in the guinea pig brain ex vivo and their partial purification. J. Neurochem. *58,* 967-974.

Kauppinen, R.A., Niskanen, T., Hakumaki, J., and Williams, S.R. (1993). Quantitative analysis of 1H NMR detected proteins in the rat cerebral cortex in vivo and in vitro. NMR Biomed. *6,* 242-247.

Kelly, D.F., Kordestani, R.K., Martin, N.A., Nguyen, T., Hovda, D.A., Bergsneider, M., McArthur, D.L., and Becker, D.P. (1996). Hyperemia following traumatic brain injury: relationship to intracranial hypertension and outcome. J. Neurosurg. *85,* 762-771.

Kelly, D.F., Martin, N.A., Kordestani, R., Counelis, G., Hovda, D.A., Bergsneider, M., McBride, D.Q., Shalmon, E., Herman, D., and Becker, D.P. (1997). Cerebral blood flow as a predictor of outcome following traumatic brain injury. J. Neurosurg. *86,* 633-641.

Kharatishvili, I., Immonen, R., Grohn, O., and Pitkanen, A. (2007). Quantitative diffusion MRI of hippocampus as a surrogate marker for post-traumatic epileptogenesis. Brain *130,* 3155-3168.

Kharatishvili, I., Nissinen, J.P., McIntosh, T.K., and Pitkanen, A. (2006a). A model of posttraumatic epilepsy induced by lateral fluid-percussion brain injury in rats. Neuroscience *140,* 685-697.

Kharatishvili, I., Nissinen, J.P., McIntosh, T.K., and Pitkanen, A. (2006b). A model of posttraumatic epilepsy induced by lateral fluid-percussion brain injury in rats. Neuroscience *140,* 685-697.

Kharatishvili, I., Nissinen, J.P., McIntosh, T.K., and Pitkanen, A. (2006c). A model of posttraumatic epilepsy induced by lateral fluid-percussion brain injury in rats. Neuroscience *140,* 685-697.

King, M.D., van Bruggen, N., Ahier, R.G., Cremer, J.E., Hajnal, J.V., Williams, S.R., and Doran, M. (1991). Diffusion-weighted imaging of kainic acid lesions in the rat brain. Magn. Reson. Med. *20,* 158-164.

Kuo, Y.T., Herlihy, A.H., So, P.W., and Bell, J.D. (2006). Manganese-enhanced magnetic resonance imaging (MEMRI) without compromise of the blood-brain barrier detects hypothalamic neuronal activity in vivo. NMR Biomed. *19,* 1028-1034.

Kuo, Y.T., Herlihy, A.H., So, P.W., Bhakoo, K.K., and Bell, J.D. (2005). In vivo measurements of T1 relaxation times in mouse brain associated with different modes of systemic administration of manganese chloride. J. Magn. Reson. Imaging *21,* 334-339.

Kurth, S.M., Bigler, E.D., and Blatter, D.D. (1994). Neuropsychological outcome and quantitative image analysis of acute haemorrhage in traumatic brain injury: preliminary findings. Brain Inj. *8,* 489-500.

Le Bihan, D., Mangin, J.F., Poupon, C., Clark, C.A., Pappata, S., Molko, N., and Chabriat, H. (2001). Diffusion tensor imaging: concepts and applications. J. Magn. Reson. Imaging *13,* 534-546.

Lee, J.H., Silva, A.C., Merkle, H., and Koretsky, A.P. (2005). Manganese-enhanced magnetic resonance imaging of mouse brain after systemic administration of MnCl2: dose-dependent and temporal evolution of T1 contrast. Magn. Reson. Med. *53,* 640-648.

Lehericy, S., Marjanska, M., Mesrob, L., Sarazin, M., and Kinkingnehun, S. (2007). Magnetic resonance imaging of Alzheimer's disease. Eur. Radiol. *17,* 347-362.

Lenzlinger, P.M., Morganti-Kossmann, M.C., Laurer, H.L., and McIntosh, T.K. (2001). The duality of the inflammatory response to traumatic brain injury. Mol. Neurobiol. *24,* 169-181.

Leon-Carrion, J., Dominguez-Morales Mdel, R., Barroso y Martin, J.M., and Murillo-Cabezas, F. (2005a). Epidemiology of traumatic brain injury and subarachnoid hemorrhage. Pituitary *8,* 197-202.

Leon-Carrion, J., Dominguez-Morales Mdel, R., Barroso y Martin, J.M., and Murillo-Cabezas, F. (2005b). Epidemiology of traumatic brain injury and subarachnoid hemorrhage. Pituitary *8,* 197-202.

Lewine, J.D., Davis, J.T., Bigler, E.D., Thoma, R., Hill, D., Funke, M., Sloan, J.H., Hall, S., and Orrison, W.W. (2007). Objective documentation of traumatic brain injury subsequent to mild head trauma: multimodal brain imaging with MEG, SPECT, and MRI. J. Head Trauma Rehabil. *22,* 141-155.

Mac Donald, C.L., Dikranian, K., Song, S.K., Bayly, P.V., Holtzman, D.M., and Brody, D.L. (2007). Detection of traumatic axonal injury with diffusion tensor imaging in a mouse model of traumatic brain injury. Exp. Neurol. *205,* 116-131.

Malisza, K.L., Kozlowski, P., and Peeling, J. (1998). A review of in vivo 1H magnetic resonance spectroscopy of cerebral ischemia in rats. Biochem. Cell Biol. *76,* 487-496.

Marino, S., Zei, E., Battaglini, M., Vittori, C., Buscalferri, A., Bramanti, P., Federico, A., and De Stefano, N. (2007). Acute metabolic brain changes following traumatic brain injury and their relevance to clinical severity and outcome. J. Neurol. Neurosurg. Psychiatry. *78,* 501-507.

Marmarou, A., Fatouros, P.P., Barzo, P., Portella, G., Yoshihara, M., Tsuji, O., Yamamoto, T., Laine, F., Signoretti, S., Ward, J.D., Bullock, M.R., and Young, H.F. (2000). Contribution of edema and cerebral blood volume to traumatic brain swelling in head-injured patients. J. Neurosurg. *93,* 183-193.

Martin, N.A., Patwardhan, R.V., Alexander, M.J., Africk, C.Z., Lee, J.H., Shalmon, E., Hovda, D.A., and Becker, D.P. (1997). Characterization of cerebral hemodynamic phases following severe head trauma: hypoperfusion, hyperemia, and vasospasm. J. Neurosurg. *87,* 9-19.

Mathern, G.W., Babb, T.L., Vickrey, B.G., Melendez, M., and Pretorius, J.K. (1994). Traumatic compared to non-traumatic clinical-pathologic associations in temporal lobe epilepsy. Epilepsy Res. *19,* 129-139.

Mathern, G.W., Cifuentes, F., Leite, J.P., Pretorius, J.K., and Babb, T.L. (1993). Hippocampal EEG excitability and chronic spontaneous seizures are associated with aberrant synaptic reorganization in the rat intrahippocampal kainate model. Electroencephalogr. Clin. Neurophysiol. *87,* 326-339.

McIntosh, T.K. (1994). Neurochemical sequelae of traumatic brain injury: therapeutic implications. Cerebrovasc. Brain Metab. Rev. *6,* 109-162.

McIntosh, T.K., Smith, D.H., Meaney, D.F., Kotapka, M.J., Gennarelli, T.A., and Graham, D.I. (1996). Neuropathological sequelae of traumatic brain injury: relationship to neurochemical and biomechanical mechanisms. Lab. Invest. *74,* 315-342.

McIntosh, T.K., Vink, R., Noble, L., Yamakami, I., Fernyak, S., Soares, H., and Faden, A.L. (1989). Traumatic brain injury in the rat: characterization of a lateral fluid-percussion model. Neuroscience *28,* 233-244.

Mello, L.E., Cavalheiro, E.A., Tan, A.M., Kupfer, W.R., Pretorius, J.K., Babb, T.L., and Finch, D.M. (1993). Circuit mechanisms of seizures in the pilocarpine model of chronic epilepsy: cell loss and mossy fiber sprouting. Epilepsia *34,* 985-995.

Mello, L.E., Cavalheiro, E.A., Tan, A.M., Pretorius, J.K., Babb, T.L., and Finch, D.M. (1992). Granule cell dispersion in relation to mossy fiber sprouting, hippocampal cell loss, silent period and seizure frequency in the pilocarpine model of epilepsy. Epilepsy Res. Suppl. *9,* 51-9; discussion 59-60.

Metting, Z., Rodiger, L.A., De Keyser, J., and van der Naalt, J. (2007). Structural and functional neuroimaging in mild-to-moderate head injury. Lancet Neurol. *6,* 699-710.

Michaeli, S., Oz, G., Sorce, D.J., Garwood, M., Ugurbil, K., Majestic, S., and Tuite, P. (2007). Assessment of brain iron and neuronal integrity in patients with Parkinson's disease using novel MRI contrasts. Mov. Disord. *22,* 334-340.

Minematsu, K., Li, L., Fisher, M., Sotak, C.H., Davis, M.A., and Fiandaca, M.S. (1992a). Diffusion-weighted magnetic resonance imaging: rapid and quantitative detection of focal brain ischemia. Neurology *42,* 235-240.

Minematsu, K., Li, L., Sotak, C.H., Davis, M.A., and Fisher, M. (1992b). Reversible focal ischemic injury demonstrated by diffusion-weighted magnetic resonance imaging in rats. Stroke *23,* 1304-10; discussion 1310-1.

Mintorovitch, J., Moseley, M.E., Chileuitt, L., Shimizu, H., Cohen, Y., and Weinstein, P.R. (1991). Comparison of diffusion- and T2-weighted MRI for the early detection of cerebral ischemia and reperfusion in rats. Magn. Reson. Med. *18,* 39-50.

Mlynarik, V., Cudalbu, C., Xin, L., and Gruetter, R. (2008). 1H NMR spectroscopy of rat brain in vivo at 14.1Tesla: improvements in quantification of the neurochemical profile. J. Magn. Reson. *194,* 163-168.

Morais, D.F., Spotti, A.R., Tognola, W.A., Gaia, F.F., and Andrade, A.F. (2008). Clinical application of magnetic resonance in acute traumatic brain injury. Arq. Neuropsiquiatr. *66,* 53-58.

Morganti-Kossmann, M.C., Rancan, M., Stahel, P.F., and Kossmann, T. (2002). Inflammatory response in acute traumatic brain injury: a double-edged sword. Curr. Opin. Crit. Care *8,* 101-105.

Mori, S., and van Zijl, P.C. (1995). Diffusion weighting by the trace of the diffusion tensor within a single scan. Magn. Reson. Med. *33,* 41-52.

Muir, J.K., Boerschel, M., and Ellis, E.F. (1992). Continuous monitoring of posttraumatic cerebral blood flow using laser-Doppler flowmetry. J. Neurotrauma *9,* 355-362.

Nairismagi, J., Grohn, O.H., Kettunen, M.I., Nissinen, J., Kauppinen, R.A., and Pitkanen, A. (2004). Progression of brain damage after status epilepticus and its association with epileptogenesis: a quantitative MRI study in a rat model of temporal lobe epilepsy. Epilepsia *45,* 1024-1034.

Nairismagi, J., Pitkanen, A., Narkilahti, S., Huttunen, J., Kauppinen, R.A., and Grohn, O.H. (2006a). Manganese-enhanced magnetic resonance imaging of mossy fiber plasticity in vivo. Neuroimage *30,* 130-135.

Nairismagi, J., Pitkanen, A., Narkilahti, S., Huttunen, J., Kauppinen, R.A., and Grohn, O.H. (2006b). Manganese-enhanced magnetic resonance imaging of mossy fiber plasticity in vivo. Neuroimage *30,* 130-135.

Narayana, P.A. (2005). Magnetic resonance spectroscopy in the monitoring of multiple sclerosis. J. Neuroimaging *15,* 46S-57S.

Natt, O., Watanabe, T., Boretius, S., Radulovic, J., Frahm, J., and Michaelis, T. (2002). High-resolution 3D MRI of mouse brain reveals small cerebral structures in vivo. J. Neurosci. Methods *120,* 203-209.

Nissinen, J., Halonen, T., Koivisto, E., and Pitkanen, A. (2000a). A new model of chronic temporal lobe epilepsy induced by electrical stimulation of the amygdala in rat. Epilepsy Res. *38,* 177-205.

Nissinen, J., Halonen, T., Koivisto, E., and Pitkanen, A. (2000b). A new model of chronic temporal lobe epilepsy induced by electrical stimulation of the amygdala in rat. Epilepsy Res. *38,* 177-205.

Nissinen, J., Large, C.H., Stratton, S.C., and Pitkanen, A. (2004). Effect of lamotrigine treatment on epileptogenesis: an experimental study in rat. Epilepsy Res. *58,* 119-132.

Nissinen, J., Lukasiuk, K., and Pitkanen, A. (2001). Is mossy fiber sprouting present at the time of the first spontaneous seizures in rat experimental temporal lobe epilepsy? Hippocampus *11,* 299-310.

Obenaus, A., Robbins, M., Blanco, G., Galloway, N.R., Snissarenko, E., Gillard, E., Lee, S., and Curras-Collazo, M. (2007). Multi-modal magnetic resonance imaging alterations in two rat models of mild neurotrauma. J. Neurotrauma *24,* 1147-1160.

Obrenovitch, T.P., Garofalo, O., Harris, R.J., Bordi, L., Ono, M., Momma, F., Bachelard, H.S., and Symon, L. (1988). Brain tissue concentrations of ATP, phosphocreatine, lactate, and tissue pH in relation to reduced cerebral blood flow following experimental acute middle cerebral artery occlusion. J. Cereb. Blood Flow Metab. *8,* 866-874.

Okunieff, P.G., Koutcher, J.A., Gerweck, L., McFarland, E., Hitzig, B., Urano, M., Brady, T., Neuringer, L., and Suit, H.D. (1986). Tumor size dependent changes in a murine fibrosarcoma: use of in vivo 31P NMR for non-invasive evaluation of tumor metabolic status. Int. J. Radiat. Oncol. Biol. Phys. *12,* 793-799.

Onyszchuk, G., Al-Hafez, B., He, Y.Y., Bilgen, M., Berman, N.E., and Brooks, W.M. (2007). A mouse model of sensorimotor controlled cortical impact: characterization using longitudinal magnetic resonance imaging, behavioral assessments and histology. J. Neurosci. Methods *160,* 187-196.

Overgaard, J., and Tweed, W.A. (1974). Cerebral circulation after head injury. 1. Cerebral blood flow and its regulation after closed head injury with emphasis on clinical correlations. J. Neurosurg. *41,* 531-541.

Ozawa, Y., Nakamura, T., Sunami, K., Kubota, M., Ito, C., Murai, H., Yamaura, A., and Makino, H. (1991). Study of regional cerebral blood flow in experimental head injury: changes following cerebral contusion and during spreading depression. Neurol. Med. Chir. (Tokyo) *31,* 685-690.

Pasco, A., Lemaire, L., Franconi, F., Lefur, Y., Noury, F., Saint-Andre, J.P., Benoit, J.P., Cozzone, P.J., and Le Jeune, J.J. (2007). Perfusional deficit and the dynamics of cerebral edemas in experimental traumatic brain injury using perfusion and diffusion-weighted magnetic resonance imaging. J. Neurotrauma *24,* 1321-1330.

Pautler, R.G., and Koretsky, A.P. (2002). Tracing odor-induced activation in the olfactory bulbs of mice using manganese-enhanced magnetic resonance imaging. Neuroimage *16,* 441-448.

Paxinos, G., and Watson, C. (1986). The Rat Brain in Stereotaxic Coordinates.

Petroff, O.A., Hyder, F., Rothman, D.L., and Mattson, R.H. (2001). Homocarnosine and seizure control in juvenile myoclonic epilepsy and complex partial seizures. Neurology *56,* 709-715.

Petroff, O.A., Prichard, J.W., Ogino, T., Avison, M., Alger, J.R., and Shulman, R.G. (1986). Combined 1H and 31P nuclear magnetic resonance spectroscopic studies of bicuculline-induced seizures in vivo. Ann. Neurol. *20,* 185-193.

Philips, M.F., Mattiasson, G., Wieloch, T., Bjorklund, A., Johansson, B.B., Tomasevic, G., Martinez-Serrano, A., Lenzlinger, P.M., Sinson, G., Grady, M.S., and McIntosh, T.K. (2001). Neuroprotective and behavioral efficacy of nerve growth factor-transfected hippocampal progenitor cell transplants after experimental traumatic brain injury. J. Neurosurg. *94,* 765-774.

Pierce, A.R., Lo, E.H., Mandeville, J.B., Gonzalez, R.G., Rosen, B.R., and Wolf, G.L. (1997). MRI measurements of water diffusion and cerebral perfusion: their relationship in a rat model of focal cerebral ischemia. J. Cereb. Blood Flow Metab. *17,* 183-190.

Pierce, J.E., Smith, D.H., Trojanowski, J.Q., and McIntosh, T.K. (1998). Enduring cognitive, neurobehavioral and histopathological changes persist for up to one year following severe experimental brain injury in rats. Neuroscience *87,* 359-369.

Pirttila, T.R., Pitkanen, A., Tuunanen, J., and Kauppinen, R.A. (2001). Ex vivo MR microimaging of neuronal damage after kainate-induced status epilepticus in rat: correlation with quantitative histology. Magn. Reson. Med. *46,* 946-954.

Pitkanen, A., Nissinen, J., Jolkkonen, E., Tuunanen, J., and Halonen, T. (1999). Effects of vigabatrin treatment on status epilepticus-induced neuronal damage and mossy fiber sprouting in the rat hippocampus. Epilepsy Res. *33,* 67-85.

Pitkanen, A., Nissinen, J., Lukasiuk, K., Jutila, L., Paljarvi, L., Salmenpera, T., Karkola, K., Vapalahti, M., and Ylinen, A. (2000). Association between the density of mossy fiber sprouting and seizure frequency in experimental and human temporal lobe epilepsy. Epilepsia *41 Suppl 6,* S24-9.

Prichard, J., Rothman, D., Novotny, E., Petroff, O., Kuwabara, T., Avison, M., Howseman, A., Hanstock, C., and Shulman, R. (1991). Lactate rise detected by 1H NMR in human visual cortex during physiologic stimulation. Proc. Natl. Acad. Sci. U. S. A. *88,* 5829-5831.

Racine, R.J. (1972). Modification of seizure activity by electrical stimulation. II. Motor seizure. Electroencephalogr. Clin. Neurophysiol. *32,* 281-294.

Raghupathi, R., Conti, A.C., Graham, D.I., Krajewski, S., Reed, J.C., Grady, M.S., Trojanowski, J.Q., and McIntosh, T.K. (2002). Mild traumatic brain injury induces apoptotic cell death in the cortex that is preceded by decreases in cellular Bcl-2 immunoreactivity. Neuroscience *110,* 605-616.

Rink, A., Fung, K.M., Trojanowski, J.Q., Lee, V.M., Neugebauer, E., and McIntosh, T.K. (1995). Evidence of apoptotic cell death after experimental traumatic brain injury in the rat. Am. J. Pathol. *147,* 1575-1583.

Roberts, T.P., Vexler, Z., Derugin, N., Moseley, M.E., and Kucharczyk, J. (1993). High-speed MR imaging of ischemic brain injury following stenosis of the middle cerebral artery. J. Cereb. Blood Flow Metab. *13,* 940-946.

Roch, C., Leroy, C., Nehlig, A., and Namer, I.J. (2002a). Magnetic resonance imaging in the study of the lithium-pilocarpine model of temporal lobe epilepsy in adult rats. Epilepsia *43,* 325-335.

Roch, C., Leroy, C., Nehlig, A., and Namer, I.J. (2002b). Predictive value of cortical injury for the development of temporal lobe epilepsy in 21-day-old rats: an MRI approach using the lithium-pilocarpine model. Epilepsia *43,* 1129-1136.

Rodriguez-Paez, A.C., Brunschwig, J.P., and Bramlett, H.M. (2005). Light and electron microscopic assessment of progressive atrophy following moderate traumatic brain injury in the rat. Acta Neuropathol. *109,* 603-616.

Ross, B.D., Ernst, T., Kreis, R., Haseler, L.J., Bayer, S., Danielsen, E., Bluml, S., Shonk, T., Mandigo, J.C., Caton, W. *et al*. (1998). 1H MRS in acute traumatic brain injury. J. Magn. Reson. Imaging *8,* 829-840.

Salazar, A.M., Jabbari, B., Vance, S.C., Grafman, J., Amin, D., and Dillon, J.D. (1985). Epilepsy after penetrating head injury. I. Clinical correlates: a report of the Vietnam Head Injury Study. Neurology *35,* 1406-1414.

Salmond, C.H., Menon, D.K., Chatfield, D.A., Williams, G.B., Pena, A., Sahakian, B.J., and Pickard, J.D. (2006). Diffusion tensor imaging in chronic head injury survivors: correlations with learning and memory indices. Neuroimage *29,* 117-124.

Sanacora, G., Gueorguieva, R., Epperson, C.N., Wu, Y.T., Appel, M., Rothman, D.L., Krystal, J.H., and Mason, G.F. (2004). Subtype-specific alterations of gamma-aminobutyric acid and glutamate in patients with major depression. Arch. Gen. Psychiatry *61,* 705-713.

Sanacora, G., Mason, G.F., Rothman, D.L., Behar, K.L., Hyder, F., Petroff, O.A., Berman, R.M., Charney, D.S., and Krystal, J.H. (1999). Reduced cortical gamma-aminobutyric acid levels in depressed patients determined by proton magnetic resonance spectroscopy. Arch. Gen. Psychiatry *56,* 1043-1047.

Sanchez-Pernaute, R., Garcia-Segura, J.M., del Barrio Alba, A., Viano, J., and de Yebenes, J.G. (1999). Clinical correlation of striatal 1H MRS changes in Huntington's disease. Neurology *53,* 806-812.

Santyr, G.E., Fairbanks, E.J., Kelcz, F., and Sorenson, J.A. (1994). Off-resonance spin locking for MR imaging. Magn. Reson. Med. *32,* 43-51.

Sato, M., Chang, E., Igarashi, T., and Noble, L.J. (2001). Neuronal injury and loss after traumatic brain injury: time course and regional variability. Brain Res. *917,* 45-54.

Scheid, R., Ott, D.V., Roth, H., Schroeter, M.L., and von Cramon, D.Y. (2007). Comparative magnetic resonance imaging at 1.5 and 3 Tesla for the evaluation of traumatic microbleeds. J. Neurotrauma *24,* 1811-1816.

Schmidt, R.H., and Grady, M.S. (1993). Regional patterns of blood-brain barrier breakdown following central and lateral fluid percussion injury in rodents. J. Neurotrauma *10,* 415-430.

Schmued, L.C., Albertson, C., and Slikker, W.,Jr. (1997). Fluoro-Jade: a novel fluorochrome for the sensitive and reliable histochemical localization of neuronal degeneration. Brain Res. *751,* 37-46.

Schuhmann, M.U., Stiller, D., Skardelly, M., Thomas, S., Samii, M., and Brinker, T. (2002). Long-time in-vivo metabolic monitoring following experimental brain contusion using proton magnetic resonance spectroscopy. Acta Neurochir. Suppl. *81,* 209-212.

Sepponen, R.E., Pohjonen, J.A., Sipponen, J.T., and Tanttu, J.I. (1985). A method for T1 rho imaging. J. Comput. Assist. Tomogr. *9,* 1007-1011.

Serrano, F., Deshazer, M., Smith, K.D., Ananta, J.S., Wilson, L.J., and Pautler, R.G. (2008). Assessing transneuronal dysfunction utilizing manganese-enhanced MRI (MEMRI). Magn. Reson. Med. *60,* 169-175.

Sherman, W.R., Packman, P.M., Laird, M.H., and Boshans, R.L. (1977). Measurement of myo-inositol in single cells and defined areas of the nervous system by selected ion monitoring. Anal. Biochem. *78,* 119-131.

Shutter, L., Tong, K.A., Lee, A., and Holshouser, B.A. (2006). Prognostic role of proton magnetic resonance spectroscopy in acute traumatic brain injury. J. Head Trauma Rehabil. *21,* 334-349.

Sidaros, A., Engberg, A.W., Sidaros, K., Liptrot, M.G., Herning, M., Petersen, P., Paulson, O.B., Jernigan, T.L., and Rostrup, E. (2008). Diffusion tensor imaging during recovery from severe traumatic brain injury and relation to clinical outcome: a longitudinal study. Brain *131,* 559-572.

Sierra, A., Michaeli, S., Niskanen, J.P., Valonen, P.K., Grohn, H.I., Yla-Herttuala, S., Garwood, M., and Grohn, O.H. (2008). Water spin dynamics during apoptotic cell death in glioma gene therapy probed by T1rho and T2rho. Magn. Reson. Med. *59,* 1311-1319.

Signoretti, S., Marmarou, A., Aygok, G.A., Fatouros, P.P., Portella, G., and Bullock, R.M. (2008). Assessment of mitochondrial impairment in traumatic brain injury using high-resolution proton magnetic resonance spectroscopy. J. Neurosurg. *108,* 42-52.

Silva Afonso C. , L.J.H., Aoki Ichio and Koretsky Alan P. (2004). Review Article Manganese-enhanced magnetic resonance imaging (MEMRI): methodological and practical considerations. NMR Biomed. *17,* 532-543.

Simister, R.J., McLean, M.A., Barker, G.J., and Duncan, J.S. (2003a). A proton magnetic resonance spectroscopy study of metabolites in the occipital lobes in epilepsy. Epilepsia *44,* 550-558.

Simister, R.J., McLean, M.A., Barker, G.J., and Duncan, J.S. (2003b). A proton magnetic resonance spectroscopy study of metabolites in the occipital lobes in epilepsy. Epilepsia *44,* 550-558.

Simister, R.J., McLean, M.A., Salmenpera, T.M., Barker, G.J., and Duncan, J.S. (2008). The effect of epileptic seizures on proton MRS visible neurochemical concentrations. Epilepsy Res.

Simmons, M.L., Frondoza, C.G., and Coyle, J.T. (1991). Immunocytochemical localization of N-acetyl-aspartate with monoclonal antibodies. Neuroscience *45,* 37-45.

Sloviter, R.S. (1994). The functional organization of the hippocampal dentate gyrus and its relevance to the pathogenesis of temporal lobe epilepsy. Ann. Neurol. *35,* 640-654.

Sloviter, R.S. (1982). A simplified Timm stain procedure compatible with formaldehyde fixation and routine paraffin embedding of rat brain. Brain Res. Bull. *8,* 771-774.

Smith, B.N., and Dudek, F.E. (2001). Short- and long-term changes in CA1 network excitability after kainate treatment in rats. J. Neurophysiol. *85,* 1-9.

Smith, D.H., Chen, X.H., Pierce, J.E., Wolf, J.A., Trojanowski, J.Q., Graham, D.I., and McIntosh, T.K. (1997). Progressive atrophy and neuron death for one year following brain trauma in the rat. J. Neurotrauma *14,* 715-727.

Soares, H.D., Hicks, R.R., Smith, D., and McIntosh, T.K. (1995). Inflammatory leukocytic recruitment and diffuse neuronal degeneration are separate pathological processes resulting from traumatic brain injury. J. Neurosci. *15,* 8223-8233.

Sorensen, A.G., Buonanno, F.S., Gonzalez, R.G., Schwamm, L.H., Lev, M.H., Huang-Hellinger, F.R., Reese, T.G., Weisskoff, R.M., Davis, T.L., Suwanwela, N. *et al.* (1996). Hyperacute stroke: evaluation with combined multisection diffusion-weighted and hemodynamically weighted echo-planar MR imaging. Radiology *199,* 391-401.

Squire, L.R., and Zola-Morgan, S. (1991). The medial temporal lobe memory system. Science *253,* 1380-1386.

Stejskal, E.O., and Tanner, J.E. (1965). Spin diffusion measurements: spin-echoes in the presence of a time-dependent fiel gradient. J Chem Phys *42,* 288-292.

Stubbs, M., Rodrigues, L.M., Gusterson, B.A., and Griffiths, J.R. (1990). Monitoring tumor growth and regression by 31P magnetic resonance spectroscopy. Adv. Enzyme Regul. *30,* 217-230.

Sutula, T., Cascino, G., Cavazos, J., Parada, I., and Ramirez, L. (1989). Mossy fiber synaptic reorganization in the epileptic human temporal lobe. Ann. Neurol. *26,* 321-330.

Tagliaferri, F., Compagnone, C., Korsic, M., Servadei, F., and Kraus, J. (2006). A systematic review of brain injury epidemiology in Europe. Acta Neurochir. (Wien) *148,* 255-68; discussion 268.

Takahashi, M., Fritz-Zieroth, B., Chikugo, T., and Ogawa, H. (1993). Differentiation of chronic lesions after stroke in stroke-prone spontaneously hypertensive rats using diffusion weighted MRI. Magn. Reson. Med. *30,* 485-488.

Takasawa, M., Jones, P.S., Guadagno, J.V., Christensen, S., Fryer, T.D., Harding, S., Gillard, J.H., Williams, G.B., Aigbirhio, F.I., Warburton, E.A., Ostergaard, L., and Baron, J.C. (2008). How reliable is perfusion MR in acute stroke? Validation and determination of the penumbra threshold against quantitative PET. Stroke *39,* 870-877.

Tanner, J.E. (1983). Intracellular diffusion of water. Arch Biochem Biophys *224,* 416-428.

Tauck, D.L., and Nadler, J.V. (1985a). Evidence of functional mossy fiber sprouting in hippocampal formation of kainic acid-treated rats. J. Neurosci. *5,* 1016-1022.

Tauck, D.L., and Nadler, J.V. (1985b). Evidence of functional mossy fiber sprouting in hippocampal formation of kainic acid-treated rats. J. Neurosci. *5,* 1016-1022.

Thomale, U.W., Kroppenstedt, S.N., Beyer, T.F., Schaser, K.D., Unterberg, A.W., and Stover, J.F. (2002). Temporal profile of cortical perfusion and microcirculation after controlled cortical impact injury in rats. J. Neurotrauma *19,* 403-413.

Thompson, H.J., LeBold, D.G., Marklund, N., Morales, D.M., Hagner, A.P., and McIntosh, T.K. (2006). Cognitive evaluation of traumatically brain-injured rats using serial testing in the Morris water maze. Restor. Neurol. Neurosci. *24,* 109-114.

Thompson, H.J., Lifshitz, J., Marklund, N., Grady, M.S., Graham, D.I., Hovda, D.A., and McIntosh, T.K. (2005). Lateral fluid percussion brain injury: a 15-year review and evaluation. J. Neurotrauma *22,* 42-75.

Tkac, I., Keene, C.D., Pfeuffer, J., Low, W.C., and Gruetter, R. (2001). Metabolic changes in quinolinic acid-lesioned rat striatum detected non-invasively by in vivo (1)H NMR spectroscopy. J. Neurosci. Res. *66,* 891-898.

Tkac, I., Starcuk, Z., Choi, I.Y., and Gruetter, R. (1999). In vivo 1H NMR spectroscopy of rat brain at 1 ms echo time. Magn. Reson. Med. *41,* 649-656.

Tokumitsu, T., Mancuso, A., Weinstein, P.R., Weiner, M.W., Naruse, S., and Maudsley, A.A. (1997). Metabolic and pathological effects of temporal lobe epilepsy in rat brain detected by proton spectroscopy and imaging. Brain Res. *744,* 57-67.

Toulmond, S., and Rothwell, N.J. (1995). Interleukin-1 receptor antagonist inhibits neuronal damage caused by fluid percussion injury in the rat. Brain Res. *671,* 261-266.

Tsai, G., and Coyle, J.T. (1995). N-acetylaspartate in neuropsychiatric disorders. Prog. Neurobiol. *46,* 531-540.

Tucciarone, J., Chuang, K.H., Dodd, S.J., Silva, A., Pelled, G., and Koretsky, A.P. (2008). Layer specific tracing of corticocortical and thalamocortical connectivity in the rodent using manganese enhanced MRI. Neuroimage

Tuunanen, J., Lukasiuk, K., Halonen, T., and Pitkanen, A. (1999). Status epilepticus-induced neuronal damage in the rat amygdaloid complex: distribution, time-course and mechanisms. Neuroscience *94,* 473-495.

van der Knaap, M.S., van der Grond, J., van Rijen, P.C., Faber, J.A., Valk, J., and Willemse, K. (1990). Age-dependent changes in localized proton and phosphorus MR spectroscopy of the brain. Radiology *176,* 509-515.

Van der Linden, A., Van Meir, V., Tindemans, I., Verhoye, M., and Balthazart, J. (2004a). Applications of manganese-enhanced magnetic resonance imaging (MEMRI) to image brain plasticity in song birds. NMR Biomed. *17,* 602-612.

Van der Linden, A., Van Meir, V., Tindemans, I., Verhoye, M., and Balthazart, J. (2004b). Applications of manganese-enhanced magnetic resonance imaging (MEMRI) to image brain plasticity in song birds. NMR Biomed. *17,* 602-612.

van der Zijden, J.P., van der Toorn, A., van der Marel, K., and Dijkhuizen, R.M. (2008). Longitudinal in vivo MRI of alterations in perilesional tissue after transient ischemic stroke in rats. Exp. Neurol. *212,* 207-212.

Van Putten, H.P., Bouwhuis, M.G., Muizelaar, J.P., Lyeth, B.G., and Berman, R.F. (2005). Diffusion-weighted imaging of edema following traumatic brain injury in rats: effects of secondary hypoxia. J. Neurotrauma *22,* 857-872.

Vink, R., Mullins, P.G., Temple, M.D., Bao, W., and Faden, A.I. (2001). Small shifts in craniotomy position in the lateral fluid percussion injury model are associated with differential lesion development. J. Neurotrauma *18,* 839-847.

Wallimann, T., Wyss, M., Brdiczka, D., Nicolay, K., and Eppenberger, H.M. (1992). Intracellular compartmentation, structure and function of creatine kinase isoenzymes in tissues with high and fluctuating energy demands: the 'phosphocreatine circuit' for cellular energy homeostasis. Biochem. J. *281 (Pt 1),* 21-40.

Watanabe, T., Frahm, J., and Michaelis, T. (2008). Manganese-enhanced MRI of the mouse auditory pathway. Magn. Reson. Med. *60,* 210-212.

Watanabe, T., Frahm, J., and Michaelis, T. (2004). Functional mapping of neural pathways in rodent brain in vivo using manganese-enhanced three-dimensional magnetic resonance imaging. NMR Biomed. *17,* 554-568.

Watanabe, T., Natt, O., Boretius, S., Frahm, J., and Michaelis, T. (2002). In vivo 3D MRI staining of mouse brain after subcutaneous application of MnCl2. Magn. Reson. Med. *48,* 852-859.

Wenzel, H.J., Woolley, C.S., Robbins, C.A., and Schwartzkroin, P.A. (2000). Kainic acid-induced mossy fiber sprouting and synapse formation in the dentate gyrus of rats. Hippocampus *10,* 244-260.

Whalen, M.J., Carlos, T.M., Kochanek, P.M., and Heineman, S. (1998). Blood-brain barrier permeability, neutrophil accumulation and vascular adhesion molecule expression after controlled cortical impact in rats: a preliminary study. Acta Neurochir. Suppl. *71,* 212-214.

Wu, E.X., Wong, K.K., Andrassy, M., Tang, H. (2003). High-resolution in vivo CBV mapping with MRI in wild-type mice. Magn Reson Med. *49*, 765-70.

Zhong, J., Petroff, O.A., Prichard, J.W., and Gore, J.C. (1995). Barbiturate-reversible reduction of water diffusion coefficient in flurothyl-induced status epilepticus in rats. Magn. Reson. Med. *33,* 253-256.

Kuopio University Publications G. - A.I.Virtanen Institute

G 51. Keinänen, Riitta et al. (eds.). The first annual post-graduate symposium of the graduate school of molecular medicine: winter school 2007.
2007. 65 p. Abstracts.

G 52. Vartiainen, Suvi. Caenorhabditis elegans as a model for human synucleopathies.
2007. 94 p. Acad. Diss.

G 53. Määttä, Ann-Marie. Development of gene and virotherapy against non-small cell lung cancer.
2007. 75 p. Acad. Diss.

G 54. Rautsi, Outi. Hurdles and Improvements in Therapeutic Gene Transfer for Cancer.
2007. 79 p. Acad. Diss.

G 55. Pehkonen, Petri. Methods for mining data from genome wide high-throughput technologies.
2007. 91 p. Acad. Diss.

G 56. Hyvönen, Mervi T. Regulation of spermidine/spermine N'-acetyltransferase and its involvement in cellular proliferation and development of acute pancreatitis.
2007. 79 p. Acad. Diss.

G 57. Gurevicius, Kestutis. EEG and evoked potentials as indicators of interneuron pathology in mouse models of neurological diseases.
2007. 76 p. Acad. Diss.

G 58. Leppänen, Pia. Mouse models of atherosclerosis, vascular endothelial growth factors and gene therapy.
2007. 91 p. Acad. Diss.

G 59. Keinänen, Riitta et al. The second annual post-graduate symposium of the graduate school of molecular medicine: winter school 2008.
2008. 57 p. Abstracts.

G 60. Koponen, Jonna. Lentiviral vector for gene transfer: a versatile tool for regulated gene expression, gene silencing and progenitor cell therapies.
2008. 71 p. Acad. Diss.

G 61. Ahtoniemi, Toni. Mutant Cu,Zn superoxide dismutase in amyotrophic lateral sclerosis: molecular mechanisms of neurotoxicity.
2008. 107 p. Acad. Diss.

G 62. Purhonen, Anna-Kaisa. Signals arising from the gastointestinal tract that affect food intake.
2008. 86 p. Acad. Diss.

G 63. Kaikkonen, Minna. Engineering baculo- and lentiviral vectors for enhanced and targeted gene delivery.
2008. 109 p. Acad. Diss.

G 64. Gureviciene, Irina. Changes in hippocampal synaptic plasticity in animal models of age-related memory impairment. 2
2008. 106 p. Acad. Diss.

G 65. Oikari, Sanna. Evaluation of phenotypic changes of Acyl-CoA binding protein / diazepam binding inhibitor overexpression in transgenic mice and rats.
2008. 79 p. Acad. Diss.

G 66. Laurema, Anniina. Adenoviral gene therapy and fertility: distribution studies in reproductive organs and risk of vertical transmission in female rabbits and rats.
2008. 79 p. Acad. Diss.